Chapter

Advanced Composites with Aluminum Alloys Matrix and Their Fabrication Processes

Leszek A. Dobrzański

Abstract

This chapter introduces advanced aluminum alloy matrix composites and their manufacturing processes. In the beginning, the state of the art is characterized and the general characteristics of aluminum and its practical applications are presented, starting with the history of aluminum. The current approximate distribution of bauxite resources in the world and the production of bauxite and alumina in the leading countries of the world, as well as the production of primary and secondary aluminum and the range of aluminum end products, are presented. Aluminum alloys intended for plastic deformation and castings, and composite materials in general and with a matrix of aluminum alloys in particular, have been characterized in general. Against this background, a detailed review of the results of the Author's own research included in numerous projects and own publications on advanced composite materials, their production technology, their structure, and properties were done. The range of aluminum alloy matrices of composite materials was adequately characterized, which include AlSi12, AlSi7Mg0.3, AlMg1SiCu, AlMg3, AlMg5, and AlMg9, respectively. Composite materials tested in terms of manufacturing technology include three groups. The first group includes gas pressure infiltration with liquid aluminum alloys of suitably formed porous preforms. Porous frameworks as a reinforcement for pressure-infiltrated composite materials with a matrix of aluminum alloys are produced by three methods. Al_2O_3 powder with the addition of 30–50% carbon fibers is uniaxially pressed, sintered, and heated to thermally degrade the carbon fibers and create the required pore sizes. In the second case, the ceramic porous skeleton is produced with the use of halloysite nanotubes HNTs by mechanical milling, press consolidation, and sintering. A third method is SLS selective laser sintering using titanium powders. Another group of manufacturing technologies is the mechanical synthesis of the mixture of AlMg1SiCu aluminum alloy powder and respectively, halloysite nanotubes HNTs in a volume fraction from 5 to 15% or multi-wall carbon nanotubes MWCNTs in a volume fraction from 0.5 to 5%, and subsequent consolidation involving plastic deformation. The third group of analyzed materials concerns composite surface layers on substrates of aluminum alloys produced by laser feathering of WC/W2C or SiC carbides. The structure and properties of the mentioned composite materials with aluminum alloys matrices are described in detail. The chapter summary provides final remarks on the importance of advanced aluminum alloy composite materials in industrial development. The importance of particular groups of engineering materials in the history and the development of the methodology for the selection of engineering materials, including the current stage of Materials 4.0, was

emphasized. The importance of material design in engineering design is emphasized. Concepts of the development of societies were presented: Society 5.0 and Industry 4.0. The own concept of a holistic model of the extended Industry 4.0 was presented, taking into account advanced engineering materials and technological processes. Particular attention was paid to the importance of advanced composite materials with an aluminum alloy matrix in the context of the current stage of Industry 4.0 of the industrial revolution. Growth in the production of aluminum, its alloys, and composites with its matrix was compared with that of steel. Despite the 30 times less production, aluminum is important due to its lower density. The challenges posed by the development in the Industry 4.0 stage, including the expectations of the automotive and aviation industry, force constant progress in the development of new materials with the participation of aluminum, including the composite materials with an aluminum alloy matrix presented in this chapter.

Keywords: Aluminum, Aluminum alloys matrix composite, pressure infiltration, halloysite nanotubes, multi-wall carbon nanotubes, additive manufacturing, selective laser sintering, mullite, mechanical synthesis, laser feathering, Industry 4.0, Sustainable Development Goals, materials science paradigm, aluminum market

1. State-of-the-art and the general characteristics of aluminium and its practical applications

1.1 General characteristics of aluminum

Aluminum is a metal of very high technical importance [1–4]. It occurs in nature in many minerals and is the third element (after oxygen and silicon) in terms of its share in the earth's crust. It is, however, the second metal after iron in terms of technical applications. Its main ore is bauxite, from which pure Al_2O_3 oxide is produced, and then by electrolysis of the oxide dissolved in the molten cryolite (sodium fluoroaluminate), blast aluminum is obtained, which can be further refined.

Aluminum has an atomic number of 13 and an atomic mass of 26.9815. It does not show allotropes and crystallizes in a wall-centered regular network of A1 type with a parameter of 0.40408 nm. The melting point of aluminum is 660.37°C and the boiling point is 2494°C. The density of aluminum is 2.6989 g/cm^3 at 20°C. Aluminum in the annealed condition is characterized by tensile strength 70–120 MPa, yield strength 20–40 MPa, elongation 30–45%, and narrowing 80–95%. Aluminum can be cold and hot worked plastic deformed. In the cold plastic deformed state with 60–80% degree of crushing, the tensile strength reaches 140–230 MPa, yield strength 120–180 MPa, hardness 40–60 HBW, with a reduced elongation 1.5–3%.

Aluminum is characterized by high electrical conductivity – 37.74 MS/m, constituting approx. 65% of the electrical conductivity of copper, and good thermal conductivity. The electrical conductivity is significantly reduced with increasing concentrations of impurities and impurities, mainly Fe and Si, as well as Cu, Zn, and Ti. These elements also reduce the plasticity but increase the strength properties. The Fe admixture hardly dissolves in aluminum, creating the brittle Al_3Fe phase. On the other hand, Si shows low solubility and does not form any phases, it is in the free form. In the case of the simultaneous presence of Fe and Si, the $Fe_3Si_2Al_{12}$ or $Fe_3Si_2Al_9$ intermetallic phases occur. Their separations, especially at the grain boundaries, significantly reduce the plastic properties of aluminum.

Aluminum is highly resistant to corrosion. In the air, it is covered with a thin layer of Al_2O_3, which protects against atmospheric corrosion, water, concentrated

nitric acid, numerous organic acids, and hydrogen sulfide. On the other hand, reducing acids HCl and HF, seawater, vapors, and mercury ions accelerate the corrosion of aluminum. In order to improve corrosion resistance, aluminum may be subjected to anodic oxidation (so-called anodization), i.e. an electrolytic process of producing an oxide coating, e.g. in a 10% sulfuric acid solution, combined with different colors of the metal surface.

Aluminum is extracted from ores in a complex process and, obviously, unknown throughout most of human history [5–7]. On the other hand, hydrated potassium-aluminum sulphate (KAl (SO_4) 2 12 H_2O) has been known for millennia as alum, or more precisely aluminum-potassium alum, which occurs naturally as a mineral in the form of granular, infiltrative clusters. Raids and efflorescence. It occurs in the weathering zone of clay rocks, coals containing pyrite, marcasite and other sulfides. It is also formed in the process of weathering igneous rocks rich in feldspar and feldspar, incl. in Uzbekistan in the Kara-kum desert, in Italy near Vesuvius, in the USA in Alaska and in Russia in Kamchatka. People have known alum since the 5th century BC and it was widely used for staining as early as antiquity [8]. It was widely distributed in international trade relations in the Middle Ages due to its use in dyeing [8–10]. Aluminum was discovered in 1825 by Hans Christian Oersted [11–13], a Danish physicist. The results of his work were extended by Friedrich Wöhler [8, 13, 14], a German chemist. In 1854, both Robert Wilhelm Bunsen, a German chemist, and Henri Étienne Sainte-Claire Deville, produced aluminum for the first time by electrolysis. Electricity supply was ineffective at the time, so their methods could not be developed in industry. At that time, aluminum was extremely valuable, and therefore its price significantly exceeded that of gold. The situation in this respect continued until 1856, when Deville first began industrial production and not through the production of electrolytes [8], which he considered impractical at the time, so he switched to chemical methods in the same year. In 1884, world aluminum production reached 3.6 tons.

In 1886, Paul Héroult, French engineer and Charles Martin Hall, American engineer, independently developed a method of producing aluminum, which became the first large-scale production technology [8]. Their process is still in use today and is known as the Hall-Héroult process (**Figure 1**) [15, 16]. This process and the process developed by Carl Joseph Bayer, an Austrian chemist, determined the wide dissemination of aluminum and its availability to the public, starting from 1889 (**Figure 2**) [8].

Nowadays, the commercial production of aluminum oxide by refining from bauxite practically covers the Bayer process [17, 18] (**Figure 2**), which consists of:

1. Digestion, in which bauxite is ground and slurried to caustic soda (NaOH) which is then pumped into large pressure fermentors where the caustic soda reacts with aluminum oxide minerals to form soluble sodium oxide $Na[Al(OH)_4]$;

2. Clarification, in which a sodium oxide solution is processed in cyclones to remove coarse particles; the remaining fluid is processed in thickeners where the flocculates are added to the solid agglomerates which are removed with fabric filters; the residue (red mud) is washed and discarded and the clarified solution (containing $Na[Al(OH)_4]$) goes to the next step;

3. Precipitation – aluminum oxide nucleating agents are added to the clarified solution in order to facilitate the separation of larger agglomerated aluminum oxide crystals; product-size crystals are separated from the small crystals (recycled serve as nucleating agents) and washed to remove caustic residues; agglomerates are transferred to the next step.

4. Calcination – $Na[Al(OH)_4]$ agglomerates are placed in rotary kilns or stationary fluidized bed calciners at a temperature higher than 960°C, ensuring dehydration and obtaining commercial grade aluminum oxide.

Both these processes are still used in the production of aluminum and it is them that have made aluminum popular in industry and everyday life. The statue of Anteros, which was erected in 1893 at Piccadilly Circus in London, Great Britain, can be considered a symbol of the growing role of aluminum and is considered the first large work made of this material (**Figure 3**).

World aluminum production reached 6,800 metric tons in 1900. **Figure 4** shows changes in the production volume and prices of aluminum in the years 1885–2020.

In the late nineteenth and early twentieth centuries, aluminum alloys began to be used more and more. The basis of modern aluminum production are the Bayer and Hall-Héroult processes, further enhanced in 1920 by Carl Wilhelm Söderberg, a Swedish chemist and his cooperators. In the twentieth century, the range of aluminum applications has significantly increased, including both in engineering and in construction, to gain use in aviation as a strategically important material during World War I. For these reasons, the importance of aluminum during the Second World War was even greater, to exceed 1,000,000 metric tons for the first time in 1941. After the war, since 1945, aluminum consumption has been increasing annually by another 10% for almost three decades, gaining popularity in construction applications, electrical cables, basic foil and the aerospace industry. In 1954, aluminum, ahead of copper, became the most widely produced non-ferrous metal, with world production increasing to 2,810,000 tons per year. In the second half of the 20th century, aluminum found its way into transport and packaging, although its production was critically assessed for environmental reasons, and as a result aluminum recycling developed. For example, in the United States, in the period from 1970 to 1980, the level of aluminum recycling increased 3.5 times, and by 1990 even 7.5 times. At the same time, mining and processing costs decreased and aluminum production increased, exceeding 10,000,000 metric tons per year for the first time in 1971. This was accompanied by a fall in aluminum prices since the beginning of

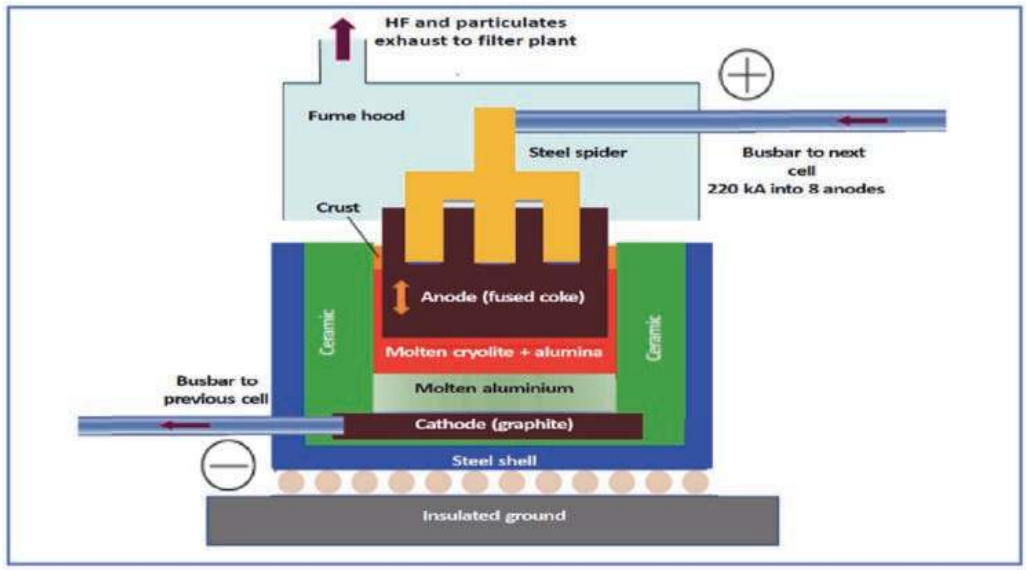

Figure 1.
The diagram of the Hall – Héroult cell for process for smelting aluminum through dissolving aluminum tained in molten cryolite, and electrolyzing the molten salt bath.

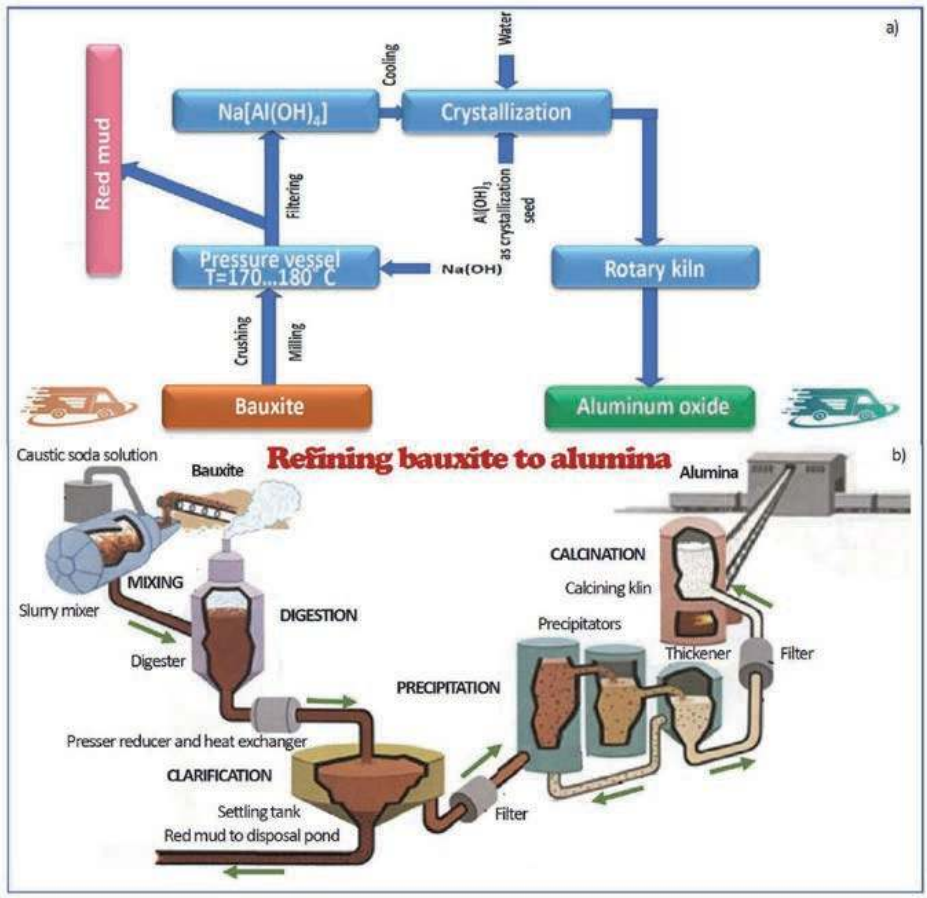

Figure 2.
The Bayer process of obtaining aluminum oxide from bauxite ores (a) the block diagram; (b) the example of the industrial application.

the 1970s. In 1973, that price was US$ 2,130 per metric ton (1998 US price level). The launch of the production of beverage cans prompted a significant increase in aluminum production in the early 1970s, despite the fact that in the 1970s and 1980s the costs of primary aluminum production increased. However, it contributed to an increase in the share of secondary aluminum in the overall production, due to its significantly increased recycling. In the 1970s, aluminum became a stock exchange commodity. In the 1970s, aluminum production from the United States, Japan and Western Europe was gradually allocated to Australia, Canada, the Middle East, Russia and China, where it was cheaper, e.g. in view of favorable tax regulations in these countries. Production costs fell in the 1980s and 1990s. In the first decade of the 21st century, the total share of the BRIC countries (Brazil, Russia, India and China) increased from 32.6% to 56.5% in primary production and from 21.4% to 47.8% in primary consumption. China amassed a particularly large share of world production thanks to abundant raw materials, cheap energy and government incentives, and its share in consumption increased from 2% in 1972 to 40% in 2010. In the United States, this share decreased to 11%. In the United States, Western Europe, and Japan, most aluminum is used in transport, engineering, construction, and packaging. World production continues to increase, surpassing 50,000,000 metric tons in 2013 and surpassing a record 58,500,000 metric tons per year in 2015. World production has now exceeded more than 62,500,000 metric tons per year [19]. Aluminum is produced in greater quantities than all other non-ferrous metals combined.

Figure 3.
Statue of Anteros, the Greek god of revered love, on Piccadilly Circus in London, UK: (a) view of Piccadilly circus; (b) detail of the monument with the figure of Anteros.

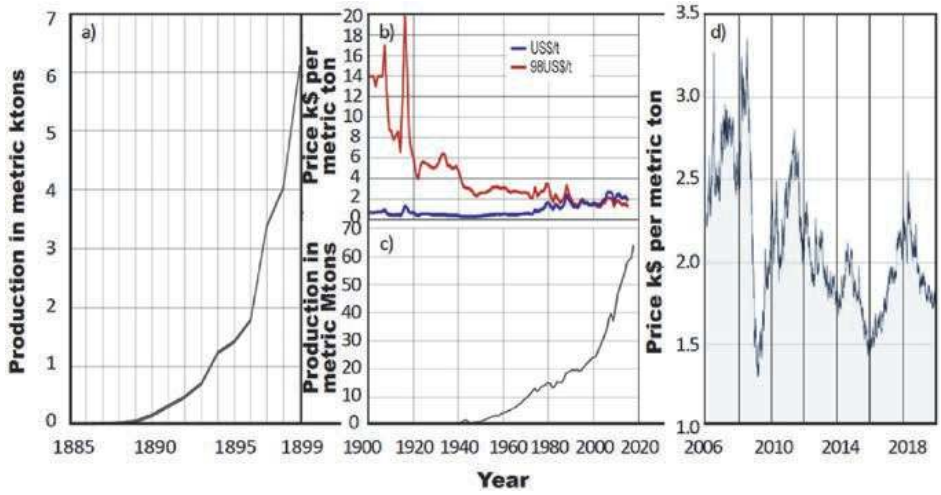

Figure 4.
Changes in the volume of aluminum production and prices in the years 1885–2020; (a) production volume in the years 1885–1900; (b) changes in aluminum prices in the years 1900–2020 – Blue line, the actual price in current values; red line – Price comparable in 1998; (c) production volume in the years 1900–2020; changes in aluminum prices in the period from 1 December 2005 to 24 November 2020 (own study based on statistical data).

The basic raw material for the production of aluminum is bauxite [20–22]. Pierre Berthier the French geologist discovered bauxite in Provence, France in 1821. Bauxite is a sedimentary rock which contains a high aluminum content as mixture of few minerals i.e. gibbsite ($Al(OH)_3$), boehmite (γ-AlO(OH)) and diaspore (α-AlO(OH)), goethite (FeO(OH)) and hematite (Fe_2O_3), clay mineral kaolinite ($Al_2Si_2O_5(OH)$) and also anatase (TiO_2) and ilmenite ($FeTiO_3$ or $FeO.TiO_2$). Australia is the largest producer of bauxite, followed by China. **Figure 5** shows the distribution of the main raw materials of bauxite in the world with the differences in their abundance. **Table 1** presents the production of bauxite and aluminum oxide in the leading countries in the world in 2018 and 2019 and the current state of bauxite raw material reserves [23].

Aluminum is produced in many grades [24] with varying degrees of purity from 99.999 to 99.0%, a few examples of which are given below:

- the purest one containing 99.995% Al is used in the production of chemical equipment and condenser films,

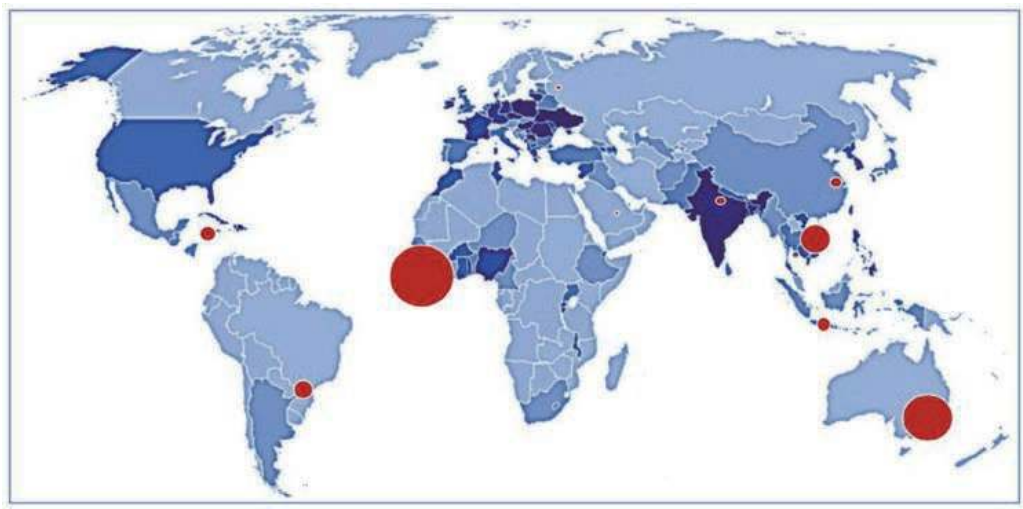

Figure 5.
Approximate distribution of bauxite reserves in the world according to data from 2019, with an indication of differences in their abundance (the diameter of the red circle corresponds to the resource size) (own study).

Country (alphabetical order)	Bauxite Reserves	Bauxite		Aluminum oxide	
		2018	2019	2018	2019
Australia	6,000,000	86,400	100,000	20,400	20,000
Brazil	2,600,000	29,000	29,000	8,100	8,900
Canada	—	—	—	1,570	1,500
China	1,000,000	79,000	75,000	72,500	73,000
Guinea	7,400,000	57,000	82,000	180	300
India	660,000	23,000	26,000	6,430	6,700
Indonesia	1,200,000	11,000	16,000	1,000	1,000
Jamaica	2,000,000	10,100	8,900	2,480	2,100
Malaysia	110,000	500	900	—	—
Russia	500,000	5,650	5,400	2,760	2,700
Saudi Arabia	200,000	3,890	4,100	1,770	1,800
Vietnam	3,700,000	4,100	4,500	1,310	1,300
United States	20,000	W	W	1,570	1,600
Other countries	5,000,000	17,000	15,000	11,400	12,000
World total (rounded)	30,000,000	327,000	370,000	131,000	130,000

Table 1.
Production of bauxite and aluminum oxide in the leading countries in the world in 2018 and 2019 and the current state of bauxite raw material reserves.

- containing 99.8% Al is used for foils, cable coatings and plating,
- containing 99.5% Al for electric wires,
- containing 99% Al for everyday products.

There are three different types of primary aluminum, corresponding to different production methods:

- commercially pure aluminum from the reduction of Al_2O_3 in the electrolyser, representing the majority of industrial production; it may contain up to 1% of impurities, and the purity very often exceeds 99.9%.
- refined aluminum produced by electrorefining commercially pure aluminum in the cell layer; its purity ranges from 99.9% to 99.99 + %.
- zone refined aluminum produced by zone refining and with the appropriate starting material and technique can produce metal with less than 1 ppm impurities.

This purity was obtained thanks to the zone refining of electrodeposited metal from organic baths.

Secondary aluminum is produced by remelting production scrap or obsolete equipment and is usually recovered as alloys. Even after remelting high-quality electrodes, the resulting "secondary pure aluminum" is less pure than the corresponding primary aluminum because contamination by other materials occurs.

Most of the impurities in primary aluminum come from raw materials (bauxite, soda, carbon). Therefore, their purity should be controlled, although it is also important to vary the chemical composition of individual shipments, even if they come from the same source, as they may differ in their composition, even by one order of magnitude.

Metallurgical aluminum grades (with limited purity) are used in the production of alloys and numerous everyday products, equipment for the food industry, for some electric cables, heat exchangers, in construction, for coatings of steel products, and in the form of foil – for food packaging. Refined aluminum (high purity) is used in electronics and electrical engineering and for the construction of special chemical apparatus.

1.2 General presentation of aluminum alloys

The relatively low strength properties of aluminum can be increased – even several times – by introducing alloying elements and heat treatment of the alloys [24–30]. **Table 2** gives the general classification of aluminum alloys according to their chemical composition.

Most generally – due to the method of manufacturing – aluminum alloys are divided into:

- for plastic deformation,
- cast.

Some of these alloys can be used both as cast and for plastic deformation.

Aluminum alloy series	Major alloy additives	Characteristic
1xxx	Lack (admixtures <1%)	Low strength properties and very high plasticity, making them susceptible to cold and hot forming; thanks to the high purity of the alloy, they are highly resistant to corrosion, and they are also characterized by high thermal and electrical conductivity
2xxx	Cu	Has an increased hardness compared to 1xxx, but the corrosion resistance is much lower
3xxx	Mn	Low strength, but susceptible to plastic deformation; they are very well weldable and corrosion resistant
4xxx	Si	High strength and corrosion resistance
5xxx	Mg	Corrosion resistance is even higher than for 4xxx
6xxx	Mg + Si	Corrosion resistant, shows good plasticity, medium mechanical strength
7xxx	Zn + Mg	Hard, high-strength aluminum alloys; they are characterized by the highest strength of all aluminum alloys, but also low corrosion resistance
8xxx	Others, no classification	Covers aluminum alloys which were not classified in the previous series

Table 2.
Classification of aluminum alloys by chemical composition.

The alloys for plastic deformation usually contain up to about 5% of alloying elements, most often Cu, Mg, Mn, sometimes also Si, Zn, Ni, Cr, Ti, or Li. Some of these alloys are used in a plastic worked or in recrystallization annealed state, and some are subjected to a precipitation hardening heat treatment. Aluminum alloys with a concentration of alloying elements greater than 5% can also be subjected to plastic deformation, under special conditions. Aluminum alloys can be shaped by various methods of plastic deformation and are supplied in the form of many metallurgical intermediates.

Cast aluminum alloys are mostly multi-component alloys with a high concentration – from 5 to 25% – of alloying elements, mainly Si, Cu, Mg, Zn, and Ni or their various combinations. Cast Al alloys are characterized by good fluidity and often low casting shrinkage. Alloys containing less than 5% alloying elements can also be used as cast. In general, aluminum alloys can be sand-molded, die-cast, pressure-cast, and lost wax methods although some of these methods are rarely used today.

1.3 General information on composite materials with aluminum alloys matrices

Advanced possibilities of shaping the properties of materials containing aluminum alloys are provided by the production of composites with an aluminum matrix (AMC), where the matrix most often used is not aluminum but aluminum alloys [31–45]. AMCs in relation to aluminum and its alloys show better physical and mechanical properties, including a very favorable strength-to-weight ratio, high strength and high modulus of elasticity, better fatigue strength, good ductility, low thermal expansion coefficient, good wear resistance and corrosion resistance and creep strength. Therefore, AMCs have found numerous applications, many times unrivaled in comparison with aluminum alloys, when high properties are required, e.g. in the automotive, aviation, manufacturing, armaments, energy and medicine industries [46–62].

Generally, a composite material, often simply referred to as a composite, is a combination of two or more materials (reinforcement members, fillers and binder constituting the matrix of the composite) differing in type or chemical composition on a macroscopic scale [3]. Components of composite materials retain their identity because they do not completely dissolve in each other and do not combine into other elements, but interact together. Typically, these components can be physically identified and exhibit interfacing surfaces.

Composite materials are usually artificially produced to obtain properties that cannot be obtained separately by any of the components present. Composite materials are used to ensure appropriate mechanical properties, but also electrical, thermal, tribological, various environmental and other properties. Composite materials most often contain fibers or phase particles and are stiffer and stronger than the continuous matrix phase. The many reinforcement elements also provide good thermal and electrical conductivity and a lower coefficient of thermal expansion and/or good wear resistance. However, there are exceptions that can also occur in composite materials, such as rubber-modified polymers, where the discontinuous phase is more compliant and more ductile than the polymer, resulting in increased impact strength. Similarly, steel wires can be used to reinforce gray cast iron in truck and tractor brake drums.

In general, composite materials can be classified on two separate levels. This classification, although it may seem a bit eclectic, is of practical importance. The first level of classification concerns the matrix material, and in this case the analysis is limited to metals and their alloys, in particular aluminum and its alloys. At the second level (**Figure 6**) the classification concerns the geometrical features of the reinforcing materials which is presented in the **Figure 7** also.

Composite materials based on non-ferrous metals, including aluminum, may contain dispersoid particles with a diameter of 10–250 nm. These particles, usually metal oxides, distributed in the matrix, affect the blocking of the dislocation movement and even if they are not coherent with the matrix, they influence its strengthening. These particles cannot dissolve in the matrix, although a low solubility may improve the adhesion of the dispersoids and the matrix. As Al_2O_3 does not dissolve in Al, the Al_2O_3 – Al system effectively enhances the dispersive hardening of such a composite material. There are numerous examples of this type of composite

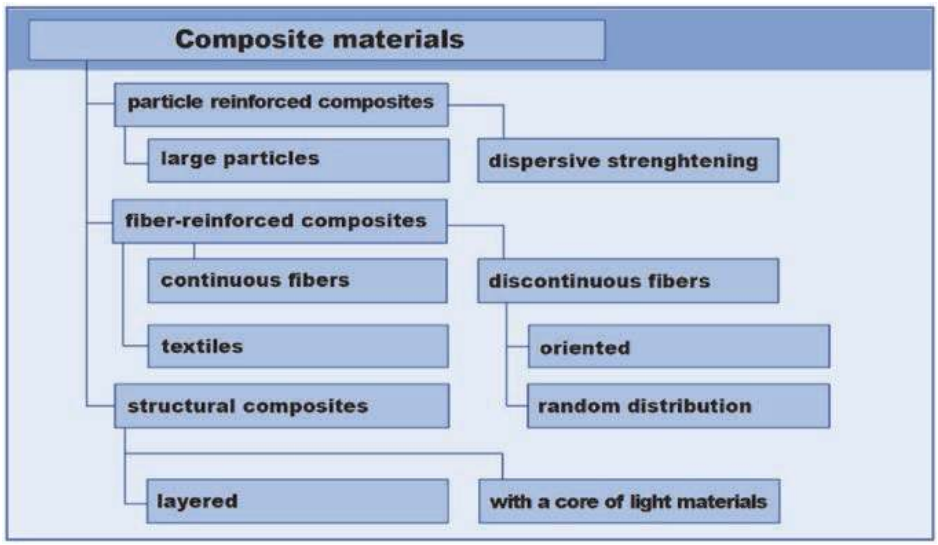

Figure 6.
Classification of composite materials according to the type and geometrical features of reinforcing elements.

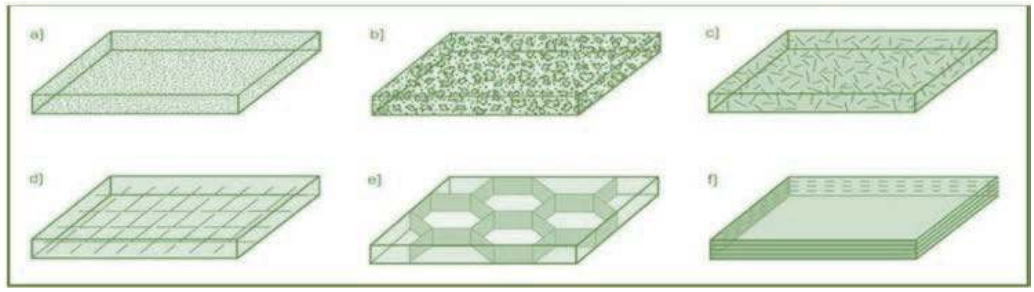

Figure 7.
Examples of different types of reinforcement elements for composite reinforced materials: (a) dispersive particles, (b) flakes, (c) discontinuous fibers, (d) continuous fibers in the form of a textile, (e) skeletally, (f) layered in laminates.

materials, including sintered aluminum powder SAP reinforced by Al_2O_3 in 14% and dispersion hardened nickel or iron alloys, oxide dispersion-strengthened ODS.

Powder metallurgy is a frequently used technology to produce metal matrix composite materials, and this distinct group of composite materials is labeled P/M MMCs (powder metallurgy metal – matrix composites) or P/M AMCs respectively for aluminum matrix.

In the case of composite materials with a non-ferrous matrix, including aluminum and its alloys, reinforced with large particles, due to the relatively large size of the reinforcing particles and the lack of their coherence with the matrix of non-ferrous metals, dispersive hardening cannot take place. These groups of composite materials, on the other hand, achieve a combination of functional properties resulting from the interaction of both the matrix and the particles of the second phase arranged therein, which often guarantee an increase in strength properties.

Fiber-reinforced composite materials are most often used to provide increased static and fatigue strength, including specific strength and stiffness, which is obtained by incorporating strong, stiff but usually brittle fibers into a soft but tough matrix. The matrix only transmits applied load to the fibers, which for the most part carry it. Composite materials of this group can show high strength properties both at room temperature and at elevated temperature.

Many reinforcement materials are used. Boron, metal and ceramic fibers are used to strengthen e.g. composite materials with a metal matrix, as well as with a composition corresponding to the intermetallic phases. The described fibers have gained a wide range of applications due to their very high utility values. However, it should be noted that their price varies by as much as 50,000 times. Glass fibers are used very commonly, although not in the case of composite materials with a non-ferrous metal matrix, because their relative specific cost (cost of 1 kg of material) ranges from 1 to 3. Aramid, carbon, ceramic oxide and an oxide fibers show very good performance properties, but at a high price, because the relative cost related to the cost of glass fibers ranges from about 15 for aramid and carbon fibers, although also not used in the case of composite materials with a non-ferrous metal matrix, to approx. 4500 for SiC fibers, which determines the limited use of these materials. In very special cases, however, sapphire fibers are used, where special reinforcing properties are required, as the relative price of this material exceeds 45,000.

Often, the fibers are stapled, their length does not exceed 10 mm, and they are arranged randomly in the matrix of composite materials, especially those with a polymer matrix.

Composite materials with a non-ferrous metal matrix including AMCs reinforced with continuous fibers are a class of materials with a wide range of applications due to their mechanical properties, wear resistance and thermal

properties. It is possible to adapt their properties to requirements and provide increased strength, stiffness, thermal conductivity, abrasion resistance, fatigue strength and dimensional stability. These composite materials are non-flammable, do not evaporate under vacuum, and are resistant to organic liquids, including fuels and solvents. The matrix of these materials consists of monolithic alloys, usually light metals, including aluminum, but also heat-resistant superalloys. They are reinforced with boron, carbide, oxide and tungsten fibers in a continuous form, usually with a volume fraction of 10–70% in the composite material, produced in addition to materials with the same matrix reinforced with discontinuous fibers. Aluminum oxide particles are a cheap solution and are most often used when the metal matrix is cast, while the most common are silicon carbide and boron carbide particles as a reinforcement in the form of discontinuous but also continuous fibers, especially in aircraft structures (**Table 3**).

Reinforcing fiber material	Manufacturing process	Application examples
Boron	Hot pressing of the fiber system between the metal foils	Tubular struts of the central part of the space shuttle hull, cold heat dissipator (diffuser) in the housings of electronic microchips of multi-layer plates, neutron radiation shielding material (e.g. in spent nuclear fuel storage facilities or containers for transporting such fuel), fan blades in turbo-jet engines, aircraft wing plating, aircraft landing gear components, bicycle frames, golf clubs; Due to the degradation of boron fibers above 480°C, high-temperature applications are impossible and manufacturing using casting or high temperature low pressure pressing
SiC	Investment casting, low pressure hot forming, superplastic forming with diffusion welding, isostatic hot pressing HIP, green tape production by winding fibers on films covering a rotating drum and their initial bonding to the film using a polymer resin, removed then in the volatilization (evaporation) process or by plasma spraying and subsequent pressure diffusion welding of several such cut tapes stacked at a temperature close to the melting point and pressure consolidation in an autoclave in a vacuum metal container, as well as in closed forms to give the required final shapes	Construction of aircraft elements, wings up to 3 m long, elements of portable bridges, small pressure vessel cylinders, bullet stabilizers, missile casings
Graphite	Vacuum diffusion welding of raw metal (aluminum) strips with longitudinally arranged fibers, diffusion rolling welding Rapi-Press, continuous pressing, direct metal infiltration process, casting	Very high strength components and stiffness, e.g. the mast of the Hubble cosmic telescope, thin-walled pipes of small and large diameters (up to 2 m), with complex shapes, produced with the near-net-shape technology
Al_2O_3	Casting	Pistons for internal combustion engines (Toyota)

Table 3.
General characteristics of composite materials with aluminum matrix reinforced by continuous fibers.

Various types of ceramics, e.g., Al_2O_3, SiC and B_4C, are widely used to reinforce aluminum matrix composites. They show very good properties, such as high strength, high hardness, abrasion resistance.

Composite materials in metal-to-metal and metal-ceramic systems are produced using liquid and solid-phase technologies. Liquid-phase technologies are based on direct (in situ) methods, during which the fibrous structure of the composite is obtained by solidifying the alloy with unidirectional heat dissipation, and on indirect (ex situ) methods using foundry technologies, plastic processing and powder engineering.

The basic manufacturing processes for AMC on an industrial scale can be divided into the following groups:

- Liquid state processes, including stir casting, extrusion casting, injection molding and in situ (reactive) process, ultrasonic assisted casting, vacuum infiltration, pressureless infiltration and dispersion methods;

- Solid-state processes involving powder mixing followed by consolidation (powder metallurgy), friction by shot-assisted high-energy powder grinding, ion bonding by diffusion and vapor deposition techniques

- Liquid–solid processes including composite casting, semi-solid molding.

Methods of manufacturing composite materials with an aluminum alloys matrix with continuous reinforcement			
With the participation of the liquid phase	Gravitational • vacuum • pressure	In solid state	Diffusion welding
			Hot rolling welding
			Hot extrusion welding
	Bonding		Bonding high-energy shaping
	Hot pressing with the participation of the liquid phase		
	Plasma spraying		
Methods of manufacturing composite materials based on aluminum alloys with discontinuous reinforcement			
With the participation of the liquid phase	Methods of mixing metal in liquid state • by mechanical methods • electromagnetic methods • gas injection	In solid state	Powder engineering methods
Thixotropic manufacturing in the liquid–solid state			
Spray methods			
In situ generation methods: • reactions in the system: liquid–liquid, liquid–gas, liquid–solid, • reactions in salt mixtures, • direct oxidation and nitriding, • reactive spray molding, • self-developing high-temperature synthesis, • reactive plasma synthesis.			

Table 4.
Classification of methods of manufacturing composite materials with a matrix of aluminum alloys with continuous and discontinuous reinforcement.

Method	Range of shape and size	Range of volume fraction	Damage to reinforcement	Cost
Stir casting	Wide range of shapes, larger size up to 500 kg	Up to 0.3	No damage	Least expensive
Squeeze casting	Limited by preform shape up to 2 cm height	Up to 0.5	Severe damage	Moderate expensive
Spray casting	Limited shape, large shape	0.3–0.7		Expensive
Powder engineering	Wide range, restricted size		Reinforcement fracture	Expensive

Table 5.
Comparative analysis of different technique of composites manufacturing.

A detailed classification can also be made, based on the type of reinforcement (continuous and discontinuous) (**Table 4**).

Table 5 compares additionally some of the methods mentioned.

During the last quarter of a century, the processes of mechanical alloying, known for a long time, have been used in the production of composite materials reinforced with particles, causing improvement in the structure and dispersion hardening of these materials and even distribution of hardening particles in the matrix [33, 47, 63–65]. The resulting nanocrystalline or submicrocrystalline structure improves the properties of newly developed composite materials [34, 37, 47, 53, 63, 65].

2. Description of the materials taken into account and the technologies used for their manufacturing

2.1 The range of matrices of aluminum alloy matrix composite materials presented in this chapter

This chapter presents a generalization of the results of numerous own studies and provides a detailed overview of the structure and properties and manufacturing technology of several AMCs selected for presentation due to their advanced manufacturing methods and unexpected properties and the resulting wide application possibilities.

Among these materials, there are basically three groups of such materials presented in this chapter, examined within the research projects [66–74] of the Author of this chapter and doctoral dissertations [75–80] carried out under the supervision of the Author of this chapter. The details were published earlier [81–112]. The description in this chapter covers the main groups of composite materials presented in **Table 6**, as follows:

1. composite materials manufactured by gas-pressure infiltration with liquid aluminum alloys,

2. nanocomposite materials manufactured by mechanical synthesis of a mixture of aluminum alloy powder with HNTs or MWCNTs nanotubes and the press consolidation,

3. composite surface layers on the substrate of aluminum alloys as a result of laser feather by introducing carbides powder.

No.	Matrix	Reinforcement	A form of reinforcement	Technology of manufacturing	Literature
1	AlSi12	Sintered Al_2O_3 powder with carbon fibers	Skeleton structure	Gas-pressure infiltration	[73–75]
2.	AlSi12	Sintered HNTs halloysite nanotubes with carbon fibers	Skeleton structure	Gas-pressure infiltration	[68, 70, 74, 78]
3	AlSi12	Selective laser sintering of titanium powder	Skeleton structure	Gas-pressure infiltration	[66, 70, 74, 80]
4	AlSi7Mg0.3	Selective laser sintering of titanium powder	Skeleton structure	Gas-pressure infiltration	[66, 70, 74, 80]
5	AlMg1SiCu	Halloysite HNTs nanotubes	Reinforcing by dispersive particles	Mechanical synthesis & press consolidation	[68, 76]
6	AlMg1SiCu	Multi-wall carbon nanotubes MWCNTs	Reinforcing by dispersive particles	Mechanical synthesis & press consolidation	[67, 79]
7	AlMg3	WC	Powder particles in remelted zone	Laser feather by introducing powder in remelted zone	[69, 70, 72, 77]
8	AlMg3	SiC	Powder particles in remelted zone	Laser feather by introducing powder in remelted zone	[69, 70, 72, 77]
9	AlMg5	WC	Powder particles in remelted zone	Laser feather by introducing powder in remelted zone	[69, 70, 72, 77]
10	AlMg5	SiC	Powder particles in remelted zone	Laser feather by introducing powder in remelted zone	[69, 70, 72, 77]
11	AlMg9	WC	Powder particles in remelted zone	Laser feather by introducing powder in remelted zone	[69, 70, 72, 77]
12	AlMg9	SiC	Powder particles in remelted zone	Laser feather by introducing powder in remelted zone	[69, 70, 72, 77]

Table 6.
General characteristics of the discussed composite materials.

In the above-mentioned composite materials, aluminum alloys listed in **Table 7** were used as the matrix.

2.2 Manufacturing technologies of porous skeletons as a reinforcement of pressure-infiltrated aluminum alloy matrix composite materials

In the case of the 1st composite material in question, porous Al_2O_3 ceramic skeleton was produced by sintering Alcoa Industrial Chemicals CL 2500 powder (**Table 8**) with the addition of 30, 40, or 50% by weight Sigrafil C10 M250 UNS carbon fibers from SGL Carbon Group (**Figure 8**) with the properties given in **Table 9**.

Al_2O_3 powder was wet-milled in a ball mill for 5 minutes to break up powder agglomerates. In order to eliminate mutual electrostatic interactions and prevent agglomeration of carbon fibers, Dolapix CE 64 was used, introduced into the Al_2O_3

Aluminum alloys	Elements concentration, wt. %							
	Si	Fe	Cu	Mn	Mg	Ti	Other	Al
AlSi12	10.0–12.0	Max 0.3	Max 0.03	0.2–0.4	0.25–0.32	0.08–0.15	—	rest
AlSi7Mg0.3	6.5–7.5	Max 0.15	Max 0.05	Max 0.10	0.25–0.45	0.08–0.15	V max 0.03	
AlMg1SiCu	0.6	0.47	0.22	0.11	0.95	0.006	Cr 0.26; Zn 0.015	
AlMg3	0.07	0.07	0.01	0	2.86	0.01	—	
AlMg5	0.08	0.07	0.01	0	5.55	0.01	—	
AlMg9	1.32	0.1	0.003	0.43	10.1	0.008	Zn 0.006	

Table 7.
Chemical composition of the aluminum alloys used.

Density, g/cm^3	Particle diameter D50, μm	Share of other phases, wt%						
		Al_2O_3	Na_2O	Fe_2O_3	SiO_2	CaO	B_2O_3	other
3.98	1.80	99.80	0.05	0.02	0.01	0.01	0.01	0.10

Table 8.
Properties Al_2O_3 Alcoa CL 2500 powder.

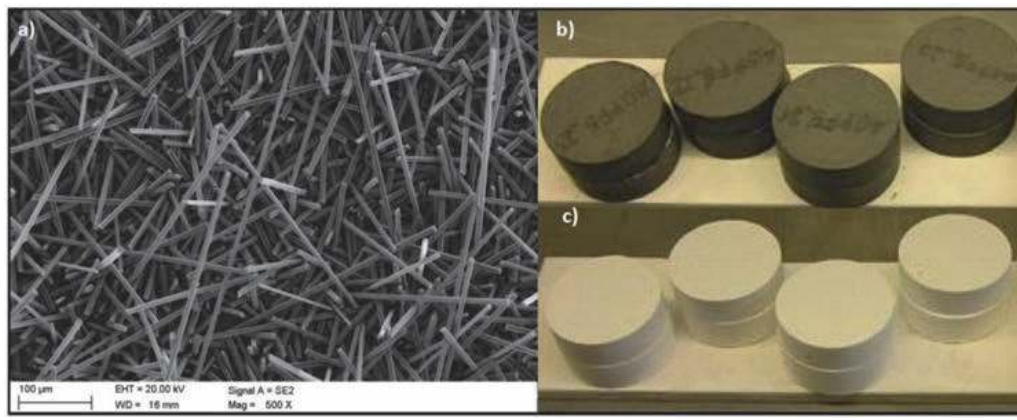

Figure 8.
(a) Morphology of Sigrafil C10 M250 UNS carbon fibers (SEM); (b, c) powder mix of aluminum oxide and carbon fibers (b) after pressing, (c) after sintering (macro).

suspension. To facilitate subsequent compression, 1% water-soluble polyvinyl alcohol Moviol 18–8 was added to the mixture. The powder was then dried by freezing and sublimating water under reduced pressure and sieved through a 0.25 mm sieve. The polyvinyl alcohol was activated after the powder was moistened with distilled water and left for 24 h in a polymer foil bag. Then the powders were pressed uniaxially in a die with a diameter of 30 mm on a manual laboratory press "Nelke" and in a rectangular die with dimensions of 65x46 mm on a hydraulic plate press Fontune TP 400 at a pressure 100MPa, for 15 seconds. The pressed preforms were sintered in Gero tubular furnace in an air atmosphere with a flow of 20 l/min, with slow heating up to 800°C at a rate of 20°C/h, heating for 10 hours for complete thermal degradation of carbon fibers, heating up to 1500°C at a rate of 300°C/h,

Diameter, μm	Average length, μm	Density, g/cm^3	Strength, GPa	Young's modulus, GPa	Carbon content, wt. %
8	135	1.75	2.5	26	>95

Table 9.
Properties of Sigrafil C10 M250 UNS carbon fibers.

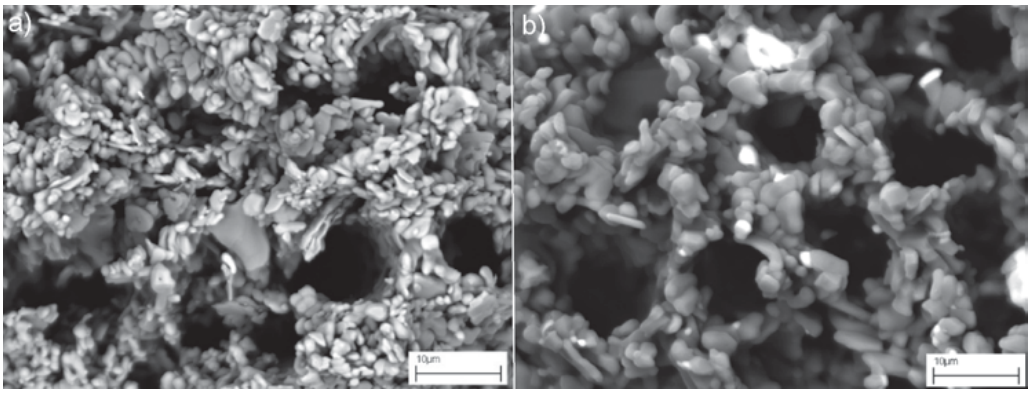

Figure 9.
The fracture's structure of the ceramic skeleton produced by sintering Al_2O_3 powder with (a) 30%; (b) 50% carbon fiber content.

sintering for 2 h and cooling with the furnace. The sintered skeletons show larger pores after the carbon fiber degradation and of much smaller dimensions around the individual ceramic particles that were intentionally not densified to the maximum extent (**Figure 9**). As a result, the created ceramic skeleton is characterized by a system of interconnected pores, ensuring high permeability of 2.48–10.56 $m^2 \cdot 10^{-13}$ and facilitates infiltration with liquid aluminum alloy.

Appropriate Al_2O_3 wettability by the liquid aluminum alloy was ensured by nickel coating the pores of the ceramic skeletons by using Atotech's Futuron technology (**Table 10**) used to make metallic coatings on polymeric materials to create a tin and palladium layer on the surface.

The solution of Noviganth Activator AK II ensures the exchange of tin on the surface with metallic palladium, after which it is possible to apply a layer of the Ni-P alloy by the chemical electroless method. The internal surfaces of the ceramic skeletons were coated using a solution pumping device which used a spiral cooler in the shape of a copper coil to ensure the required temperature. The sintered porous skeletons were glued with the two-component adhesive "UHU plus endfest 300" to the aluminum rings, which could be infiltrated with the liquid AlSi12 alloy after heating in a furnace at 800°C. The sintered ceramic skeleton in a matrix coated with graphite and heated to 450°C, was infiltrated by the AlSi12 liquid alloy at 800°C using a punch in a Fontune TP 400 hydraulic plate press with a pressing speed of 17 mm/s and a maximum press pressure of 100MPa for 120 s. They were removed from the mold and cooled with a stream of compressed air.

In the second case of the composite materials analyzed in this chapter, the ceramic porous skeleton, which is the reinforcement of the composite, was manufactured with the use of halloysite nanotubes (HNTs) by their mechanical milling, press consolidation, and sintering. HNTs are provided by NaturalNano (USA), and their phase composition is shown in **Table 11**. The nanotubes are obtained from halloysite, which is a clay mineral of volcanic origin, which is

Treatment	Reagent	Temperature, °C	Time, min
Surface activation	Futuron Activator	Room temperature	1
	Noviganth Activator AK II	40–45	3
Applying Ni-P coating by chemical electroless method	Noviganth PA Chemical Nickel	55	1.5

Table 10.
The course of coating Al_2O_3 ceramics with Ni-P alloy.

No.	Phase	Share, wt.%		
		Halloysite nanotubes	Halloysite nanotubes heated at 1100°C	Halloysite nanotubes heated at 1500°C
1	SiO_2	45.63	53.85	53.92
2	Al_2O_3	37.93	44.86	45.1
3	$Fe_2O_3^*$	0.46	0.58	0.59
4	TiO_2	0.11	0.16	0.13
5	CaO	0.01	0.02	0.01
6	MgO	0.07	0.09	0.1
7	K_2O	0.01	0.02	0.02
8	Na_2O	0.03	0.18	0.09
9	P_2O_3	0.35	0.42	0.41
10	Loss on the kiln at 1025°C	15.58	0.24	0.04

** Total Fe converted to Fe_2O_3.*

Table 11.
The phase composition of halloysite nanotubes provided by NaturalNano (USA).

characterized by high porosity, large specific surface, high ion exchange and easy chemical and mechanical processing. Halloysite is a mineral [$Al_2Si_2O_5$ $(OH)_4 \cdot H_2O$] that occurs in three deposits in the world, including in Poland. At least 30% of naturally occurring resources are in the form of nanotubes in the shape of polyhedron, hollow inside as cylindrical objects of the diameter 40–200 nm and length of up to 1–2 μm. After properly insulation HNTs can be used in nanotechnology. The morphology and particle size distribution of the powders used are shown in **Figure 10**.

For the manufacturing of porous ceramic skeletons, a mixture of halloysite powder with a mass fraction of 30, 40, 50, 60, or 70% by weight, respectively, was mechanically dry milled with Sigrafil CIO M250 UNS carbon fibers from SGL Carbon Group, analogous to that used in the previous case. Additionally, the MA7050 micronized amide wax powder with a mass fraction of 1% was used as a lubricant, also reducing the adhesion between the powder material and the mill and milling media, as well as leveling the friction between the die walls and powder particles. The technology of manufacturing the porous skeleton was very similar to that described in the 1st case. The milling of the mixture of the above-mentioned components was performed with the use of a Fritsch Pulverisette 6 centrifugal ball mill for 15 min.

The fragmented and homogeneous powder mixture obtained in this way was formed by uniaxial cold pressing in closed dies, respectively, of circular (φ30 mm)

or rectangular (12 × 35 mm) cross-section for 15 s on a LabEcon 600 Fontijne Grotnes hydraulic plate press. Preliminary tests allowed to set the pressing pressure as 50, 75, and 100 MPa. The degradation and sintering cycle of the moldings in the PRS 75 W high-temperature furnace by Czylok in the air atmosphere with the flow of 5 l/h was analogous to that in the first case, but the sintering temperature, determined on the basis of the analysis of the structure and mechanical and functional properties, is 1500°C for 1 h heating and an optimal share of HNTs of 70%. In this way, the structure of sintered porous mullite is obtained (**Figure 11**), which is subjected to pressure infiltration in the device shown schematically in **Figure 12** with the AlSi12 alloy.

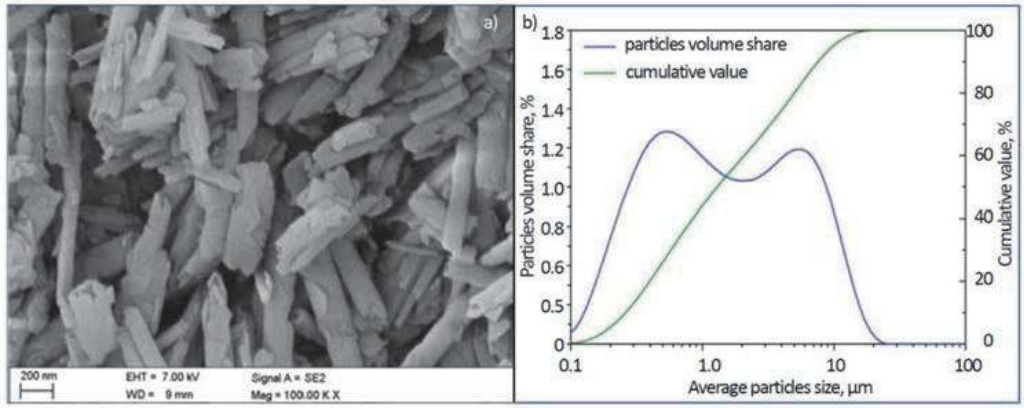

Figure 10.
Morphology of halloysite nanotubes (a) and particle size distribution (b).

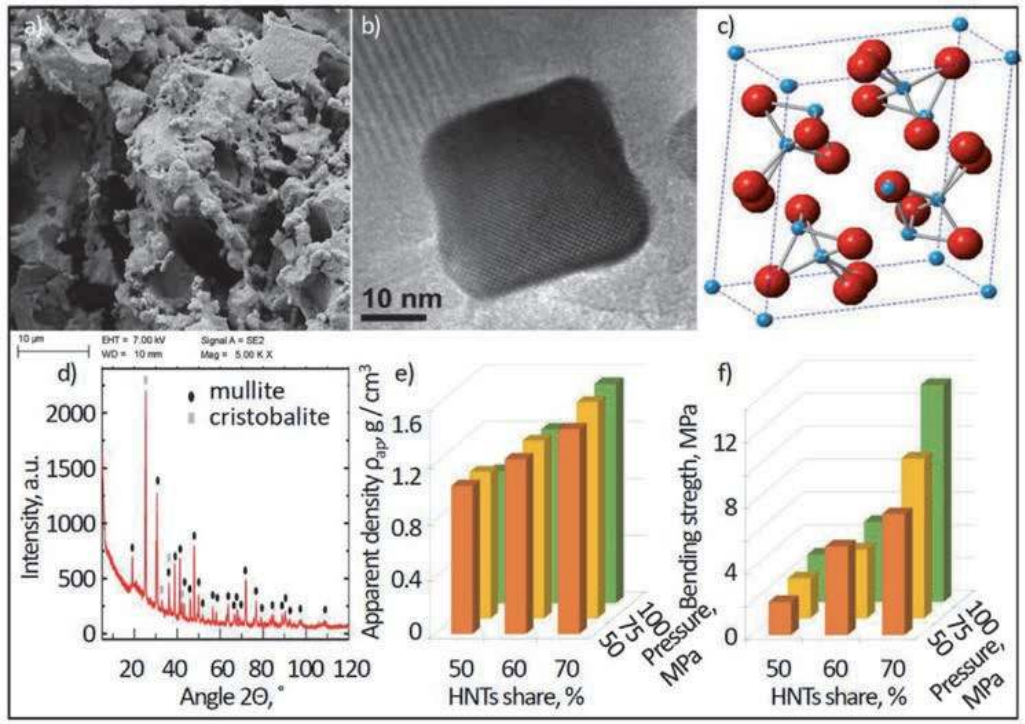

Figure 11.
Structure of the sintered skeletons (a) mullite with cristobalite nano-areas as confirmed by X-ray analysis (d); (b) nanoparticle of mullite (HRTEM); (c) mullite structure. (f) elementary crystallographic cell of mullite from fig. (b); (e), (f) influence of HNTs share and pressure on the apparent density (e) and bending strength of skeleton (f).

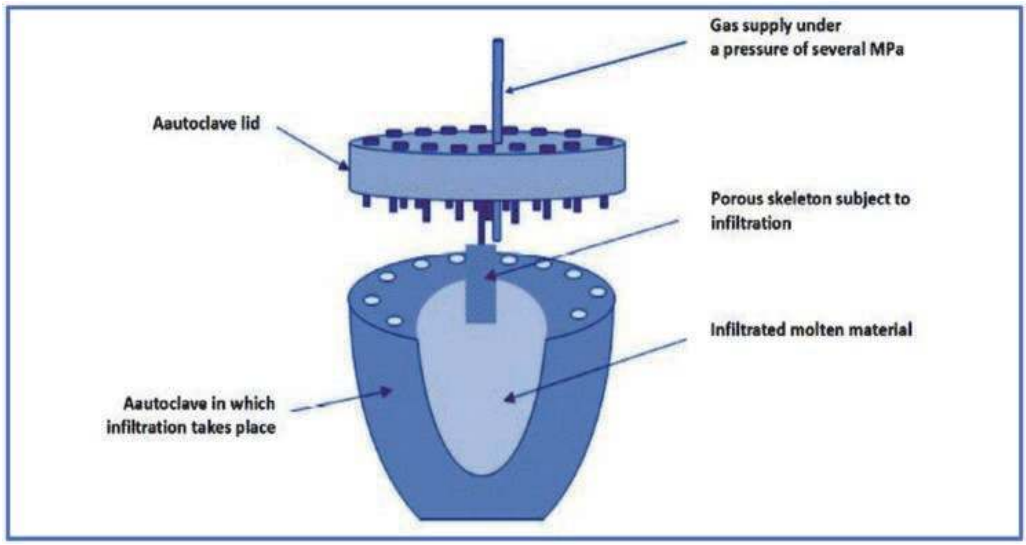

Figure 12.
Diagram of the infiltration device.

In the third and fourth cases of composite materials, selective laser sintering SLS was used for the manufacturing of a porous skeleton, divided into two main stages: design and manufacturing this skeleton (**Figure 13**).

In stage I, a given element is designed. The available specialized three-dimensional software allows for almost complete control and repeatability of the size and geometrical features of the designed elements, and also enables full control of the conditions of the manufacturing process. The design result is a three-dimensional computer-aided design CAD model in stereolithography STL format, showing the surface of the element by means of a triangle mesh. The smaller triangles are, the more precise the mapping of the surface is. By successively dividing the element into layers of a specific thickness, the optimal conditions for the manufacturing process are established, including laser power, scanning speed, layer thickness, distance between successive remelting paths, and the diameter of the laser beam. Software for Manufacturing Applications 3D Marcarm Engineering AutoFab, integrated with the Renishaw AM 125 machine, used for selective laser sintering, was used. The three-dimensional skeleton model was designed by CAD using unit cells of a defined structure and size and by subsequently multiplicating such unit cell to design a repetitive structure skeleton in which the pore size and wall thickness are fully designed by the designer, characterized by completely open pores.

On the basis of numerous technological experiments, the selection of "hexagon cross" unit cells (**Figure 14**) was made and the conditions for the manufacturing by selective laser sintering of porous titanium skeletons with a selected pore size of 250 μm (controlled unit cell dimensions 500 μm) and 350 μm (dimensions unit cell 600 μm). Experimentally, the relationship between the design arrangements and the actual pore dimensions was established (**Figure 15**).

After giving the model the appropriate size and structure, it is divided into layers with a predetermined thickness, with the number of layers corresponding to the number of layers of powder that will sinter until obtaining the accuracy of the model production depends on the laser power used: for low power 50 W it is ±20 μm in the XY plane, and for high power 200 W ± 100 μm in the XY plane with a layer thickness of 20 to 50 μm. Manufacturing conditions are transferred to the

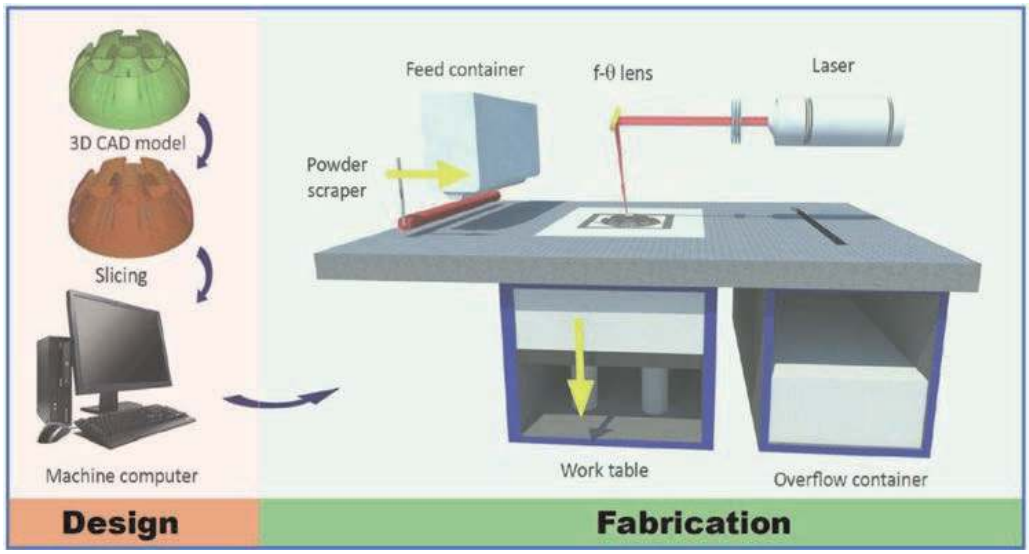

Figure 13.
Schematic diagram of the selective laser sintering technology.

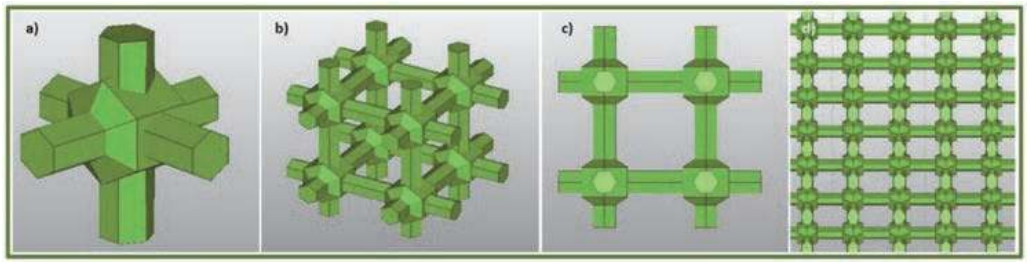

Figure 14.
(a-c) Basic hexagon cross unit cell, (d) computer model structure image showing the arrangement of unit cells at an angle of 45° to the x axis of the coordinate system.

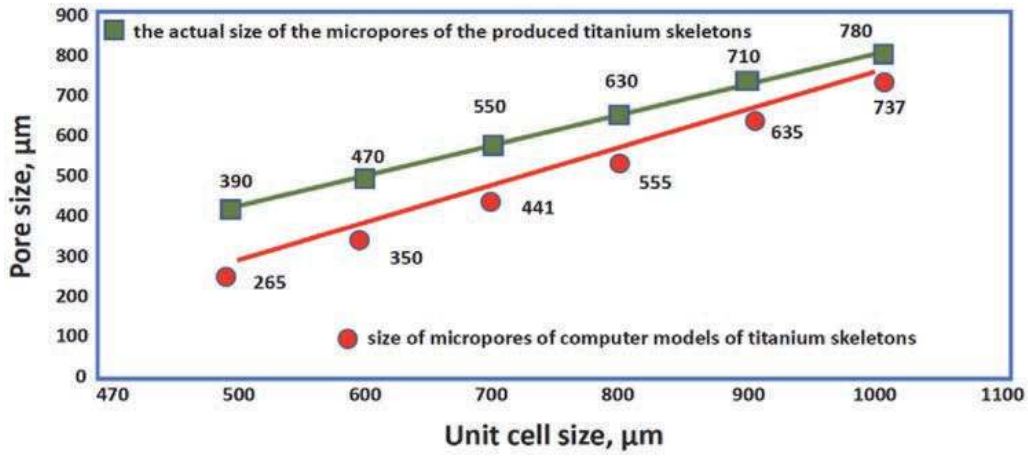

Figure 15.
Graph of the dependence of the pore size designed with the use of AutoFab software and titanium micro-skeletons produced by the selective laser sintering method on the size of the base unit cell.

designed model in STL format to the machine software for selective laser sintering. The most favorable properties of titanium skeletons with the given pore sizes are provided by the arrangement of unit cells at an angle of 45° to the x axis of the coordinate system (**Figure 11d**).

In the second stage, the previously designed element is manufactured by the method of selective laser sintering, layer by layer, until the final product is obtained. Selective laser sintering is a complex thermophysical process, the course of which depends on the type of material, the characteristics of the laser and the environment, and the thickness of the powder layer, as previously stated, as well as the diameter of the laser spot, the distance between the laser spots and the distance between the laser paths (**Figure 16**).

In the case of porous materials, the laser power of 60 W was selected and, in addition to the II laser path, the diameter of the spot was smaller than the distance between the laser spots, marked as laser path I. The AM 125 system uses a YFL fiber laser with ytterbium-doped active material and a maximum power of 200 W. The AM 125 system is equipped with a vacuum chamber, which allows the use of a unique method of emptying the working chamber of the device in such a way that all gases are first pumped out of the working chamber, and then an inert gas such as argon or nitrogen is introduced, providing an operating environment in which the oxygen concentration does not exceed 100 ppm.

The technology of selective laser sintering can be treated as a modern technology of powder engineering, where the process of building an element begins with the distribution of the powder layer on a working table with position adjustable in relation to the z-axis. This layer acts as a substrate for the created object. The laser beam is guided along the surface of the powder in accordance with the previously entered and appropriately configured information concerning the successive layers of the cross-section of the spatial image of the object. Next, the working table with the powder is lowered by the height (layer thickness) set by the user, another thin layer of powder is spread, where the grains sintering, which takes place by surface melting of another layer of metal powder grains with the previously sintered layers of the manufactured element. Whether the powder is sintered or fused depends on the manufacturing conditions. The process involves sintering with a liquid phase. Successive layers of the cross-section are sintered together. The process is repeated until a coherent element is obtained. After the construction is completed and the temperature is lowered, the element is removed from the powder bed and subjected to a finishing treatment, depending on the application, e.g. sandblasting or grinding. The AM 125 device has a powder container with automatic valves delivering an additional portion of the powder during the entire process, and its excess after the distribution of the next layer in the working chamber is drained to the container, which can be easily and quickly dismantled and placed at the powder sieving or

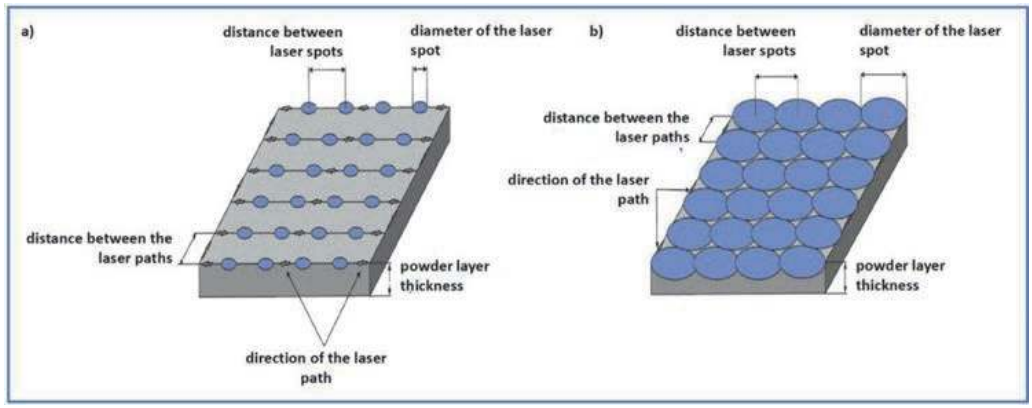

Figure 16.
Characteristics of a laser beam with a spot diameter: (a) smaller than the distance between the laser spots, (b) greater than the distance between the laser spots.

selection station thanks to which it is possible to reuse the powder in the next process.

For the production of porous titanium skeletons, titanium powder was used with the composition presented in **Table 12** with the purity grade 2 and the grain size up to 45 μm with a spherical shape. The powder used for the tests also has a reduced oxygen concentration down to 0.14% (in titanium powders the average oxygen concentration is about 0.5%).

The technology of selective laser sintering allows the production of microporous titanium skeletons with completely open pores, with the full possibility of controlling the shape and size of these pores, and also allows the production of elements of any designed shape, which makes it very competitive in relation to other material manufacturing technologies of porous materials.

The mechanical properties of selectively laser-sintered titanium micro-skeletons depend on the spatial orientation with respect to the main axes of the applied external stress, the assumed pore size, the laser power, the size of the laser spot, and the path of the laser spot. The best mechanical properties of 36 MPa (tensile strength), 97 MPa (bending strength), and 125 MPa (compressive strength) are obtained after selective laser sintering according to spatial orientation 45° in relation to the x-axis, with a laser spot width of 50 μm, laser power 60 W, an assumed porosity of 50–60%, corresponding to a pore size of 250 μm, for the course of a laser spot for which the distance between the laser spots and the laser remelting paths in relation to the diameter of the laser spot is equal to or smaller than the diameter of the laser spot. The lowest mechanical properties of 8 MPa (tensile strength), 15 MPa (flexural strength), 14 MPa (compressive strength), respectively, are ensured by the 45° orientation in relation to the y axis and 45° in relation to the x-axis for the same pore size ~250 μm. The smaller assumed pore size influences the greater the strength, and it varies from 8 MPa (tensile strength), 17 MPa (bending strength), 12 MPa (compressive strength) to 18 MPa, 43 MPa, 37 MPa, respectively, with a reduction the pore size from 450 μm to 250 μm. As the pore size decreases, the diameter of the laser spot also decreases from 90 to 50 μm, respectively, which helps to increase the strength. With the increase of the laser power from 50 W to 60 W, the mechanical properties increase, changing from 28 MPa (tensile strength), 72 MPa (bending strength), 74 MPa (compressive strength) to 36 MPa, 97 MPa, 125 MPa respectively. Using the same technological conditions for selective laser sintering, changing the ratio of the diameter of the laser spot to the value of the distance between the spots and paths of laser remelting from ≥1 to <1 results in more than double the strength of porous titanium.

The titanium porous elements after selective laser sintering were subjected to preliminary cleaning in isopropanol solution using an ultrasonic cleaner. After the excess powder was removed from the pores of the titanium skeleton, the specimens were digested with aqua regia for 1 hour using an ultrasonic bath to remove excess powder loosely attached to the titanium skeleton that had not been removed in the pre-treatment. Composite engineering materials, the model of which structure is shown in **Figure 14a**, were produced by pressure infiltration of microporous

Mass concentration of elements, %							
C	**O**	**N**	**H**	**Fe**	**Other**		**Ti**
					Each	**Together**	
0.01	0.14	0.01	0.004	0.03	<0.01	<0.4	rest

Table 12.
Chemical composition of titanium powder.

titanium skeletons produced by the selective laser sintering technology at a temperature of 800°C under a pressure of 2–3 MPa for 2 minutes in a manner analogous to the second case, using casting matrix material aluminum alloys, respectively AlSi12 in third case and AlSi7Mg0.3 in fourth case (**Figure 17**).

2.3 Manufacturing technologies by mechanical synthesis and subsequent plastic consolidation of aluminum alloy matrix composite materials

In cases 5 and 6, the composite materials were manufactured by mechanical synthesis and subsequent plastic consolidation of the mixture of aluminum alloy AlMg1SiCu powders as a matrix and reinforcement, respectively for variant 5 halloysite nanotubes HNTs as in variant 2 in the volume fraction of 5 to 15% and in the variant 6 multi-wall carbon nanotubes MWCNTs in the volume fraction of 0.5 to 5% (**Figure 18**).

By using the mechanical alloying method, it is possible to produce nanostructured composite materials with the controlled particle size of the reinforcing phase and their uniform distribution and resulting in increased mechanical properties. Air-atomized aluminum alloy powder with nominal particle size <63 μm was obtained from ECKA, Austria. Multiwalled carbon nanotubes MWCNTs with the properties given in **Table 13** were supplied by Cheap Tubes (USA).

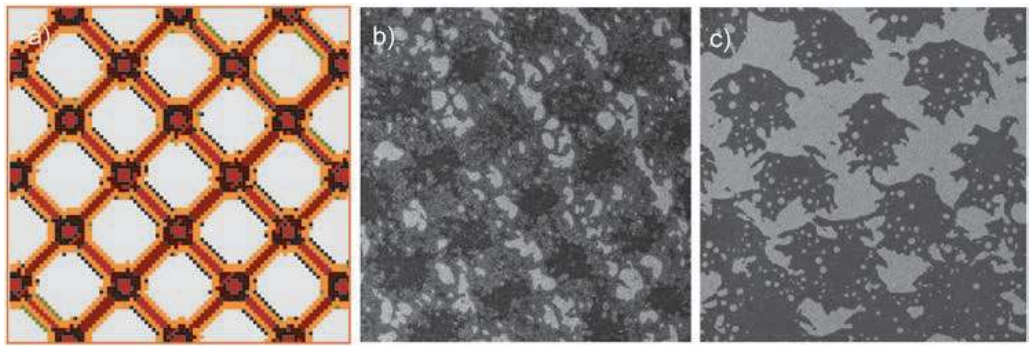

Figure 17.
Structure diagram of engineering composite materials with reinforcement of a titanium skeleton laser selectively sintered and pressure infiltrated with casting aluminum alloys; (a) diagram; (b) with AlSi12 matrix; (c) with AlSi7Mg0.3 matrix (b, c: SEM).

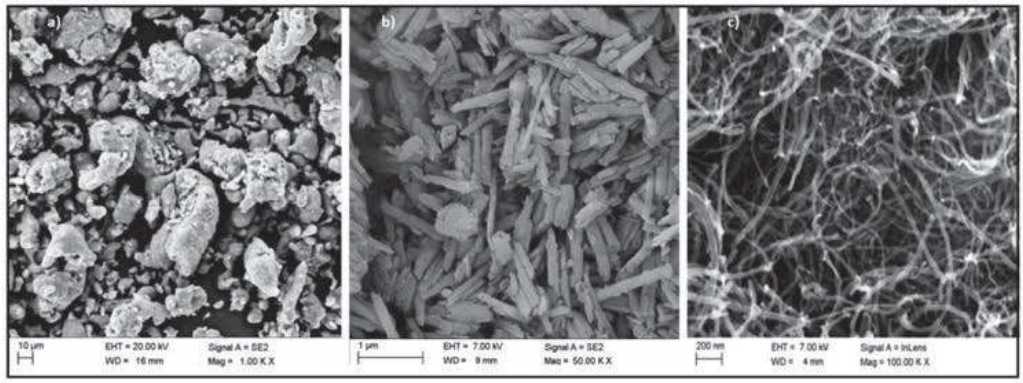

Figure 18.
Structure comparison in the delivered state; (a) AlMg1SiCu aluminum alloy powder; (b) halloysite nanotubes HNTs; (c) multi-wall carbon nanotubes MWCNTs (SEM).

As before, the lubricant MA7050 was used for all powders as a process control agent PCA reducing the adhesion between the feed and mill material with a mass fraction of 1%. The four stations planetary ball mill Pulverisette 5 by the Fritsch Company was used for mechanical synthesis using high energy mechanical milling for 0.5 to 20 hours at 200 rpm. Detailed conditions are given in **Table 14**.

In the case 5th, halloysite nanotubes had to be annealed prior to high-energy milling. A series of structural changes takes place in the halloysite, starting from dehydroxylation causing a metastable state, during heating of halloysite nanotubes at a temperature of ~100°C, associated with the 1st endothermic reaction consisting in the release of adsorption water (about 2% by weight), through the transformation into a regular spinel phase, in the temperature range of 400–600°C (peak at 548°C), when the 2nd endothermic reaction occurs, associated with hydroxylation (OH- ions in the octaendric layer are exchanged for O_2- ions (approx. 13% by mass), ending with the formation of mullite at a temperature close to 950°C as a result of an exothermic reaction associated with the reconstruction of the halloysite structure and the formation of the Si-Al spinel phase as a transition form [113–115] (15% by mass) [115]. These phenomena are confirmed by the thermogravimetric analysis (**Figure 19**) performed with the use of a corundum crucible in the range it is 20–1000°C in the air atmosphere to which 0.5018 g of halloysite nanotubes was subjected. The halloysite nanotubes used for the tests were therefore annealed at the temperature of 100, 500 or 700°C (HNT_{100}, HNT_{500} and HNT_{700}).

No.	Properties	Dimension	Value
1	Outer diameter	nm	20–30
2	Inner diameter	nm	5–10
3	Ash	wt. %	<1,5
4	Purity	wt. %	>95
5	Length	μm	10–30
6	Inner diameter	m^2/g	110
7	Electrical conductivity	S/cm	>100
8	Bulk density	g/cm^3	0.28
9	True density	g/cm^3	~2.1

Table 13.
Properties of multi-wall carbon nanotubes.

No.	Description	Reinforcement type	
		HNTs	MWCNTs
1	Reinforcement's concentration	5; 10; 15 wt.%	0.5; 2; 3.5; 5 wt.%
2	Time of milling	0.5; 1; 1.5; 2; 2.5; 3; 3.5; 4; 5; 6 h	0.5; 1; 1.5; 2; 3; 4; 5; 10; 15; 20 h
3	Ball material	AISI 420 quenched stainless steel	
4	Ball diameter	20 mm	
5	Ball-to-powder weight ratio	20:1	

Table 14.
Milling process parameters.

As a result of high-energy mechanical milling, crushed and permanently bonded composite powders were manufactured. Composite powders obtained as a result of high-energy mechanical milling were then cold pressed in a mold with a seat diameter of 26 mm and pressure of 300 MPa, and then pressed at a temperature of 460–500°C using a graphite suspension in oil as a lubricant, without degassing, in a cover made of AlMg1SiCu alloy. Co-extrusion of cold-pressed powders of rod-shaped composite materials consisted of placing the molded part in a thick-walled sleeve closed on one side by a punch, and on the other – by a die with a forming hole. At elevated temperature, under the pressure of the punch, the material was extruded through the die opening, obtaining a rod with a circular cross-section and a diameter of 8 mm in the case of using HNTs or 6 mm in the case of using MWCNTs, respectively.

2.4 Manufacturing technologies of the composite layers on the substrates of aluminum alloy

All other cases 7–12 concern composite layers of several millimeters obtained on the surface of casting aluminum alloys containing 3–10% magnesium. The desired composite layer of the tested aluminum alloys was obtained as a result of smelting the surface of the elements with the high-power HPDL ROFIN DL020 diode laser and fusing ceramic powders directly into the liquid metal pool using a gravity feeder (**Figure 20**). This laser is characterized by a very high beam power density, up to 107 W/cm^2, which means that the thermal impact on the surface of the element is limited, and thus causes only slight stresses and thermal deformations. The use of a diode laser for feathering ceramic powders into the surface layer of Al-Mg alloys allows for a predictable and repeatable way to obtain a composite layer on the surface of the analyzed aluminum alloys.

In order to minimize the power of the laser beam, shorten the time of the beam's impact on the surface and reduce the absorption of surface radiation, e.g. by grinding, anodizing, or tarnishing with the use of etching chemicals. The use of a flux, e.g. lithium chloride, is preferred. If this flux is not used, it would be necessary to reduce the scanning speed and increase the power of the laser beam, which results in increased linear energy and can lead to structure's changes in a larger volume of the material, making the technology less predictable and more difficult to control than with laser feathering using flux on surfaces of aluminum-magnesium alloys.

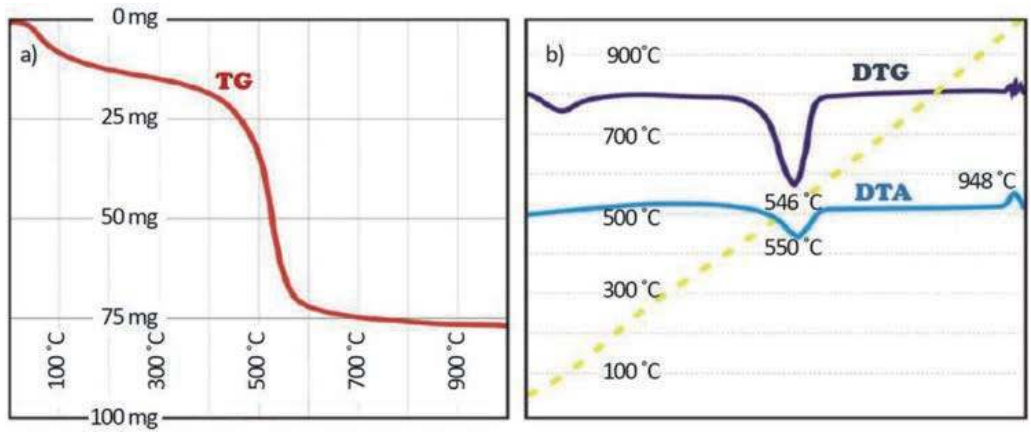

Figure 19.
Thermogravimetric curve of TG (a) and DTG and DTA (b) curves of halloysite nanotubes and the course of temperature changes during the tests (yellow dashed line).

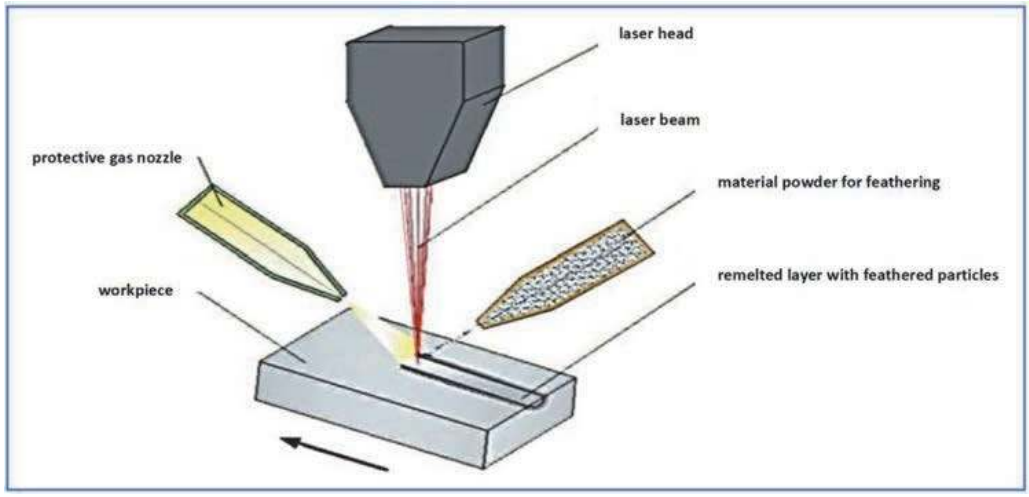

Figure 20.
Diagram of laser feathering of ceramic powder particles.

The purpose of selecting and optimizing the technological conditions of laser feathering is to produce a surface durable composite layer of aluminum with embedded carbides, characterized by a high coefficient of friction without the need for additional heat and surface treatment. The surface of the elements before laser feathering was mechanically processed by grinding with sandpaper with a gradation of 60 μm and then covered with a lithium chloride-based flux under the trade name "AluFlux". Lithium chloride powder was mixed with anhydrous ethyl alcohol in a ratio by volume of 1:5, resulting in a liquid suspension which was uniformly covered over the entire surface of the laser-processed part. The surface prepared in this way was dried for 30 minutes in a furnace at 50°C in order to evaporate the alcohol and moisture from the element surface. WC/W_2C and SiC powders were selected for laser surface treatment, taking into account the wettability of their powders (**Figure 21**). The conditions of the laser surface treatment, including the scanning speed and power of the laser beam, the method of powder feeding, and the shape of the laser spot, were determined on the basis of numerical calculations of the Finite Elements Method FEM computer simulation. In the numerical model, the laser beam power ranging from 0.5 to 2.5 kW, the beam scanning speed ranging from 0.2 to 0.8 mm/s, and the method of feeding the feathered powder through a paste consisting of a mixture of water glass and powder, milled on the surface of two or

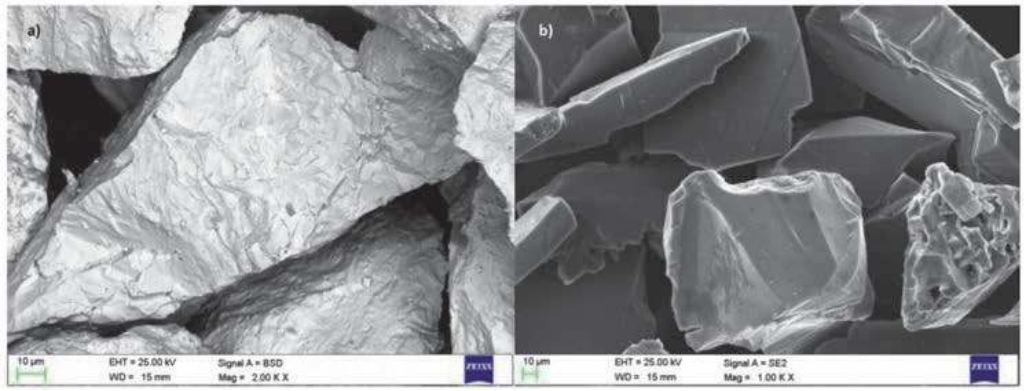

Figure 21.
Feathering powder of a) WC/W_2C tungsten carbide; b) SiC silicon carbide.

No.	Technical characteristic	Value	
1	Laser beam power, kW	1.8; 2.0; 2.2	
2	Laser beam scanning speed, m/min	0.5	
3	Spot size, mm	1.8 x 6.8	
4	Protective gas	Argon	
5	Protective gas flow, l/s	20	
6	Alloying powder	SiC	WC
7	Powder particle size, μm	45–180	45–180
8	The amount of powder fed, g/min	1	8
9	Theoretical powder density, g/cm^3	3.21	15.7
10	Melting point, °C	2730	2870

Table 15.
Technical conditions of the laser feathering process and general characteristics of the ceramic powders used.

three grooves with a depth of 0.5 and 1 mm and a gravity feeder with a speed depending on the density of the fed powder from 0.5 to 12 g/min. **Table 15** presents the decided experimental technical conditions of the laser feathering process and basic information on the ceramic powders used. The method of feeding the feathering particles into the area of the molten metal pool by means of a gravity feeder at a speed of 1 g/min for SiC and 8 g/min for WC/W_2C was selected. After the laser surface treatment, no other thermal or thermo-mechanical treatments were performed.

3. Structure and properties of the composite materials with aluminum alloys matrices taken into account in this chapter

3.1 Structure and properties of the composite materials with reinforcement in form of skeletons infiltrated with aluminum alloys matrices

In the first case of composite materials obtained by infiltration of porous skeletons, it is them that largely determine the properties. Pressure infiltration of porous skeletons with liquid metal alloys is increasingly used in the production of metal-matrix composite materials [116–140]. The benefits of using this technology include near-net-shape mapping and high surface quality, the possibility of local product strengthening and the use of a wide range of matrix and reinforcement materials, high efficiency also at mass production scale with relatively low production costs [87, 88, 141]. The interest in using aluminum oxide as the backbone of this group of materials has increased significantly in the current two decades [88, 141–145]. In the case of composite materials with reinforcement in the form of skeletons and an infiltrated matrix of aluminum alloys, a metal-ceramic connection also plays an important role due to the lack of wettability of aluminum oxide by aluminum alloys [82–84, 87, 88, 141–143, 146–154]. It has been improved by applying Ni-P coatings on Al_2O_3. A small proportion of pores with small dimensions ensures that after infiltration a density close to theoretical, which increases with the increase of the Al_2O_3 proportion. It was confirmed that composite materials with aluminum alloy matrix can be manufactured by pressure infiltration of porous ceramic skeletons made of a mixture of carbon fibers and Al_2O_3 particles, and the distribution of the

DOI: http://dx.doi.org/10.5772/intechopen.98677

reinforcing phase in the matrix is uniform. The infiltration is complete, and the fracture is mixed because the matrix is plastically deformed around the reinforcing phase, while at the metal-ceramic interface, the fracture is brittle (**Figure 22**). The Ni-P layer has a continuous structure with a thickness that does not clog the pores of the sintered ceramic skeletons.

The hardness of composite materials reinforced with porous skeletons made of Al_2O_3 particles increases with the increase in the proportion of the ceramic phase, obtaining 48.88 and 51.74 HRA, respectively, with a 30% share of reinforcement covered by Ni-P, and without it, which is more than 2.5 times increase in relation to the matrix with a hardness of 19.19 HRA (**Figure 23**). The tensile strength of the composite material reaches its maximum value with 25% reinforcement and amounts to 299.07 MPa and 320.14 MPa, respectively, in the case of the material with the reinforcement not covered or covered with Ni-P respectively. It proves the desirability of covering the internal surfaces of porous frameworks with a Ni-P layer in order to improve Al_2O_3 wettability by the liquid aluminum alloy and to improve the metal-ceramic bond.

The abrasion resistance of these composite materials increases with the increase in the proportion of the ceramic phase, and composite materials are characterized by much lower wear than their matrix, and the smallest of them is the material with a 25% ceramic phase (**Figure 23c**). Potentiodynamic studies confirm that the

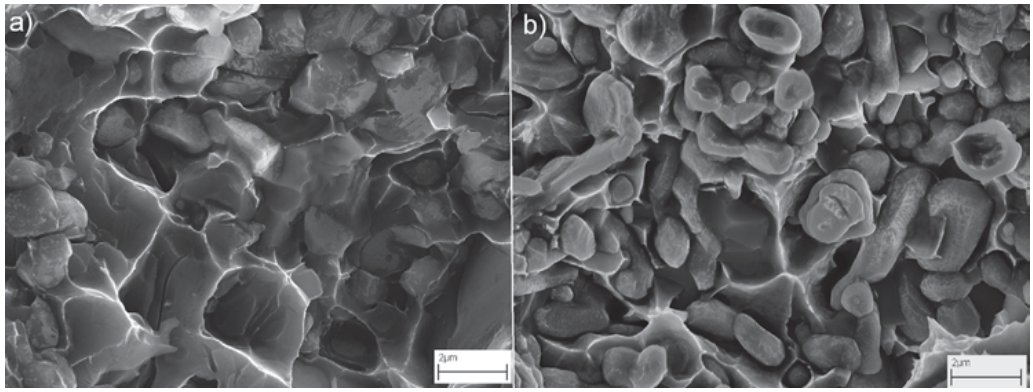

Figure 22.
The fracture's structure of the composite material a) without b) with an N-Pi layer on the Al_2O_3 skeleton.

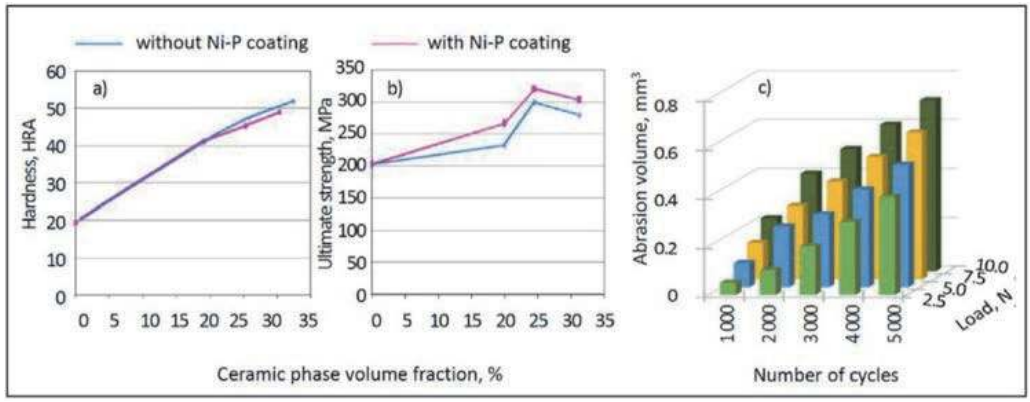

Figure 23.
Dependence of (a) hardness; (b) tensile strength from the proportion of Al_2O_3 reinforcement in the form of a porous sintered skeleton; (c) wear resistance with 30% Al_2O_3 reinforcement.

corrosion resistance of composite materials reinforced with ceramic skeletons in this way increases with the increase of the reinforcing phase. The presence of the Ni-P coating applied to the surface of the ceramic, however, promotes corrosion acceleration compared to the cases where this coating is absent, although the corrosion resistance also improves in these cases along with the increase in the proportion of the ceramic phase.

Composite materials reinforced with porous ceramic skeletons obtained from Al_2O_3 particles or fibers consisting in their pressure infiltration with liquid AlSi12 alloy constituting the matrix provides the required structure, as well as mechanical properties and wear resistance much more favorable than the aluminum alloy constituting the matrix.

In the second case, composite materials are manufacturing using liquid AlSi12 alloy for infiltration of the skeleton from sintered mineral nanotubes obtained from halloysite. Halloysite, like other secondary layered silicates, such as kaolinite or montmorillonite, and in general aluminosilicates or aluminum silicates, can be used to produce alternative reinforcement of composite materials with a matrix of light metals, especially aluminum, reinforced with ceramic particles [155–168]. These minerals can be used to produce mullite $3Al_2O_3{\cdot}2SiO_2$, among others by sintering, melting, or mechanical or chemical synthesis [169–173]. The mullite has good mechanical and physicochemical properties, meeting the requirements for porous skeletons as reinforcement for composite materials [174–177]. The porous skeletons produced in this way are an alternative to preforms commonly used for the production of composites based on aluminum alloys by infiltration methods, which are ceramic skeletons or foams formed from particles or short fibers, with high porosity 60–90% [119, 163, 177–189]. They replace the particles of oxides, carbides, nitrides, graphite, carbon, boron, glass, Al_2O_3 and SiC fibers, intermetallic phases used in their production; fly ash microspheres and microgranules; Al_2O_3, SiC, SiO_2 nanotubes; multi-walled carbon nanotubes, graphene and most often SiC and Al_2O_3 fibers. For economic reasons, it is beneficial to replace Al_2O_3 fibers with particles, which also increases the strength of infiltrated materials by approx. 35%, despite a slight reduction in abrasion resistance [84, 86, 87, 106, 148]. Halloysite in the form of NHTs can be an alternative for both economic and mechanical properties reasons. Among the sintered, porous ceramic skeleton, it is most preferable to sinter HNTs at 1500°C with the share of 70% HNTs, while the differentiation of the pressing pressure in the range of 50 to 100 MPa is of little importance (compare **Figure 19**). All composite materials analyzed here are characterized by an infiltrated structure with complete filling of the pores of the ceramic skeleton with the matrix alloy and good adhesion at the phase boundary of the ceramic reinforcement and the metallic matrix (**Figure 24**).

Composite materials manufactured according to the technology described as the second case are characterized by a structure of evenly interpenetrating phases with a contrasting structure. The matrix material is an α-solution with numerous precipitates of the coarse-crystalline β phase and fine precipitates of the iron-rich phase, while the reinforcement is an evenly distributed, continuous mineral phase in the form of irregularly shaped mullite. The strengthening of the above-mentioned composites in the form of fine-grained mullite and cristobalite occurs as a result of sintering mineral nanotubes and the accompanying series of structural changes. The gas-pressure infiltration of these ceramic skeletons leads to the diffusion dissolution of the cristobalite formed during sintering in the liquid aluminum alloy. As a result, the excess of silicon in the liquid solution crystallizes in the form of coarse precipitates, analogous to hypereutectoid Al-Si alloys. The relatively short infiltration time does not affect the dissolution of mullite in the liquid solution. The mechanical and functional properties of the discussed composite materials with

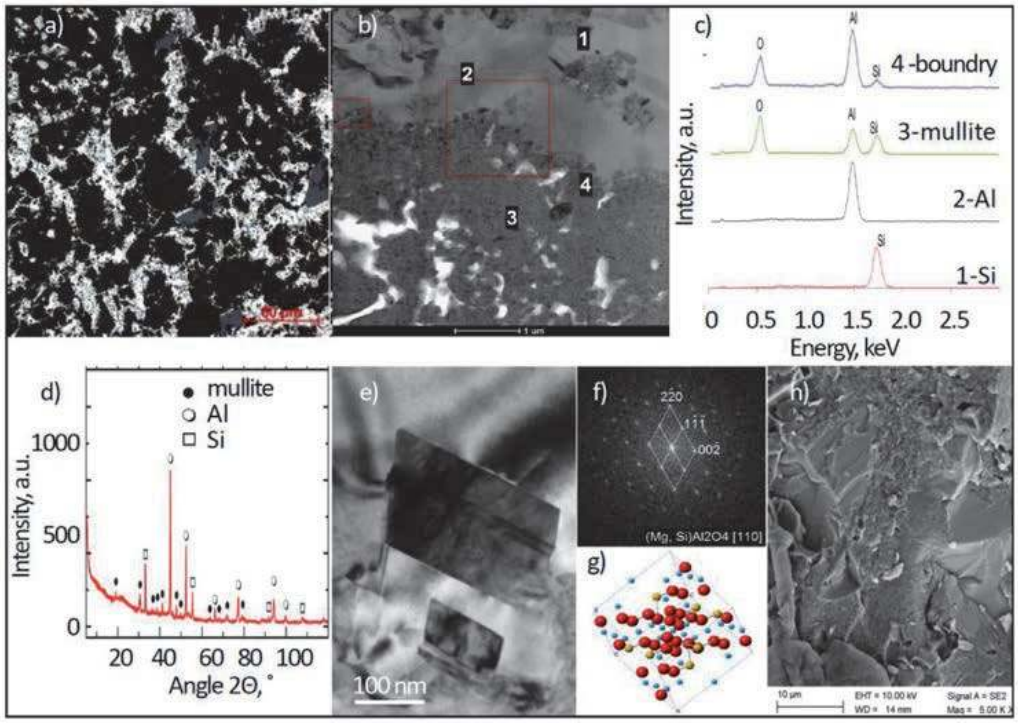

Figure 24.
Structure (a) of composite material with Al12Si matrix with reinforcement of sintered HNTs in 70% share; (a) light microscope; (b) structure of intermediate zone between the reinforcement and the matrix with marked points of analysis by EDS method (SEM); (c) results of the local EDS analysis; (d) X-ray analysis of the surface of the composite material; (e) thin foil structure in the intermediate zone between ceramic and metal (HRTEM); (f) solution of the FFT of the nano diffraction from the area (e); (g) $MgAl_2O_4$ unit cell model; (h) fracture morphology of the composite material with 70% HNTs after the bending test (SEM).

HNTs reinforcement are the best in the case of sintering ceramic skeletons at 1500°C and at 70% HNTs (**Figure 25**).

The mentioned technology enables the manufacturing of composite materials with enhanced mechanical properties and wears resistance, significantly exceeding the functional properties of the alloy used as a matrix, providing the prospect of their implementation on structural elements, e.g. in the aviation and automotive industries.

The third and fourth cases of composite materials concern the use of microporous titanium skeletons manufactured by selective laser sintering with an adjustable pore size and their controlled spatial orientation as reinforcement, manufactured by pressure infiltration with liquid alloys AlSi12 or AlSi7Mg0.3, respectively.

Additive technologies have found a very wide application in numerous industries, including military, automotive, aviation, machine, household goods, but also in medicine, both for the production of solid and porous elements [128, 190–218]. Porous materials produced with this technology can be used as skeletons for the production of infiltrated composite materials with a matrix of aluminum alloys. The structure of these composite materials with aluminum alloys matrix and titanium skeleton reinforcement manufactured by additive technology does not contain any local voids and pores. It is made of a matrix corresponding to the chemical composition of the alloys used, respectively, AlSi12 or AlSi7Mg0.3 (**Figure 26**) inside the pores of a titanium skeleton with a size of 250–350 μm, which is a reinforcement with a shoulder thickness of 200–300 μm depending on the sintering conditions. The matrix and reinforcement composition was confirmed by X-ray diffraction (**Figure 26i-k**). The results of the X-ray diffraction tests of the structure AlSi12/Ti

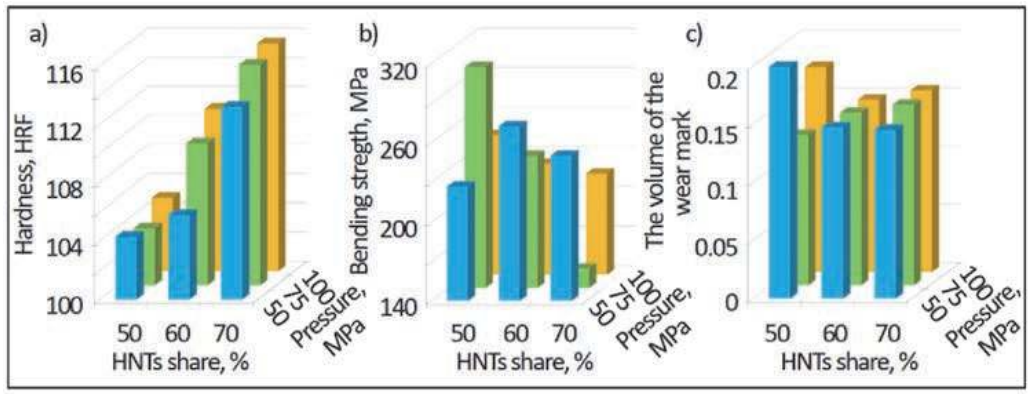

Figure 25.
The relationship of (a) hardness, (b) bending strength, (c) the volume of the wear mark on the share of HNTs and compaction pressure.

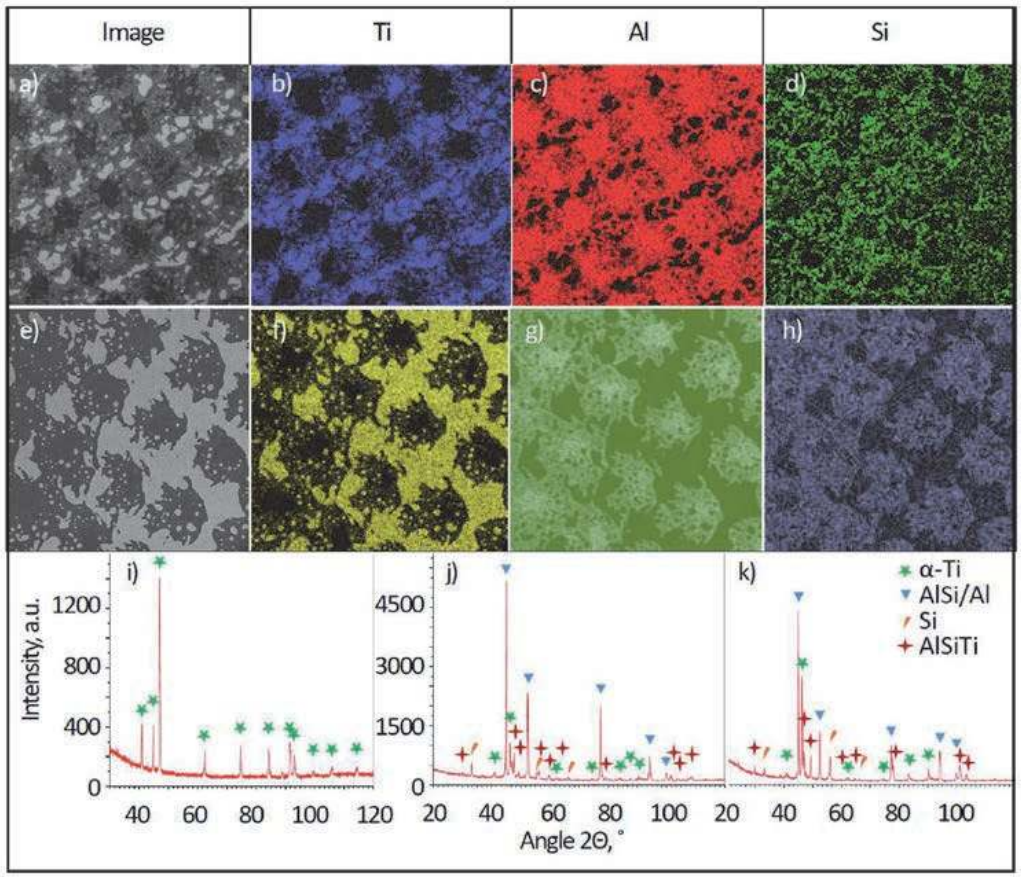

Figure 26.
The structure of the surface layer of the composite material with the reinforcement in the form of a titanium skeleton manufactured by selective laser sintering SLS and a matrix made of aluminum alloy: (a-d) AlSi12, (e-h) AlSi7Mg0.3; (a, e) SEM; (b-d, f-h) surface distribution of elements: (b, f) Ti, (c, g) Al, (d, h) Si; (i-k) X-ray diffraction from the (e) image; (i) Ti skeleton; (j, k) composite materials with the matrix (j) AlSi12; (k) AlSi7Mg0.3.

(**Figure 26j**) and AlSi7Mg0.3/Ti (**Figure 26k**) composite materials show that during infiltration, phases with the participation of individual elements of the composite material, such as Al, Si, may be formed as well as Ti, AlSi and the AlSiTi phase. The AlSiTi phase is formed in the area between the matrix material and the

DOI: http://dx.doi.org/10.5772/intechopen.98677

reinforcement (**Figure 27**), and its chemical composition differs from that of the reinforcement and the matrix, as Al, Ti, and Si were identified in the qualitative and quantitative EDS method. In the matrix material, Mg, Cu, Ni can also be identified, the concentration of which in the matrix is less than 1%.

The mechanical properties of pressure-infiltrated composite materials with a matrix of selected aluminum AlSi12 or AlSi7Mg0.3 casting alloys (**Figure 28**) depend on the spatial orientation with respect to the main axes of the titanium micro-skeleton produced by selective laser sintering, the size of the pores in the micro-skeleton and the sintering conditions, especially laser power and the size of the laser spot. The bending strength is 280–430 MPa, and the compressive strength is 480–600 MPa. The most advantageous mechanical properties: bending strength of 430 MPa and compressive strength of 600 MPa, these composite materials obtain after laser sintering of the skeleton with a laser power of 60 W, with a laser spot

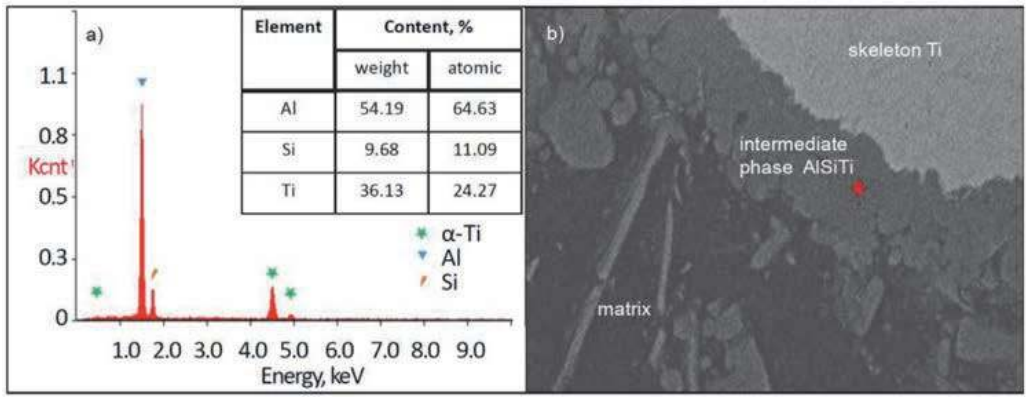

Figure 27.
The structure of the AlSi7Mg0.3/Ti composite material (SEM) (b) and the scattered X-ray energy diagram and the results of the quantitative analysis of the chemical composition of the AlSiTi phase of the place marked with a red cross (a).

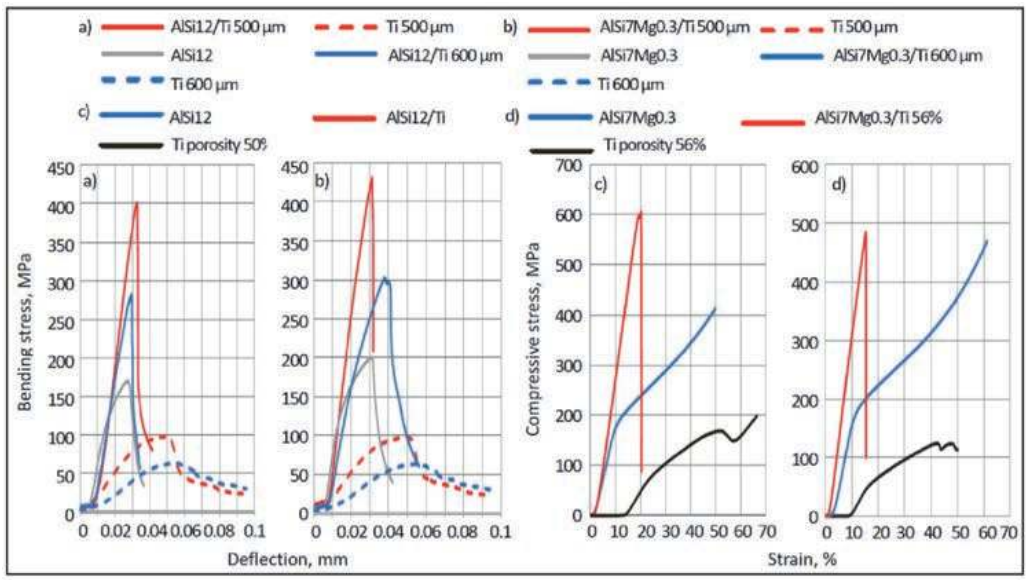

Figure 28.
Diagrams of the dependence of bending stress on deflection (a, b) and compressive stress on deformation (c, d) for the AlSi12 alloy, titanium skeleton and AlSi12/Ti composite material (a, c) and AlSi7Mg0.3 alloy, titanium skeleton and composite material AlSi7Mg0.3/Ti (b, d) with pore sizes of 500 or 600 μm (a, b) or with a porosity of 50% (c) and 56% (d), respectively.

with a diameter of 50 μm, the distance between the laser spots and between laser remelting paths equal or smaller than the diameter of the laser spot when the spatial orientation is 45° to the x-axis and if the pore size is 200–250 μm with a porosity of approx. 50–60%.

Therefore, reinforcing the aluminum alloy with porous titanium skeletons has a positive effect on the mechanical properties of the analyzed composite materials. The AlSi12 alloy is characterized by a bending strength of about 170 MPa, while in the case of the AlSi12/Ti composite material, the maximum bending strength was obtained using a titanium skeleton with a porosity of 56%, obtaining a bending strength of about 400 MPa, and with a titanium skeleton with a porosity of 66%. strength of about 280 MPa was obtained. The strength of the AlSi12/Ti composite material compared to the strength of solid titanium (1682 MPa) is more than four times lower, however, compared to the strength of the AlSi12 alloy itself, it increases twice. The use of a titanium skeleton with lower porosity, i.e. a skeleton of greater strength, in the composite material with the AlSi12 alloy matrix, increases the bending strength by about 230 MPa compared to the matrix material, while when the skeleton with lower strength and higher porosity is used, the increase in bending strength is not so significant at about 110 MPa compared to the matrix material. In the case of a composite material with the AlSi7Mg0.3 matrix with the use of titanium skeletons, the increase in bending strength compared to the matrix material is approximately 100 and 130 MPa, respectively. When the same titanium skeletons and different matrix materials are used, the matrix bending strength has a dominant effect on the bending strength of composite materials, while if the same matrix materials are used, the strength of the composite material is mainly determined by the strength of the titanium matrix.

The comparison of the fracture structure of the aluminum alloys constituting the matrix of the composite materials discussed with the fracture structure of the composite material after bending tests shows significant differences. The breakthroughs of aluminum alloys are flat, with visible planes along which the material cracked, while in the case of composite materials, places characteristic of titanium are distinguished (**Figure 29**). The studies of the breakthrough of the AlSi12/Ti and AlSi7Mg0.3/Ti composite materials indicate that the combination of titanium and aluminum alloys is durable and does not break when the bending force is applied. The structure of the breakthroughs after the compression test is significantly different from the breakthroughs after bending. After the compression test, such a clear separation of the matrix material from the reinforcement material cannot be noticed, which is so clearly visible in the structure of breakthroughs after bending.

Micro-skeletal composite materials, manufactured by pressure infiltration with selected aluminum casting alloys AlSi12 or AlSi7Mg0.3 to give the final shape and geometric form, dedicated, among others for the automotive, machine-building, and aerospace industries, as well as for medical and dental applications.

3.2 Structure and properties of the aluminum alloy matrix composite materials manufactured by mechanical synthesis and subsequent plastic consolidation

In cases 5 and 6 for mechanical synthesis of the composite materials in a planetary mill (the so-called high-energy process) of AlMg1SiCu alloy powder and respectively nanotubes obtained from halloysite or MWCNTs carbon nanotubes, was used to produce the composite materials. In the initial stage of mechanical synthesis, the originally spherical particles are deformed, flattened, and have a lamellar shape. After 5 hours of mechanical milling, it was found out that most of the particles were equiaxed with no flake shaped particles present. Changes in the

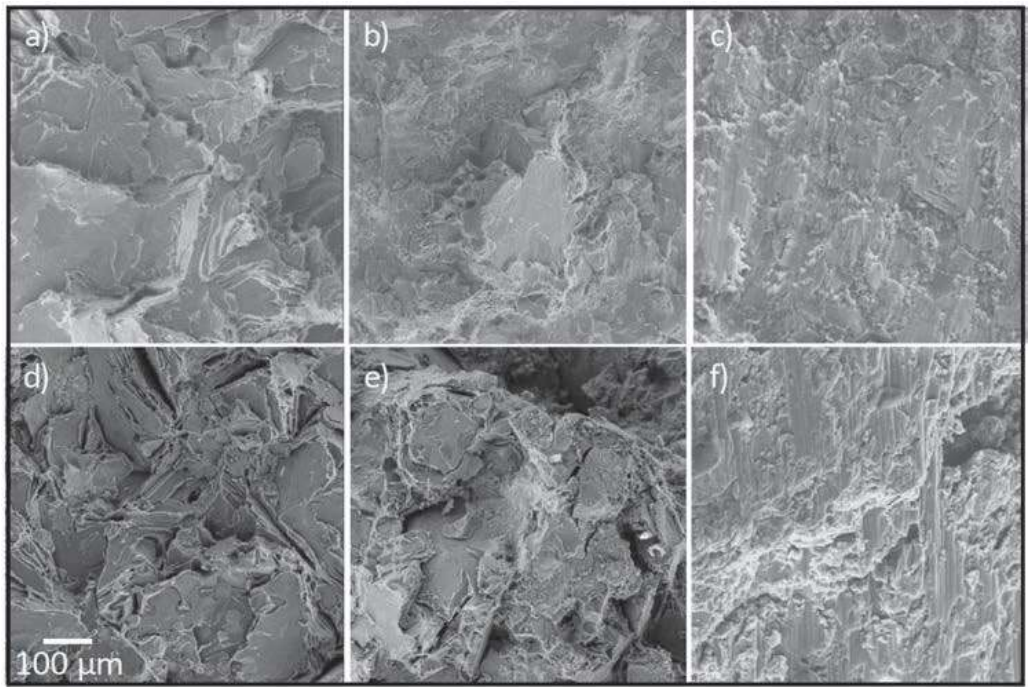

Figure 29.
Breakthrough structure (a) AlSi12 alloy; (d) AlSi7Mg0.3 alloy; and composite materials based on (b, c) AlSi12 alloy; (e, f) an AlSi7Mg0.3 alloy; after tests; (a, b, d, e) of static bending; (c, f) static compression.

shape and size of the milled powders are caused by the welding of individual particles as a result of collisions with the milling media or the walls of the mill. The flattened particle conglomerates formed as a result of welding become significantly hardened, hard, and therefore prone to cracking. As the milling progresses, these particles become fragmented and reassembled, which ultimately affects the random orientation of the boundaries of the particles to be welded. The fact that the process has reached a steady-state is provided by the relatively equiaxial shape of the milled powder particles. In contrast to the milled powder of the AlMg1SiCu alloy, in the case of the powder of the composite material, it was found out that the deformed particles joined tightly, creating a morphologically homogeneous structure, free of pores and discontinuities. Despite the twice longer milling time, the powder of the AlMg1SiCu alloy consists of fine particles, which to a large extent form porous conglomerates with irregular, non-aligned shapes and sizes varying in a wide range from 10 to 200 μm. Extending the milling time results in a homogeneous distribution of the reinforcing particles, and it is also possible to produce powders with equiaxed particles. The influence of the presence of reinforcement subject to fracture under the conditions of mechanical alloying of the ductile aluminum matrix is given in the diagram of the successive stages during mechanical alloying (**Figure 30**). The examples of the corresponding structure for the case respectively 5 and 6 are given in **Figure 31**. Examples of correctly and incorrectly made rods in the stage of plastic consolidation are shown in **Figure 32**.

In the case of 5th, the composite materials with the AlMg1SiCu matrix are reinforced with nanotubes obtained from halloysite. The use of HNTs particles reduces the bulk density of the mixture with the matrix powder of the AlMg1SiCu alloy even by more than 50%, and this effect becomes present with the increase in the proportion of the reinforcing phase. Reinforcement material particles are characterized by a larger specific surface, irregular, often oblong shape, and form porous conglomerates, thus characterized by a much lower bulk density compared to globular AlMg1SiCu particles. In the case of mechanical milling of a plastic

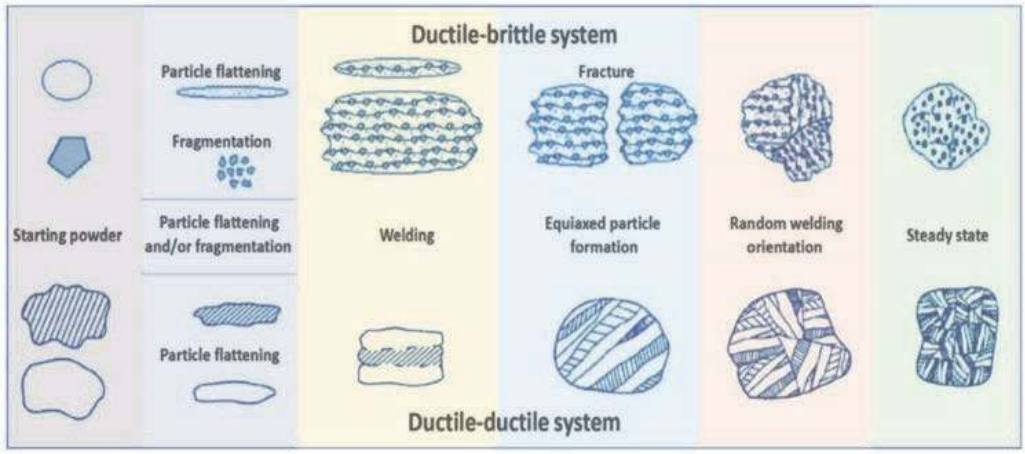

Figure 30.
Diagram of the successive stages of the ductile-brittle/ductile-ductile systems during mechanical alloying.

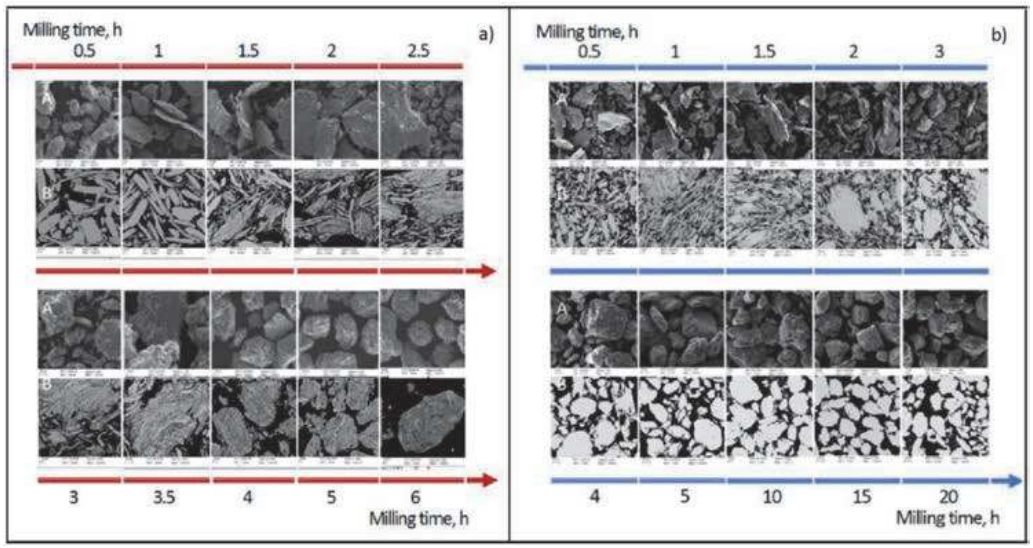

Figure 31.
Morphology (A), structure (B) after high-energy mechanical milling of a powder mixture of AlMg1SiCu alloy with (a) 15% of halloysite nanotubes (red) or (b) 2% MWCNTs carbon nanotubes (blue) respectively in the range of (a) 0.5–6 h or (b) 0.5–20 h.

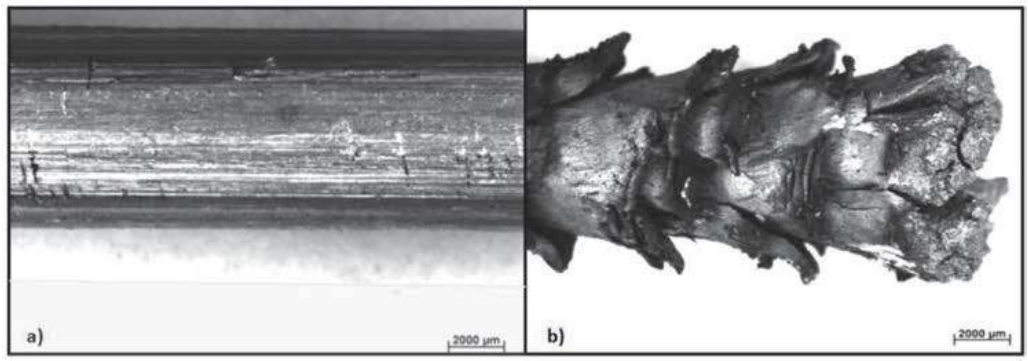

Figure 32.
Exemplary view of bars containing AlMg1SiCu alloy with (a) 5% and (b) 2% of multi-wall carbon nanotubes MWCNTs extruded at 460°C (a) and 500°C (b).

powder of an aluminum alloy with a brittle reinforcing phase in the form of halloysite nanotubes with a mass fraction of 15%, the increase of the bulk density takes place in 2 times shorter time than in the case of matrix powder. As a result of high energy milling, an equiaxial shape of the particles is obtained and an even distribution of fine reinforcing particles confirming that the process has reached a steady state. Further milling does not significantly affect the obtained structure and properties of the powders. In the initial stage, the particle size distribution is characterized by two peaks (**Figure 33**), because the tested powders are a mixture of particles with a significant difference in size (the aluminum alloy powder has a median of 62.30 μm, and halloysite nanotubes – 2.58 μm). The particle size of the powders undergoes continuous, non-linear changes during milling. As the milling time increases, the deformed particles are joined together and the peak on the particle size distribution curve becomes wider at the base, and then with the increase of the milling time and the associated increase in the proportion of large particles resulting from repeated welding, an asymmetric deviation is achieved. Due to the breakage of large particles, the asymmetry that has arisen gradually disappears. Eventually, the process reaches a steady state, corresponding to a balance between the powder particle aggregation and fragmentation mechanisms, which is represented by symmetrical or a narrow particle size distribution curve (**Figure 33**).

Mechanical synthesis, in addition to the effect on the morphology and structure of the manufactured composite powders, also affects their phase composition, and increasing the milling time also affects the generation of a large number of defects and results in the fragmentation of the crystal structure [219–221]. Already after several minutes of milling, low-angle reflections from mineral halloysite crystals disappear, leaving only reflections identified as α-Al on the diffraction patterns. Structural changes occur during annealing of halloysite [169, 222–226]. The interplanar distance of all halloysite powders is 0.72 nm, which proves permanent dehydration [113, 114]. Annealing of halloysite nanotubes at the temperature of 500–700°C causes disorder of their crystal structure, which with increasing temperature causes amorphization of halloysite as a result of disordering the packet structure [227–230]. Mechanical high energy milling improves the distribution of HNT_{100} reinforcement particles in the AlMg1SiCu matrix, more advantageously than when using HNT_{500} and HNT_{700}. With a short milling time, this ensures a homogeneous structure of the nanocomposite material with an even distribution of reinforcing particles without their agglomeration after consolidation. The consolidation of powders consists in their successive cold pressing and hot extrusion, resulting in a lack of discontinuities of the structure in the form of pores or cracks and obtaining a material with a very fine structure (**Figure 34a**), devoid of agglomerates of reinforcing particles. In the produced material, there are grains with a size of several nanometers (**Figure 34b-d**) in the structure of the solid

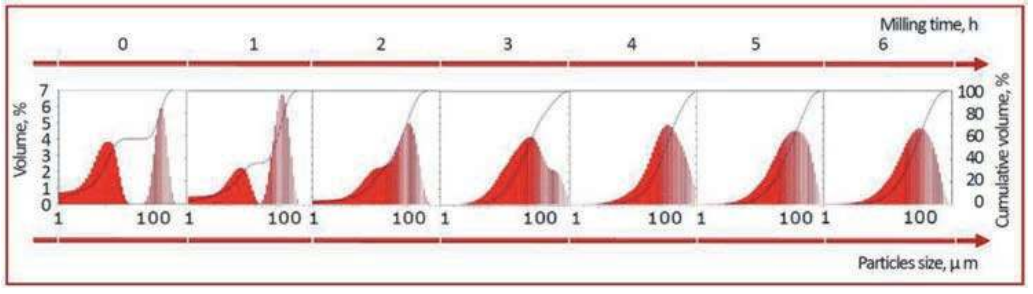

Figure 33.
Relationship between the size of the mixture of AlMg1SiCu particles and HNT_{100} halloysite nanotubes in a share of 10% from the time of high-energy milling.

solution of the AlMg1SiCu alloy in a metastable state (**Figure 34e-h**). There are also many regular, parallel, rhomboidal regions not exceeding a few nanometers (**Figure 34e**), which most likely constitute the Guinier–Preston zones with the concentration of Cu atoms [1, 231–233].

Based on the results of the X-ray phase analysis, the presence of only the matrix phase in the analyzed composite materials, i.e. solid aluminum solution (**Figure 35**).

In addition to the nanometric grains of the Alα solution (**Figure 36a**) in the matrix, there are precipitations of the Al_2O_5Si phase (**Figure 36b**) probably formed during mechanical milling and the intermetallic primary phases $AlFe_3$ and Al_4 (Fe, Cr, Mn) $Si_{0.74}$ (**Figure 36c**) [234].

The high degree of plastic deformation caused by mechanical milling, nanometric fragmentation of the structure, and dispersion hardening with particles

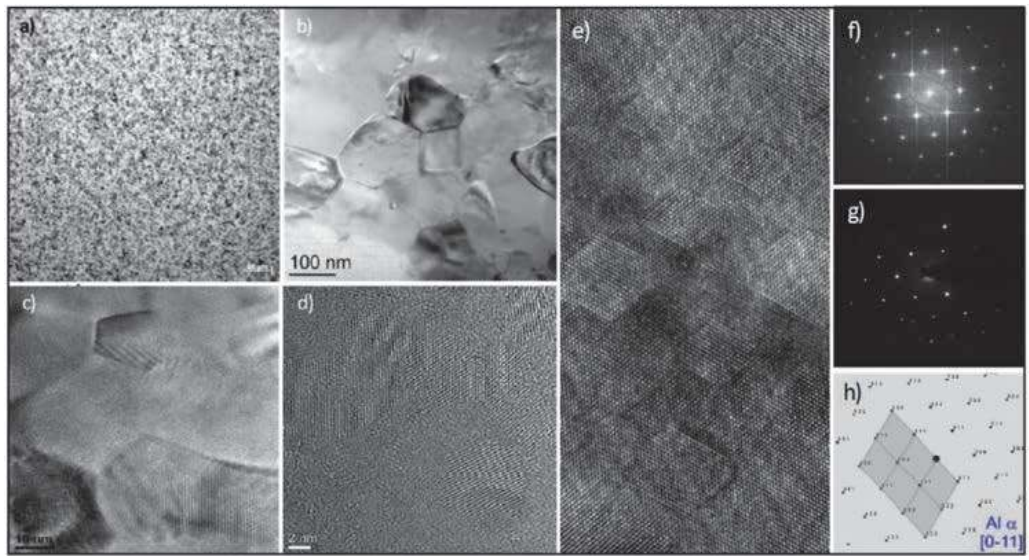

Figure 34.
The structure of the nanocomposite with AlMg1SiCu matrix with the share of 15% HNTs: (a) uniform structure (light microscope); (b-d) very fine grains matrix structure (HRTEM); (e) rhomboidal nanostructured regions in the matrix (HRTEM); (f) Fourier transform; (g) nano diffraction; (h) solution of the diffraction pattern from Figure e.

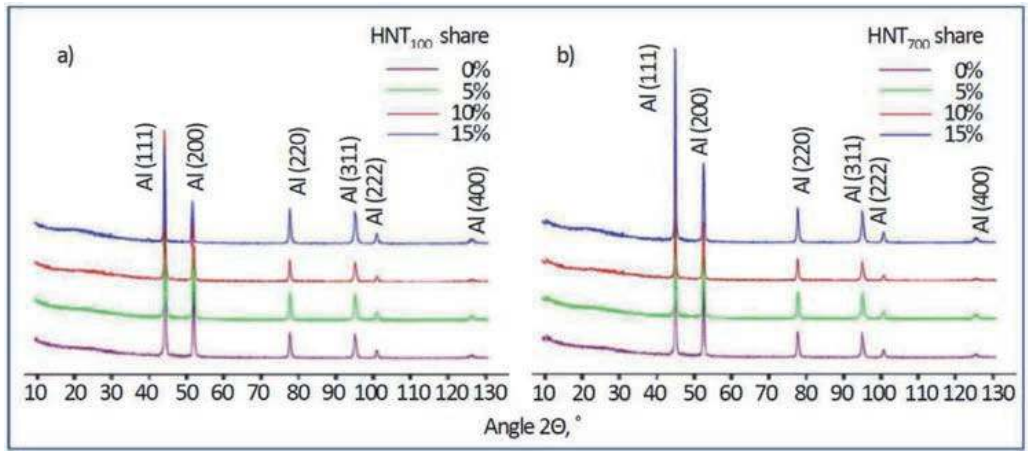

Figure 35.
Results of X-ray diffraction analysis using a Cu lamp of AlMg1SiCu alloy powders and high energetic milled nanocomposite materials with a matrix of this alloy with the participation of 5, 10, or 15% strengthening with halloysite nanotubes, respectively (a) HNT_{100}; (b) HN_{700}.

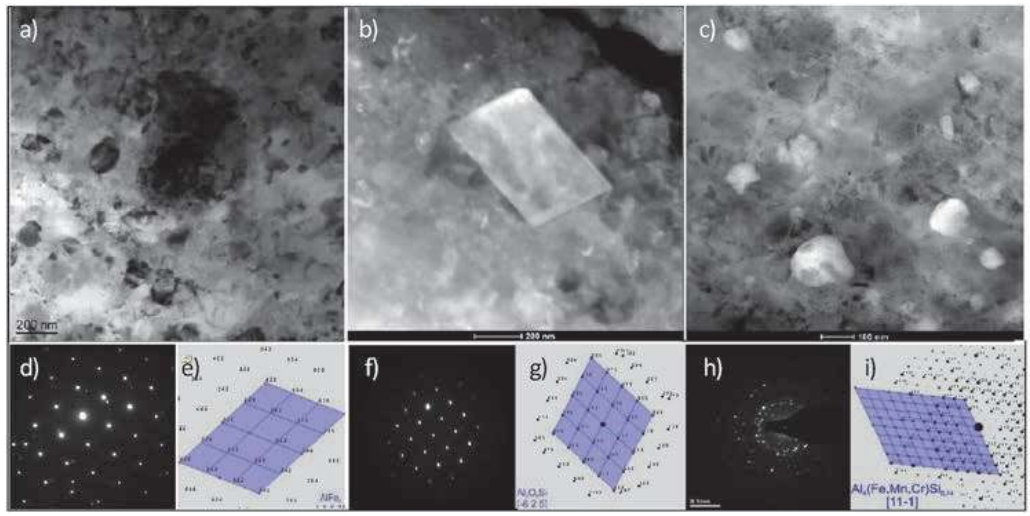

Figure 36.
The structure of nanocomposite with AlMg1SiCu matrix with 15% HNTs (TEM): (a) nanometric grains of Alα solution; (b) Al_2O_5Si phase precipitations probably during mechanical milling; (c) intermetallic primary phases Al_4 (Fe, Cr, Mn) $Si_{0.74}$; (d, f, h) diffraction patterns; (e, g, i) solutions of diffraction patterns.

of halloysite and oxides results in an almost 3-fold increase in the microhardness of powders than before milling and despite its reduction by about 30% after plastic consolidation, the produced nanocomposite materials show microhardness 110–150 $HV_{0.1}$ (**Figure 37a**), higher than the Mg1SiCu alloy. The introduction of HNTs particles into the Mg1SiCu alloy matrix using high-energy milling causes more than a twofold increase in the yield point under compression, because the yield point for compression with HNT_{100} nanotubes is 450–495 MPa at the test temperature of 25° C (**Figure 37b**), and at the test temperature of 225°C is 265–280 MPa depending on HNTs share. When using nanotubes HNT_{500} and HNT_{700}, respectively, it is slightly smaller (**Figure 37c**). **Figure 37f-j** show the course of compression diagrams at various temperatures of 25–225°C. The tested nanocomposite materials show a characteristic "dimple fracture" [235–238], sometimes also referred to as a ductile foveal fracture [239] (**Figure 38**). Nanocomposite materials reinforced with HNTs nanotubes are more resistant to frictional wear, as measured by changes in the surface layer related to permanent deformation, mainly weight loss [1, 240, 241], therefore they are characterized by a lower abrasion trace volume than the AlMg1SiCu alloy (**Figure 37d,e**). Nanocomposite materials reinforced with HNT_{100} halloysite nanotubes with a mass fraction of 15% are characterized by over 180% higher yield strength under compression, over 200% higher microhardness, and nearly 250% higher friction wear resistance compared to the AlMg1SiCu alloy, which is the matrix of the composite material.

In the case of 6th composite materials with AlMg1SiCu matrix reinforced with MWCNTs, the main problem during manufacturing is the homogeneous distribution of carbon nanotubes in the matrix material. Of the several methods of dispersing nanotubes in a metal matrix, such as mechanical milling, mixing in a turbulent mixer or mixing with an ultrasonic homogenizer, only high-energy mechanical milling leads to an homogeneous distribution of the reinforcement in the matrix material, without agglomerating the MWCNTs on the surface [242–250]. Carbon nanotubes can be placed between particles of a gas-atomized or spheroidal cold-alloyed aluminum alloy. After mechanical milling on the surface of the ground particles, no carbon nanotubes are present on the surface of any of the powders ground for 5 or more hours [95, 242, 244, 246, 251–255]. With the increased share of MWCNTs, the particle size decreases (**Figure 39**).

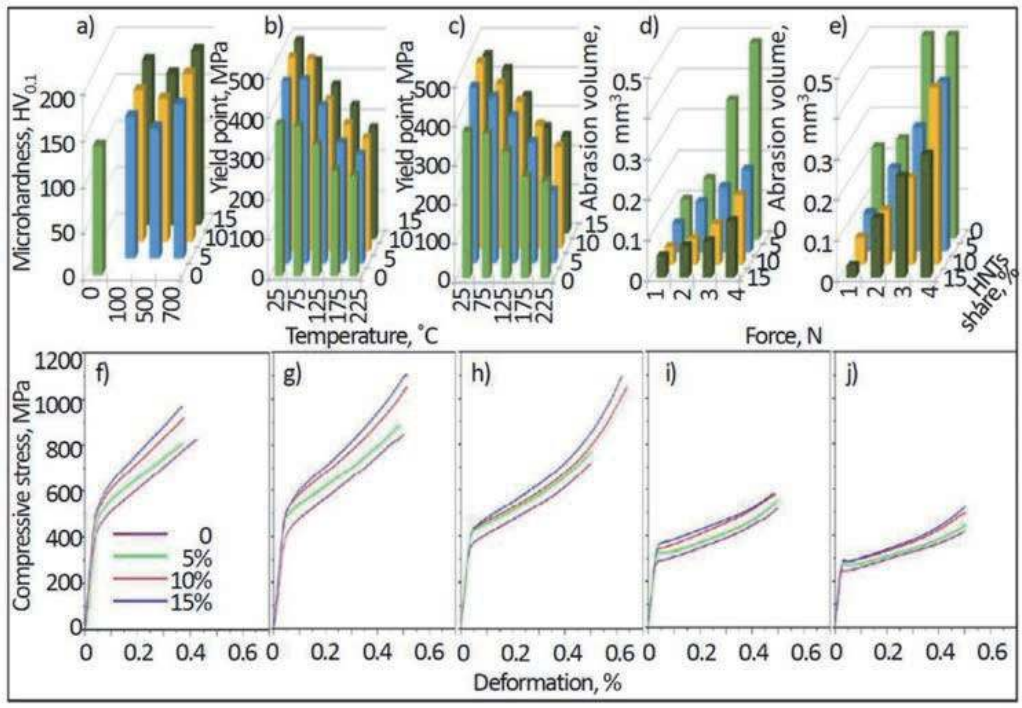

Figure 37.
Characteristics of the properties of a nanocomposite material with AlMg1SiCu matrix reinforced by HNTs in the proportion of 0–15%: (a) the influence of the HNTs annealing temperature on the microhardness; (b, c) influence of test temperature on compression yield point of nanotubes (b) HNT_{100}; (c) HNT_{700}; (d, e) effect of a load in the range 1–4 N on abrasion volume after post-measurement; (d) 1000 cycles; (e) 2000 cycles; (f-j) compressive stress curves as a function of deformation at temperature; (f) 25°C; (g) 75°C; (h) 125°C; (i) 175°C; (j) 225°C.

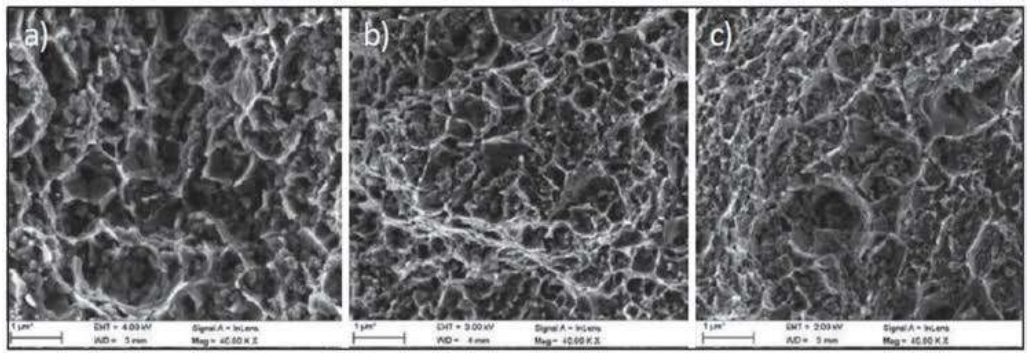

Figure 38.
The breakthrough of samples as dimple fracture style after the static compression test of nanocomposite materials with the participation of halloysite nanotubes (a) 5%; (b) 10%; (c) 15%.

As a result of mechanical milling, the order of the structure of carbon nanotubes and the interaction between the reinforcement and the matrix are degraded as a result of breaking the sp2 bonds. The results of the Raman analysis confirm the defect of the structure and the amorphization of carbon nanotubes (**Figure 40**), indicating a reduction in the intensity of the G and G' bands as well as an increase in the intensity of the D band, which is confirmed by the ID/IG and IG'/IG intensity factors ratios (**Figure 40**).

Carbon nanotubes during high-energy mechanical milling were dispersed and placed between deformed aluminum alloy particles, which increases the density of

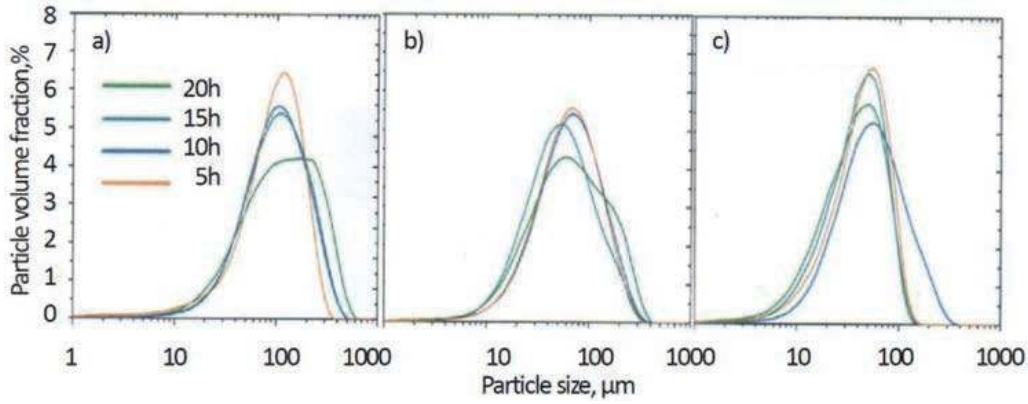

Figure 39.
The particle size distribution of the powder after high-energy mechanical milling for 5, 10, 15, and 20 h, respectively, depending on the share of MWCNTs nanotubes: (a) 0%; (b) 2%; (c) 5%.

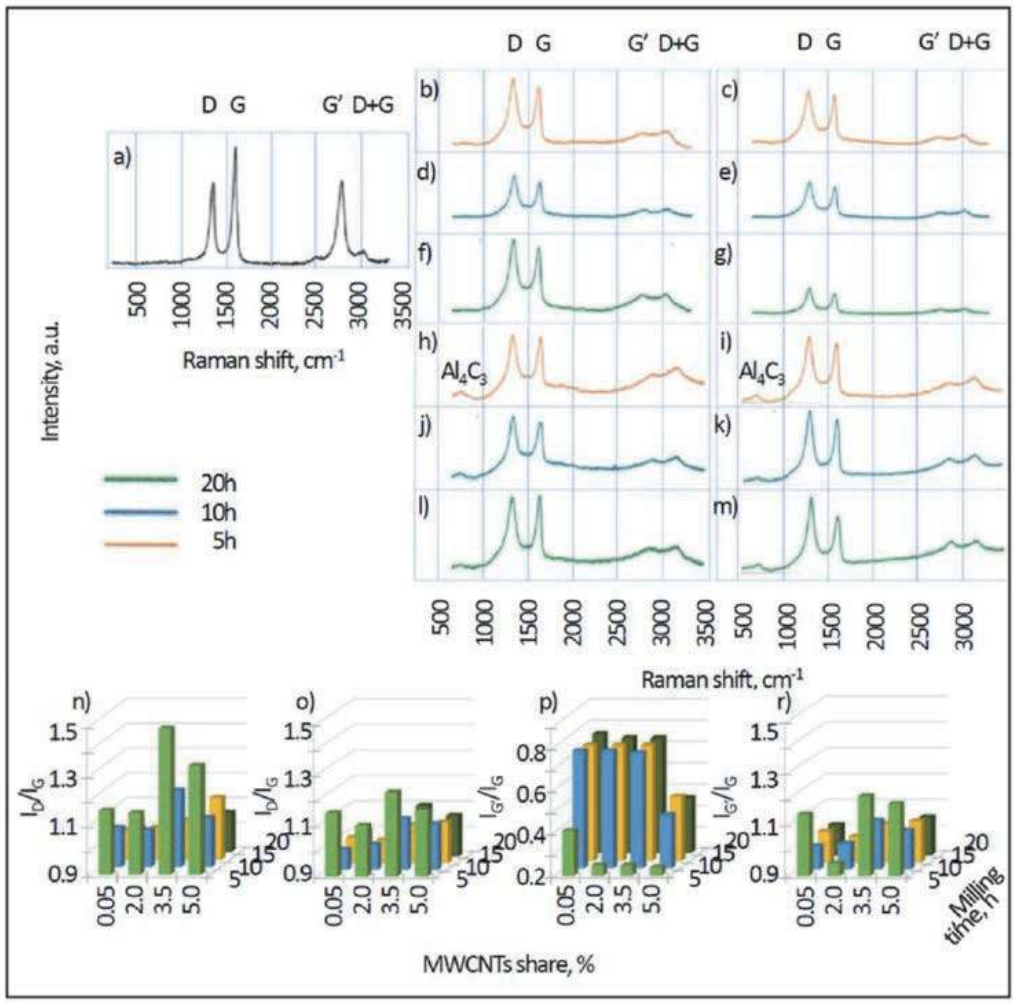

Figure 40.
Results of (a-m) Raman analysis and (n-r) distribution of intensity factors ratios (n, o) I_D/I_G and (p, r) $I_{G''}/I_G$: a) MWCNTs nanotubes; (b-g, n, p) powder obtained from high-energy mechanical milling and (h-m, o, r) after plastic consolidation, with milling time respectively for (b, c, h, i) 5 h; (d, e, j, k) 10 h; (f, g, l, m) 20 h, depending on the share of MWCNTs nanotubes: (b, d, f, h, j, l) 2%; (c, e, g, i, k, m) 5% and (n-r) depending on MWCNTs share and milling time 5, 10, 15 and 20 h.

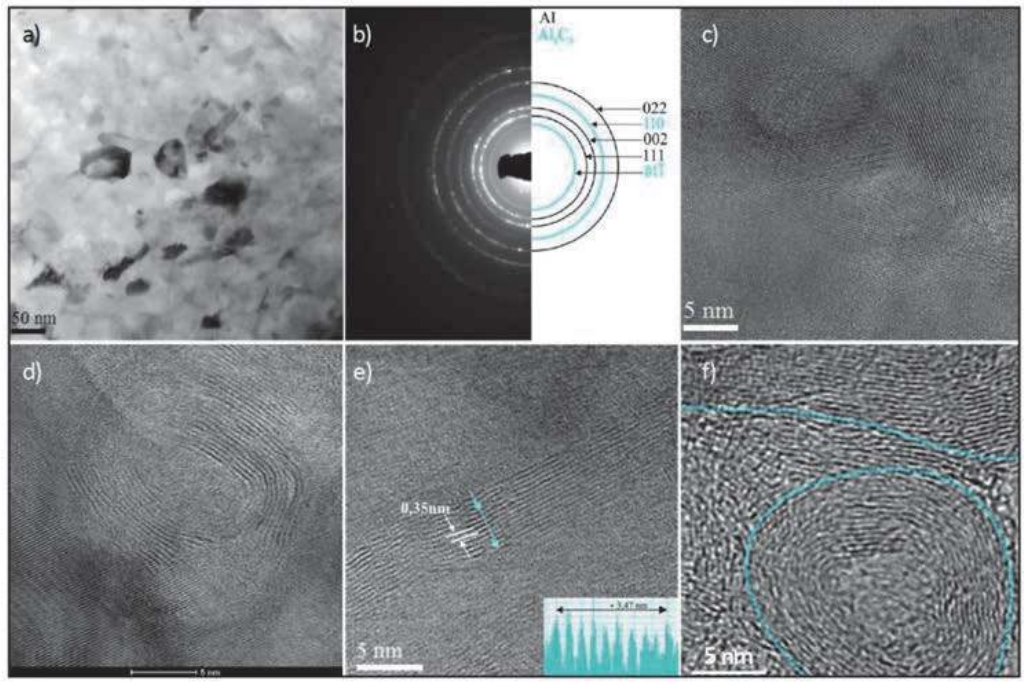

Figure 41.
The results of the thin foils investigations in the high-resolution transmission electron microscope HRTEM of the nanocomposite with the share of 5% by volume of MWCNTs after plastic consolidation; (a) structure; (b) the SAED diffraction pattern and the solution of the diffraction pattern from fig, a; (c) structure of nanograins; (d, e) nano-areas of the nanocomposites inherited from carbon nanotubes; (f) the structure of carbon nanotubes remaining after the HCl digestion of the material after high-energy mechanical milling for 10 h.

powders of nanocomposite materials (**Figure 41a, b**). The structure of the nanocomposite material with the matrix of the AlMg1SiCu aluminum alloy reinforced with MWCNTs is homogeneous (**Figure 41c**) with symmetrical, approximately spherical grains, with a size of about 50–70 nm. Carbon nanotubes show homogeneous dispersion and are strongly deformed (**Figure 41d,e**), which was revealed after complete removal of the matrix by etching with HCl (**Figure 41f**). However, literature reports [244, 251, 255–263] concerning the degree of degradation of carbon nanotubes are not unequivocal.

However, extending the milling time from 5 to 20 hours causes increased degradation of the structure of carbon nanotubes. It is accompanied by the amorphization of nanotubes, which is associated with a reduction in the intensity of the G 'bands (**Figure 40n-r**). It has been found, however, that the structure of carbon nanotubes may even be completely destroyed. Regardless of the share of MWCNTs above 0.5% and the mechanical milling the time the manufactured materials show a brittle fracture (**Figure 42**). The structure of the fractures also shows the fine grain structure of the material.

Defective nanotubes are much more reactive, so during the next consolidation involving plastic deformation at elevated temperature, as a result of the interaction of carbon nanotubes with the AlMg1SiCu alloy matrix, in places where there are nanotube defects and amorphous areas on their surface, probably intercalation of aluminum atoms occurs between the carbon layers in MWCNTs. It is the direct cause of the following precipitation of Al_4C_3 carbides (**Figure 43**) with a diameter of approx. 5–10 nm and a length of 20–30 nm. The precipitation of these carbides was also confirmed by X-ray analysis (**Figure 44**). Information on the Al_4C_3 carbides precipitation is also available in the literature in many cases of composite materials involving carbon nanotubes [264–274]. However, neither X-ray structural

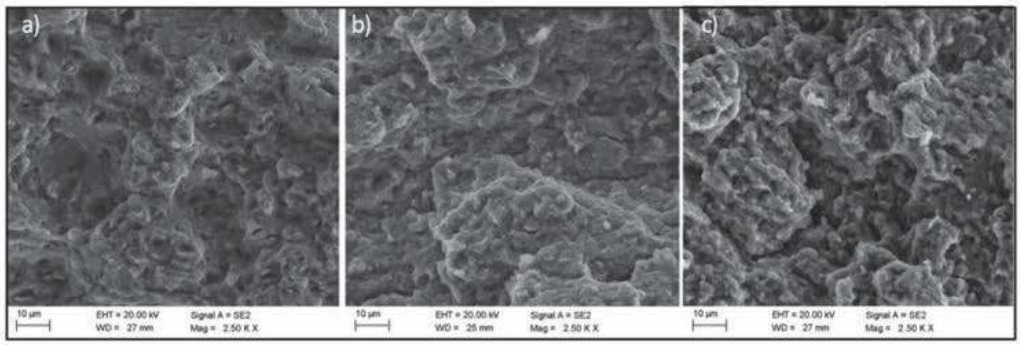

Figure 42.
Breakthrough structure of a nanocomposite material manufactured with (a, b) 2% (c) 5% by volume MWCNTs after high-energy mechanical milling for (a) 10 h; (b, c) 20 h (SEM).

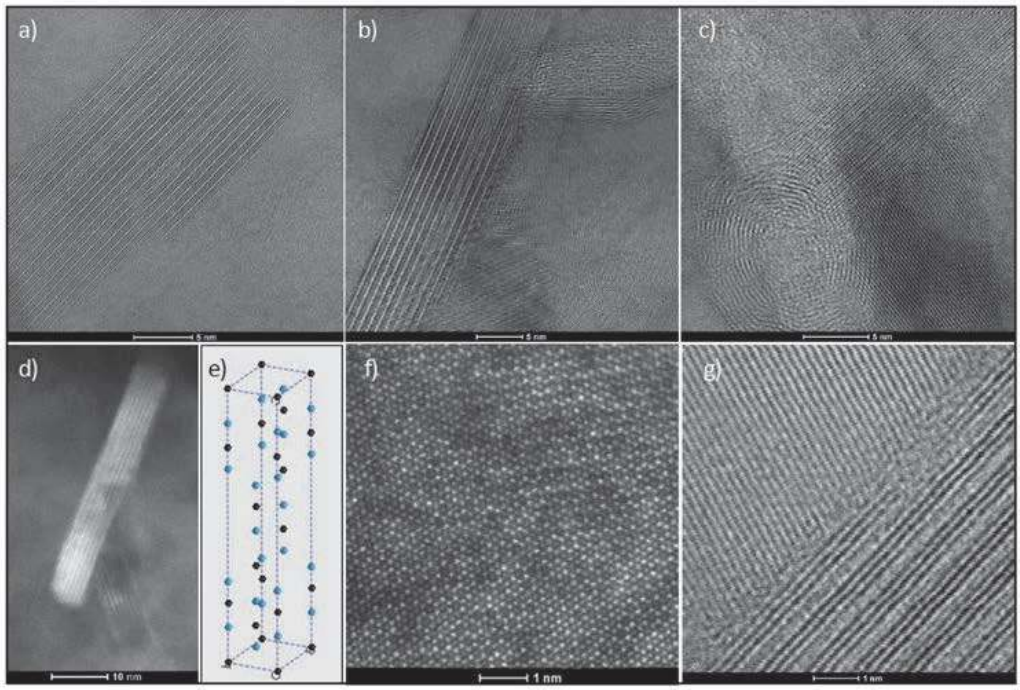

Figure 43.
Structure of thin foils of a nanocomposite material reinforced with 5% by volume MWCNTs (STEM-BF); (a) longitudinal section of the Al_4C_3 carbide in an AlMg1SiCu matrix; (b) MWCNT nanotube in longitudinal section and Al_4C_3 carbide in longitudinal section in an AlMg1SiCu matrix; (c) MWCNT nanotube in cross-section and Al_4C_3 carbide in longitudinal section in an AlMg1SiCu matrix; (d) Al_4C_3 carbide in an AlMg1SiCu matrix; (e) scheme of the distribution of Al (blue) and carbon (black) atoms in the Al_4C_3 carbide crystallographic cell; (f) Al_4C_3 carbide in cross-section – [001] direction; (g) Al_4C_3 carbide in longitudinal section and an AlMg1SiCu matrix.

analysis nor literature data indicate that Al_4C_3 is secreted directly as a result of mechanical synthesis by milling for up to 50 h [275].

The share of MWCNTs and the manufacturing conditions of nanocomposite materials have a relatively small effect on their density 2.56–2.57 g/cm^3 (**Figure 45a**), in contrast to the microhardness (**Figure 45b**). The manufactured nanocomposite materials reinforced with carbon nanotubes are characterized by increased microhardness by up to 300% (**Figure 45b**), greater ultimate tensile strength by over 200% (**Figure 45c, e-g**) and five times higher frictional wear resistance to the unground AlMg1SiCu alloy, because with the increase of share of MWCNTs, the volume of the wear mark decreases (**Figure 45d**). The coefficient of

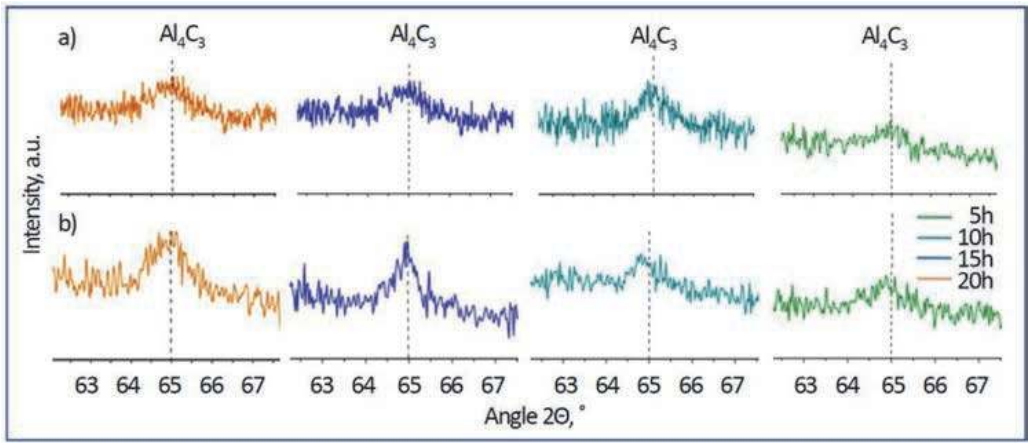

Figure 44.
Fragments of X-ray diffraction patterns confirming the precipitation of Al_4C_3 carbides in nanocomposite materials with AlMg1SiCu matrix reinforced by 2% (a) and 5% (b) MWCNTs carbon nanotubes as a result of plastic consolidation after prior high-energy mechanical milling for 5, 10, 15 or 20 h, respectively.

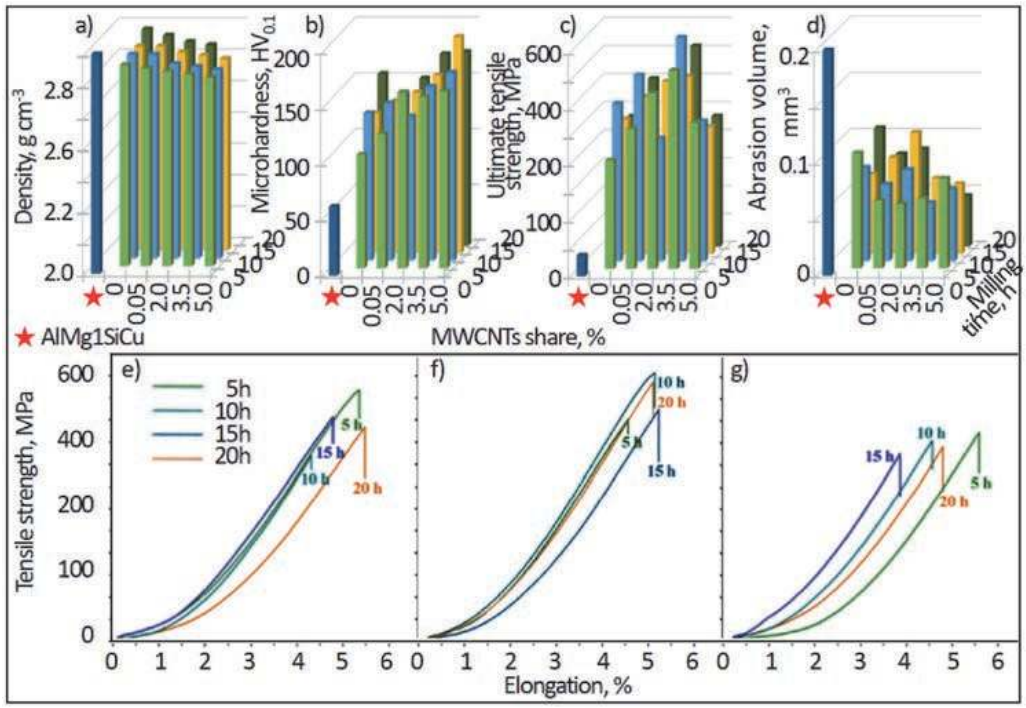

Figure 45.
Comparison of (a-d) properties of nanocomposite material obtained by consecutive high-energy mechanical milling and plastic consolidation depending on MWCNTs share 0.05; 2.0; 3.5 and 5.0% and milling time 5,10,15 and 20 h respectively comparing to AlMg1SiCu; (a) density; (b) microhardness HV 0.1; (c) ultimate tensile strength; (d) abrasion track volume; (e-g) the course changes the strength as a function of elongation during a static tensile test of a nanocomposite material manufactured after high-energy mechanical milling for 5, 10, 15, and 20 h with MWCNTs share (e) 2%; (f) 3.5%; (g) 5%.

friction of nanocomposite materials is not only lower than the coefficient of friction of materials made of the AlMg1SiCu alloy without MWCNTs, but also occurs in a much smaller range, which is also confirmed by the literature [276].

The reason for such a significant strengthening of nanocomposite materials with AlMg1SiCu alloy matrix, reinforced with MWCNTs carbon nanotubes, is dispersion nanostructured precipitates of Al_4C_3 carbide. Without the precipitation of these

carbides, these positive effects would not exist. However, note that this carbide is highly hygroscopic and completely hydrolyzes in an aqueous medium to form aluminum hydroxide and gaseous hydrocarbons such as methane or acetylene, according to the reaction:

$$Al_4C_3 + 12\ H_2O \rightarrow 3\ CH_4 + 4\ Al(OH)_3 \quad (1)$$

Similarly, the reaction with hydrochloric acid also causes decomposition of aluminum carbide according to the reaction:

$$Al_4C_3 + 12\ HCl \rightarrow 3\ CH_4 + 4\ AlCl_3 \quad (2)$$

It leads to a deterioration of the corrosion resistance of the composite materials and is a common factor contributing to mechanical failure. Even a small share of aluminum carbide destroys composite materials with the participation of aluminum and nano additives of allotropic forms of carbon in aggressive environmental conditions, and even in atmospheric conditions, causing uneven pitting corrosion. It limits the practical use of such composite materials [277]. Al resistance to electrochemical corrosion improves with the formation of Al_4C_3 on the Al surface, which prevents the dissolution of the metal in the chloride-based solution [278, 279]. The practical use of such nanocomposite materials will therefore be possible only in cases where their surface will be tightly covered with appropriate, durable coatings that effectively prevent contact of the material surface with water and other aggressive environmental media that can be applied. It is obvious that the technological process of applying the coatings cannot dissolve Al_4C_3 carbides. This requires further detailed studies as well as the eventual application of other coatings described as preventing corrosion of various alloys and composite materials based on aluminum or its alloys [280] including also the polymeric ones [281–284] and maybe it could be also possible to use the atomic layers deposition ALD technology while ensuring the required adhesion of such layers [285–288].

3.3 Structure and properties of the composite layers on the substrates of aluminum alloy

In all other cases, 7th–12th, the result of the work carried out is to obtain a hard and abrasion-resistant composite surface layer by introducing tungsten carbide or silicon carbide powder, respectively, through the interaction of a laser beam on the surfaces of aluminum AlMg3, AlMg5, AlMg9 alloys. Due to the use of laser treatment, the surface of the aluminum material is characterized by a relatively low density, receives better mechanical and tribological properties. Laser technologies are now widely used in surface treatment not only in the treatment of aluminum alloys, but many other alloys [289–317].

The share of feathering carbides WC/W_2C or SiC in the surface layer of the AlMg alloys depends on the conditions of the laser treatment. The largest share of the feathered WC/W_2C powder occurs for the AlMg9 alloy when a laser beam power is 1.8 kW. The surface layer manufactured in this case is characterized by a uniform distribution of the embedded particles in the matrix at a depth of up to 150 μm (**Figure 46a**), analogous to the laser treatment of the AlMg5 alloy surface (**Figure 46i, j**). Increasing the power of the laser beam causes an increase in the depth of remelting zone (**Figure 47a**), which results in greater dispersion of the feathered particles in the remelted layer, and the accompanying increase in the intensity of convection movements in the liquid pool affects the displacement of a part of the powder to a depth of about 1.5 mm both in the case of AlMg9 alloy

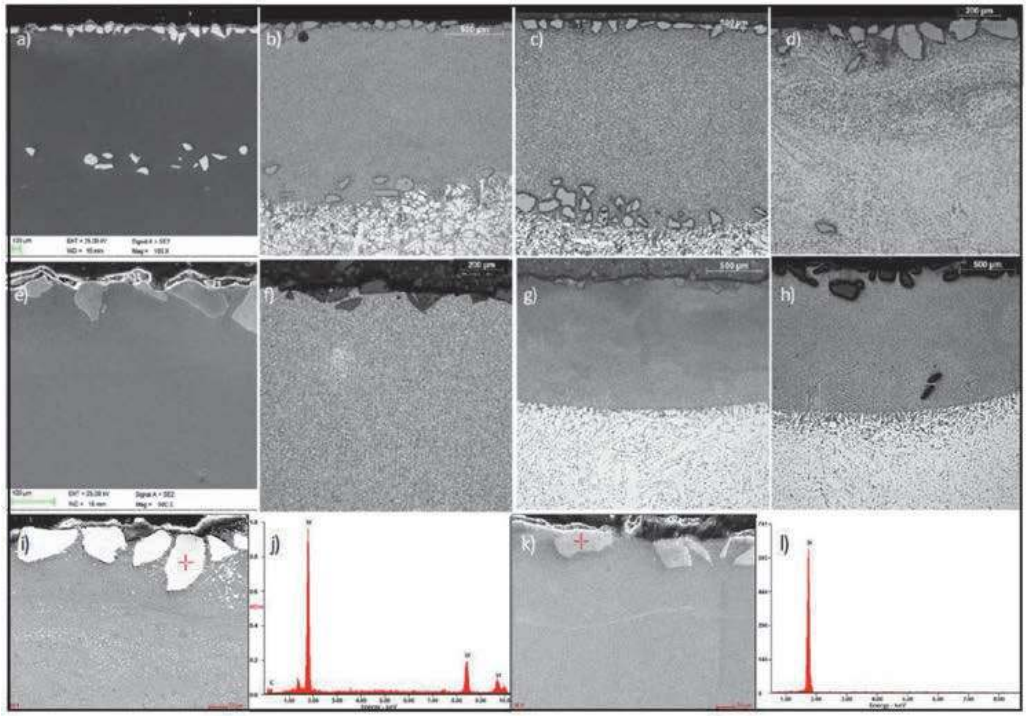

Figure 46.
Structure after laser feathering with (a-d, i, j) WC/W_2C carbides; (e-h, k, l) SiC carbides; (a-c, e, f) AlMg9 alloy; (d, g, i, j) an AlMg3 alloy; (h, k, l) AlMg5 alloy; using a laser beam with power: (a, b, f, g, h) 1.8 kW; (e) 2.0 kW; (c, d, g, i-l) 2.2 kW; (a, e, i-l) SEM; (j, l) SEM-EDS; (b-d, f-h) light microscope.

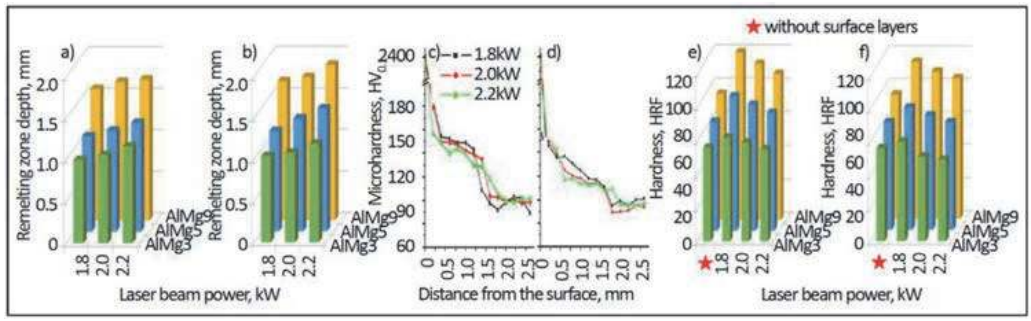

Figure 47.
The effect of laser beam power of AlMg3, AlMg5, and AlMg9 alloys when feathering carbides (a, c, e) WC/W_2C; (b, d, f) SiC; on (a, b) depth of the remelting zone; (c, d) course of hardness changes depending on the distance from the surface of the AlMg9 alloy; (e, f) the surface hardness versus the hardness of non-laser treated alloys.

(**Figure 46c, d**) and AlMg5 alloy (**Figure 46i, j**). The AlMg3 alloy after laser feathering of tungsten carbide with 1.8 kW laser beam power into the surface of the AlMg3 alloy results in an even distribution of carbides both at a depth of up to 160 μm and at the bottom of the layer. On the other hand, increasing the power of the laser beam causes gaps between the individual particles at a distance of up to 100 μm (**Figure 46d**).

The smallest proportion of the feathered powder occurs for the AlMg3 alloy after laser feathering of SiC carbide powder with a laser beam power of 2.2 kW (**Figure 46e**). As a result of laser feathering with a beam power of 2.0 and 2.2 kW, the carbides are evenly distributed in the near-surface part of the layer at a depth of up to 100 μm (**Figures 46e,g** and **47b**). The best results for laser feathering of silicon carbide are for the AlMg5 alloy (**Figure 46k,l**). Composite layers

manufactured with a laser beam power of 2.0 and 1.8 kW contain evenly distributed embedded powder particles in the matrix of an aluminum alloy, including AlMg9 (**Figure 46e,f**), with the largest share of feathered SiC powder in the case of alloy fusion AlMg5 with 1.8 kW laser beam power (**Figure 46h**). Single carbides with an average diameter of 100 μm occur in the central part of remelting zone also at the maximum power of the laser beam of 2.2 kW (**Figure 46k, l**).

Structure studies with the use of transmission electron microscopy and X-ray phase analysis showed the presence of intermetallic phases and $AlMg_2$, Al_3Mg_2, Mg_5Al_{18}, Mg_2Si precipitates.

Among the AlMg3, AlMg5 and AlMg9 alloys, the AlMg9 alloy has the highest hardness (**Figure 47f**). The mechanical and tribological properties of the manufactured composite layers containing respectively WC/W_2C or SiC carbides on the above-mentioned alloys largely depend on the power of the laser beam, because too high power adversely affects the properties of these layers (**Figure 47f**). As a result of laser feathering of carbide powder, the greatest increase in hardness occurs for the AlMg9 alloy using a 1.8 kW laser beam (**Figure 47e, f**). In the case of the two other alloys, the highest hardness occurs at this laser power, and increasing the laser power causes a slight reduction in the hardness of the surface layer (**Figure 47e, f**). The highest hardness of the layer is provided by laser feathering of the WC/W_2C powder into the AlMg9 alloy matrix with a laser beam power of 1.8 kW (**Figure 47e**). The smallest increase in hardness is obtained when laser feathering SiC powder into the AlMg3 alloy matrix with a laser beam power of 2.2 kW (**Figure 47f**). Increasing the power of the laser beam causes an increase in the hardness with respect to the Al-Mg alloy substrate at a greater depth (**Figure 47c, d**). The maximum value of hardness is lower than for treatment made with a lower power of the laser beam (**Figure 47c, d**). The introduction of WC/W_2C into the Al-Mg alloys matrix enables obtaining a higher hardness of the layers than in the case of laser feathering of SiC powder (**Figure 47c-f**).

Ball-on-disk abrasion resistance tests of the obtained composite layers as well as aluminum alloy without laser treatment showed a significant increase in abrasive wear resistance of surfaces obtained as a result of laser feathering of hard powders of WC/W_2C and SiC carbides, respectively, into the remelted matrix of AlMg3 alloys, AlMg5 and AlMg9. The highest abrasive wear resistance among all alloys and laser feathering variants is obtained after laser feathering SiC powder into the AlMg9 alloy matrix with a laser beam power of 1.8 kW. The highest wear resistance among these alloys as a result of laser feathering of WC/W_2C tungsten carbide powder is demonstrated by AlMg9 alloy after feathering with a laser beam power of 1.8 kW.

The developed technology can find numerous applications, including in the mechanical engineering, automotive and aviation industries.

4. Final remarks on the importance of advanced composite materials based on aluminum alloys in the development of Industry

4.1 The general importance of engineering materials and the technology of their manufacturing and processing

Already a dozen or so years ago, the concept of a half-life of detailed knowledge was introduced by analogy to the half-life of radioactivity [318]. After this period, characteristic for a given area of knowledge, about 50% of detailed information in this area will be up-to-date, and the rest will become outdated due to new scientific and technological discoveries. It is a measure of increasing the level of general

knowledge of engineering staff, enabling them to be quickly transferred to the practice of engineering design and product manufacturing as well as a wide application area. It is undeniable that in the area of engineering materials and the technology of their manufacturing and processing, the half-life of knowledge has been greatly shortened over the course of history and now reaches only a few years (**Figure 48**).

The development of natural materials, and with time predominantly engineering materials, has become the basic determinant of the development of material culture and human civilization in general, largely determining the level and quality of life of societies achieved. It should be realized that to manufacture any product that is accepted on the market, it is necessary to use properly selected engineering materials. Initially, for thousands of years, as described in publications, including own publications [319–337], but also a hundred years ago, the selection of materials was carried out by trial and error, which is considered the Materials 1.0 stage (**Figure 48**). To date, even in 80% of cases, materials are systematically tested according to the Materials 2.0 protocol [319, 320, 324, 333, 337, 338], after the concept is developed and its subsequent verification, and then the prototype is tested in laboratory conditions and only then tested and validated in real conditions. The impact of environmental conditions should be investigated and the product life cycle designed. In the case of the Materials 3.0 protocol, the procedure is similar, except that the use of IT tools at the concept development stage is characteristic of this stage. To design the target functionality, computational and simulation methods are used, e.g. using the principles of quantum physics and chemistry, methods of artificial intelligence, and databases. Nowadays, opportunities have opened up for the use of cyber-physical systems and big data, as well as advanced methods of artificial intelligence and machine learning, including artificial neural networks and fuzzy logic, and more and more often smart systems cooperating with people, which is the essence of the Materials 4.0 approach, which is now increasingly being implemented. It is accompanied by the application of materials on-demand, when not more than two decades ago, the principle of having to choose materials only from the assortment offered by material manufacturers was in force. The task set for the designer can now be formulated in the form of the question: "what can be used to create a product interesting for the customer on the market?" On the other hand, the approach that answers the question: "What can be

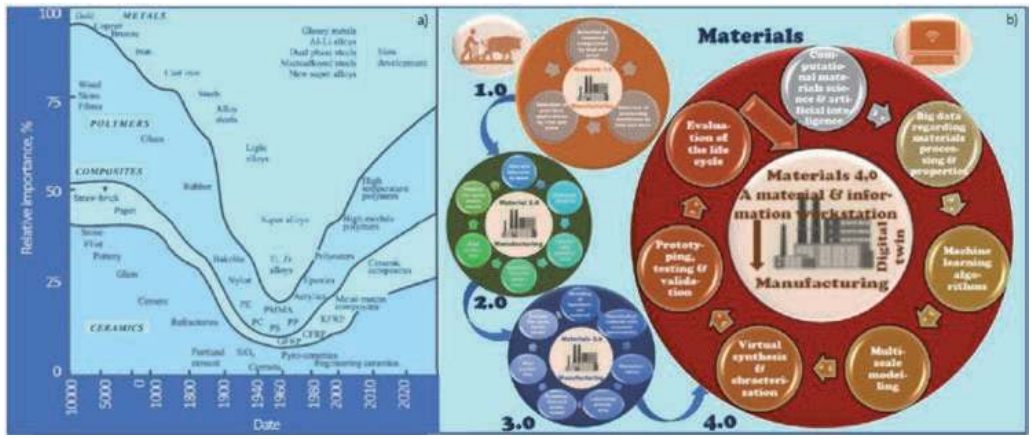

Figure 48.
Changes of: (a) the importance of individual groups of engineering materials throughout history; (b) the concept of selection of engineering materials for products from the trial and error method (materials 1.0) to the methodology using cyber-physical systems and advanced information technologies (Materials 4.0).

DOI: http://dx.doi.org/10.5772/intechopen.98677

manufactured from a material that is currently available or already known to us?" It is anachronistic. Numerous grades from among much more than 100,000 currently known and available engineering materials give new innovative potential in the implementation of products. It is impossible to correctly select engineering material for any practical application without the use of modern and highly developed Computer-Aided Design CAD tools and other Computational Material Science methods. There are two aspects to this approach. On the one hand, the material properties of each product are designed by the constructor and an appropriate engineering material should be produced that meets the requirements of a given application solution, and on the other hand, the availability of one of the ready materials having a set of properties according to the criteria should be analyzed, using the available material databases. The problem is extremely important considering that an average small car has at least 15,000 parts and a passenger aircraft may have 4.5 million or more elements. Of course, in each case, the right decision must be made regarding the selection of engineering material and the appropriate technological process. All engineering materials are in each case equivalent from the point of view of engineering design, provided that they meet a set of required criteria, and the basis for multi-criteria optimization is a set of the best functional and technological properties with the lowest possible manufacturing and processing costs, as well as the use of the material and the product manufactured of it, taking into account ecological aspects and the product life cycle. Product engineering design is essential and is not an activity extracted from the overall product manufacturing process, but an important element in satisfying market needs and at the same time is dependent on them.

Product engineering design is composed of three elements that cannot be separated and cannot exist autonomously (**Figure 49**) [3, 318–320, 324, 339–351], which include:

- structural design, ensuring the shape and geometric features of the product,
- material's design, ensuring the required physicochemical and technological properties as well as product life cycle,

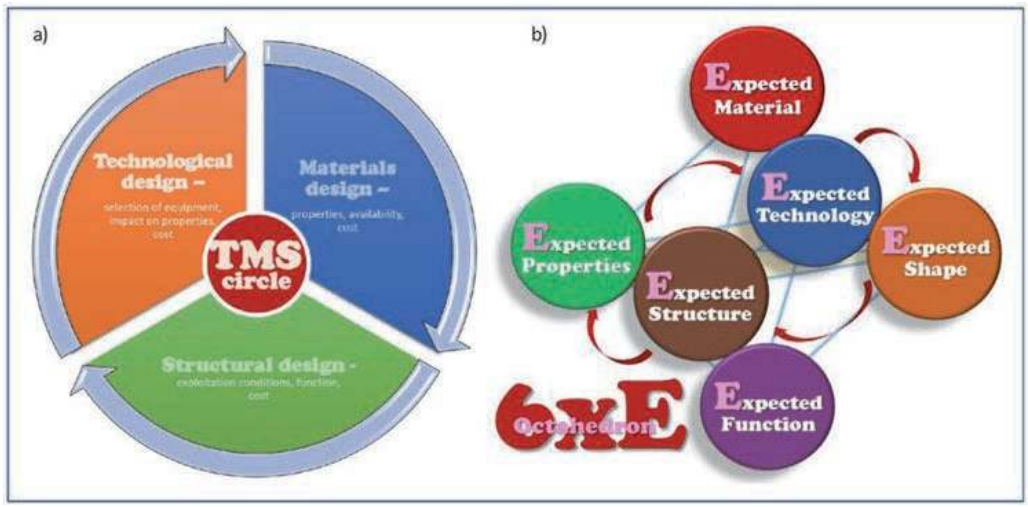

Figure 49.
Diagram of relationships between structural, material, and technological design as components of product engineering design (a) and the 6xE octahedron of expectations resulting from the material science paradigm and materials science (b).

- technological design, ensuring the manufacturing of products with the required properties, with the highest possible efficiency, the highest possible degree of automation and computer aiding, and the lowest manufacturing costs.

The functional properties of products, are including mechanical, physicochemical, thermal, magnetic, electrical, and optical properties, depending on the chemical composition and the cross-sectional structure and very often also the surface structure of the materials and the conditions of use of the products and their components. These conditions include also operate at high or low temperatures, in conditions of cyclic loads, as well as in an aggressive gaseous or liquid medium. Materials science deals with the assessment of the impact of the structure on the electronic, crystalline, micro, and macroscopic scale on the properties of materials, while material engineering covers the relationships between the structure, technological processes, and functional properties of materials used for numerous products and complex application systems, significantly determining the quality of life of modern societies. The materials science paradigm corresponds to an octahedron illustrating the 6xE rule (**Figure 49b**) [3, 318–320, 339, 340]. Expected operational functions of the product are ensured by designing the expected material, processed using the expected technology, in order to give the expected geometric characteristics and shape of the product, enabling the expected structure and deciding to obtain a set of expected properties of the designed product. The above-mentioned approach provides people with continuous access to products and consumer goods that directly affect the level and quality of life, climate, quality and potential of health protection, education, information exchange, and other aspects recognized by the United Nations as Sustainable Development Goals (**Figure 50**). It presents a deeply humanistic mission of the engineering community in order to activate the development of societies. For this reason, the real development of materials engineering, including nanotechnology and surface engineering, and the accompanying research, are an important determinant of present and future prosperity and high quality of life. Sustainable development of this area is therefore of great interest to societies.

Figure 50.
Civilization's main threats and sustainable development goals enabling counteraction them and their relationship to the development of engineering materials used on products.

4.2 The importance of engineering materials and technological processes in the context of the current stage of Industry 4.0 of the industrial revolution

All products of interest to customers, without exception, are made of engineering materials and cannot be built without them. The processes of using engineering materials and other resources such as energy, capital, and people to make products available using different machines and different technological processes organized according to a well-designed plan are called manufacturing. The development of manufacturing processes is closely related to the development of the material culture of societies, which was reflected in the Japanese approach of the Society from groups of people practicing hunting and harmoniously coexisting with nature, which was considered Society 1.0 to information and achieving the goals of Society 5.0 of the smart sustainable development, oriented to people, their well-being and high quality of life, and ensuring economic development, which goals are achieved by connecting cyberspace with the real world (**Figure 51**) [319, 320, 322, 352–357].

In Europe, a few years earlier, the German concept of Industry 4.0 was developed, already popular in many countries around the world, and also presented in Author's own works, describing the stages of the industrial revolution (**Figure 52**) [195, 293, 319, 320, 322, 323, 332–337, 349, 350, 358–414].

The introduction of steam engines at the end of the 18th century, considered Industry 1.0, marked the beginning of the industrial revolution. The current stage

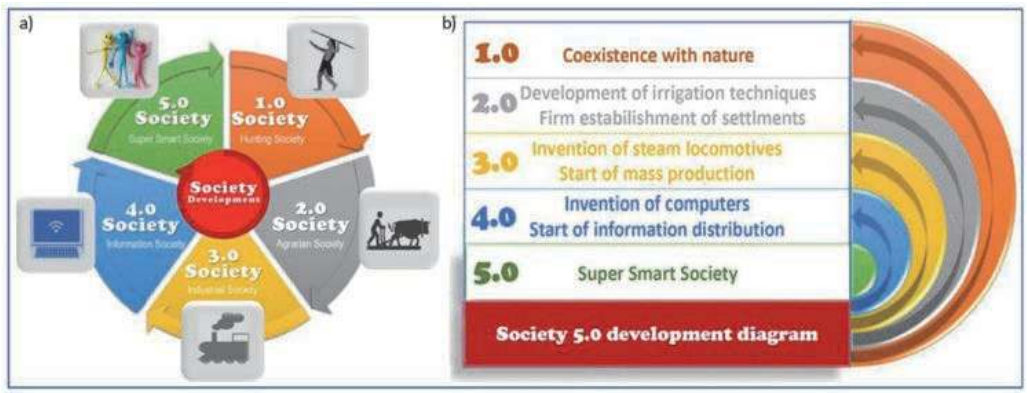

Figure 51.
The concept of development from Society 1.0 to Society 5.0 (a) and the main events determining the implementation of each of the stages (b).

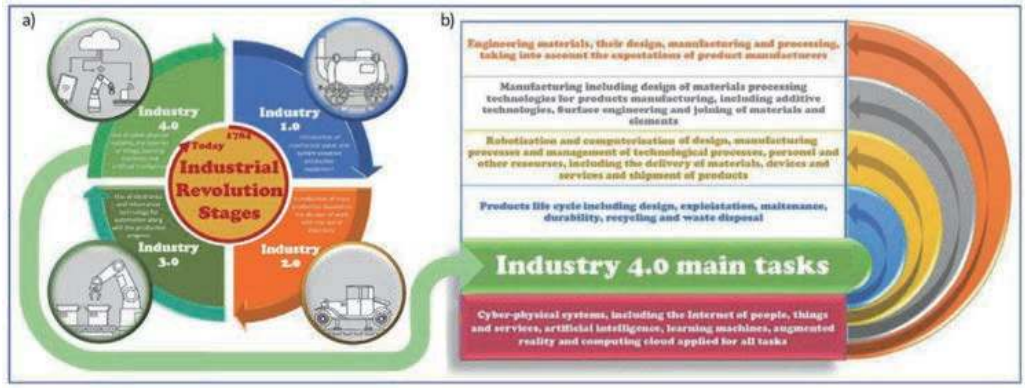

Figure 52.
The concept and tasks of Industry 4.0 (a) and main tasks in the Industry 4.0 stage (b).

of Industry 4.0 includes smart factories, supplied by smart suppliers, producing smart products. Physical production processes are monitored by manufacturing systems, making smart decisions, based on real-time communication with people, machines, and sensors, and based on experiments performed on the so-called "Digital twins" in virtual reality using the simulation of real conditions of operation and maintenance of manufactured products using cyber-physical systems (CPS), Internet of Things (IoT) and cloud computing, with the use of large data sets. In the classic Industry 4.0 model [319, 320, 322, 361, 367–369, 372–375, 378–382, 387–391, 393, 395, 402, 415, 416] it was recognized that this stage of using the nine basic technologies described in the literature was achieved (**Figure 53**) [293, 319, 320, 323, 345–349, 360–415].

It turned out that this model is one-sided and requires a significant augmentation, mainly by taking into account engineering materials, technological manufacturing processes and technological machines, and not only complex cyber-physical systems and very advanced tools and information systems (**Figure 54**).

The most important thing is that manufacturing possible only in reality, thanks to the physical system and on the condition of using real materials, usually engineering ones. No product can be manufactured without materials. Therefore, they should be absolutely included in the current Industry 4.0 model, because obviously they are and were necessary for every stage of the industrial revolution from Industry 1.0 to Industry 4.0. The simplified approach in the classic Industry 4.0 model creates the erroneous impression that the progress concerns only technologies covering monitoring, control, coordination, and integration of information and communication technologies that make up cyber-physical systems (**Figure 53**), without the need to make real progress in the field of technological machines, manufacturing technologies and necessary engineering materials to manufacture any product. It is obviously not true and therefore an adequate model must take into account all these aspects [319, 320, 322, 332–336, 365, 417]. A far-reaching simplification is also reducing the technological issues only to additive manufacturing, as it was done in the classic Industry 4.0 model. Additive manufacturing cannot be treated as ruthlessly competing with many known and used for many years, and sometimes even millennia, technologies for manufacturing products, such as foundry, machining, plastic working, heat treatment, surface engineering, joining and welding, and assembly [319, 320, 322, 332–337, 345–349, 364, 365]. The enormous technological progress that is taking place now and in the near future will not

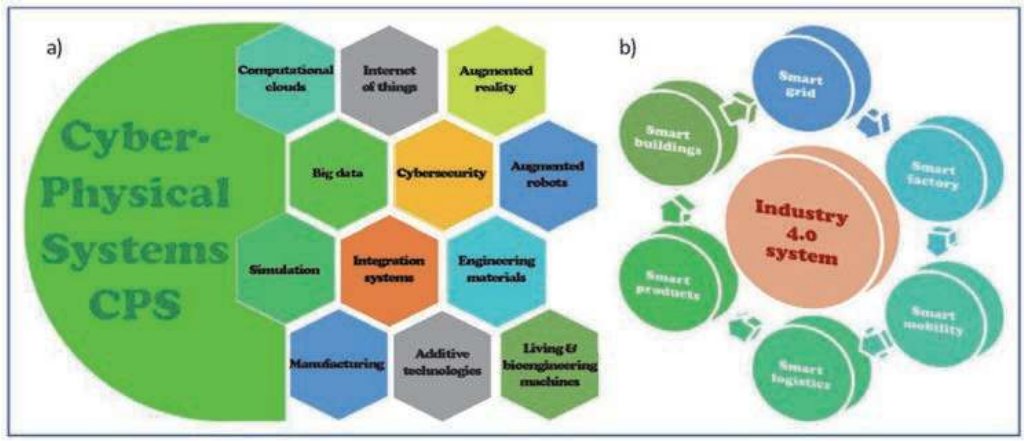

Figure 53.
The crucial components of the current industry 4.0 model: (a) augmented set of leading technologies included in cyber-physical systems; (b) smart systems included in the Industry 4.0 model.

eliminate these technologies, so it is necessary to include them in the Industry 4.0 model. It should be noted that the systematic modernization and progress in the field of these technologies concerns their mechanization, robotization, and above all computer-aided engineering design and manufacturing within cyber-physical systems. It is obvious that the classic model of Industry 4.0 in fact concerns only the computerization of technological processes, therefore, instead of it, it was necessary to introduce the appropriate holistic augmented model of Industry 4.0 [319, 320, 418] leaving cyber-physical systems as one of the elements technology platform of this new model (**Figure 53**).

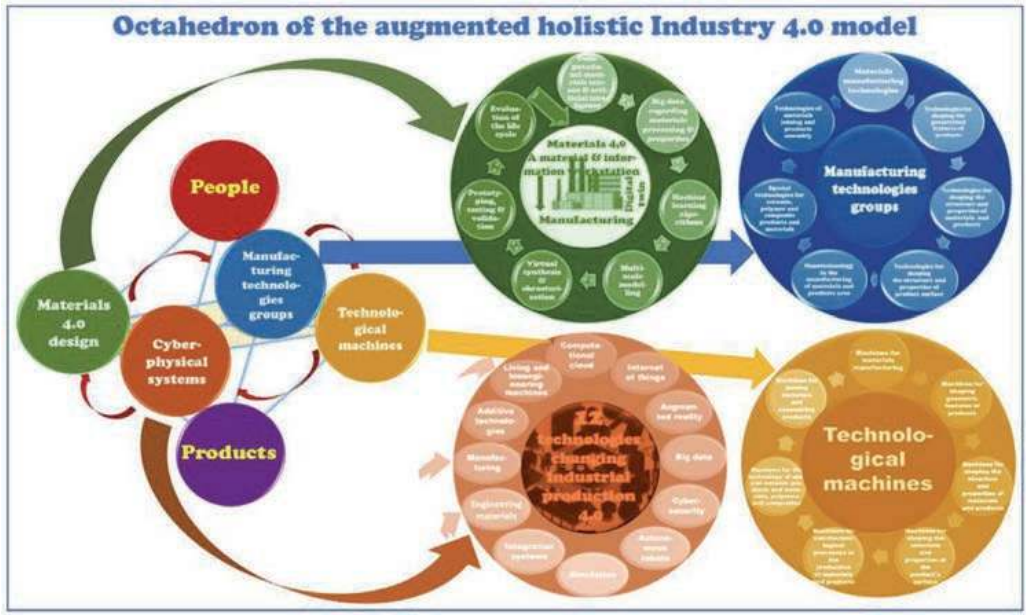

Figure 54.
The holistic augmented model of Industry 4.0 taking into account advanced engineering materials and technological processes and also the machines and production devices used, as well as twelve technologies related to cyber-physical systems conditioning the development of production in the most modern phase of the industrial revolution.

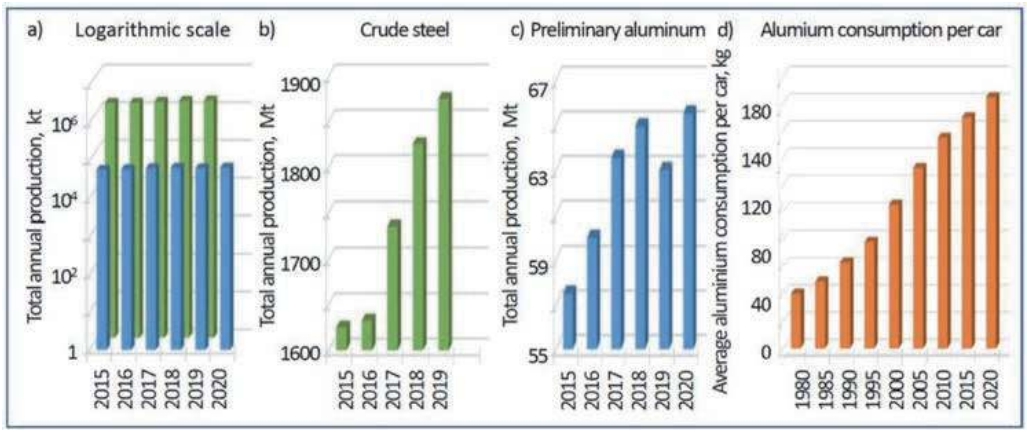

Figure 55.
Comparison of the annual total world production in 2015–2020 years of (a, b) crude steel (a, c) preliminary aluminum (a – logarithmic scale); (d) changes of the average aluminum consumption per car in 1980–2020 years.

4.3 The importance of advanced composite materials with an aluminum alloy matrix in the context of the current stage of Industry 4.0 of the industrial revolution

The growing and more sophisticated requirements set by the conditions of the current stage of the Industrial Revolution, conventionally designated as Industry 4.0, also pose challenges to designers and manufacturers of engineering materials. They apply equally to the implementation of new engineering materials, technological processes of their manufacturing and processing, advanced methods of their design, as well as the application of nanotechnology and surface engineering in this area. Among engineering materials, world steel production remains extremely high (**Figure 55**), despite reports of a decline in production in some countries due to the SARS-CoV-2 coronavirus pandemic.

The Worldsteel Association published crude steel production data in August 2020. Compared to August 2019, world production was 0.6% higher, despite the pandemic. The lowest production level, amounting to 137 million tons, was recorded in April 2020. Since then, production has been increasing and in August it amounted to 156.2 million tons. However, there has been a reshuffle in the market. Production declines were recorded in the United States (−24.4%), Japan (−20.6%), Germany (−13.4%), Russia (−4.6%), India (−4.4%) and South Korea (−1.8%). From the beginning of the year, production decreased by 19% in North America, by 18.6% in the European Union, by 15.6% in South America, and by 4.5% in the former Soviet Union countries. Production in the dominant country, i.e. China, despite the pandemic, does not decrease, but even increases. China, as the largest steel producer in the world, produced 94.8 billion tons in August, 8.4% more than in the previous year. Comparing total production in the first eight months of 2020 and 2019, China grew by 3.7%. Increases in steel production also occurred in Vietnam (32.9% compared to August 2019 and 11.5% in total since the beginning of the year), in Turkey (22.9% compared to August 2019 and 0.6% in total since the beginning of the year), in Iran (14.6%) and Brazil (6.5%).

Compared to steel, aluminum alloys are significantly lighter, and at low temperatures are characterized by higher impact strength. Aluminum alloys are the preferred structural materials used, among others, for the manufacturing of cars, in the aerospace industry and mining machines, in the processing industry for various high-performance elements for various applications, due to their relatively low weight and favorable set of properties. Ecological considerations require the reduction of the total weight of cars, which indicates the need to produce many new components from aluminum alloys (**Figure 55**). The use of lightweight materials for the manufacturing of car components allows for compliance with increasingly stringent air pollution regulations. It is obvious that a car with a lower weight allows for lower and more economical fuel consumption, which clearly reduces the emission of exhaust gases, mainly carbon dioxide, into the atmosphere.

Annual global aluminum production is expanding (**Figure 55**) at a level almost 30 times lower than that of steel, although the aluminum market may also have changed due to the COVID-19 pandemic. In 2015–2020 years, the total aluminum production amounted to 374,840 tons, and thanks to the increase in production in China in 2020, the total world production increased by a few percent compared to 2018, when it was higher than in 2019. The dynamics of aluminum production in 2015–2020 is shown in **Figure 54**. For example, in 2017, primary aluminum was produced in 41 countries. The main producers were China (55%), Russia (6%), India (5%), Canada (5%) and the United Arab Emirates (4%) in order of decreasing aluminum production. The share of China in the global aluminum production is growing year by year.

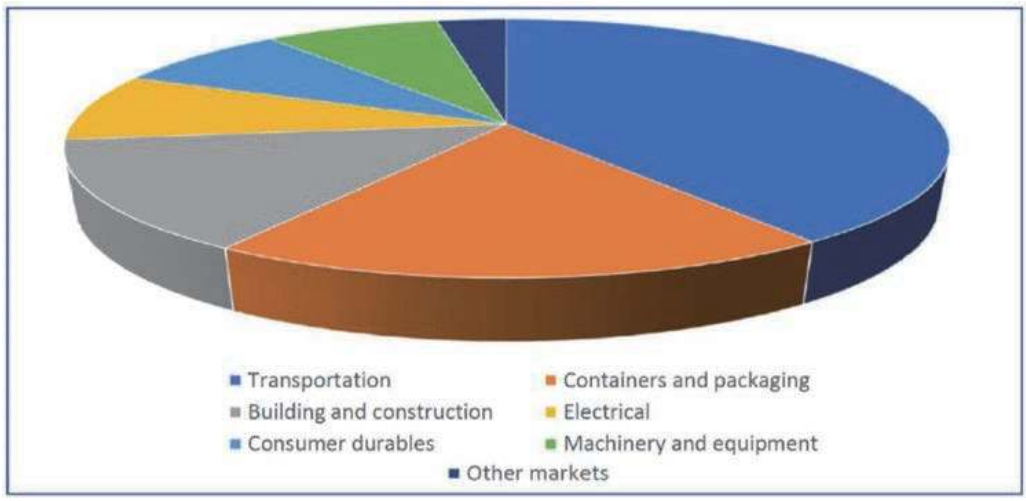

Figure 56.
Main areas of application of aluminum and its alloys in the US and Canada in 2017 (compiled according to data from the US Geological Survey and Aluminum Association 2017, available on July 15, 2018).

The end-use rate of aluminum and its alloys in various application areas has been established for many years. Aluminum has gained a good position on the world market due to its significant share in increasing the fuel efficiency of vehicles and in relation to its use in ecological construction products and ecological packaging. An example are the main areas of application of aluminum and its alloys in the United States and Canada (**Figure 56**).

According to the International Trade Center (ITC), the value of the aluminum market and its products in 2018 amounted to USD 194.32 billion [419]. It was estimated that the volume of the aluminum market in that year was 79 million tons, and it is estimated that aluminum consumption will increase with compound annual growth rate CAGR of 4.2% in the forecast period until 2025 [420]. Aluminum is widely used for packaging and construction, and is also used in machinery and equipment, and in the electrical and consumer durables industries. The main area of application of aluminum is the automotive industry. Since aluminum is a light metal, it is used mainly in car bodies and engines parts, what is an essential factor in reducing car fuel consumption. It also applies to trucks, as, for example, the Ford plant launched the production of an all-aluminum F-150 trak's body in 2015 [421], which reduced the weight of the truck by more than 300 kg, resulting in a significant improvement in fuel efficiency and reduced total operating costs. International agreements on fuel economy are influencing for increase the use of aluminum in the automotive industry around the world. The expected increase in the production first of all of electric vehicles, and also semi-autonomous and autonomous vehicles as well as self-driving cars and trucks will further strengthen the aluminum automotive market. This segment is estimated to grow at a CAGR of 4.3% by 2025. Aluminum is now widely used in smartphones, tablets, laptops, flat screen TVs, monitors and other consumer electronics products. According to estimates provided by the Global System for Mobile communications Association (GSMA), the number of mobile phone users worldwide will increase from 5.1 billion in 2018 to 5.8 billion in 2025. Therefore, the global smartphone and smart TV market will be subject to a CAGR growth of 8–10% in the forecast period until 2025, which will affect the increase in demand on the aluminum market. Aluminum is the second most used metal in construction after steel, and according to the World Bank, in 2016, the gross domestic product GDP of construction was 25.4%. Aluminum is widely used

in windows, curtain walls, roofing and cladding, sunshades, solar panels, railings, shelves and other temporary structures. The growing construction activity around the world creates more and more opportunities for the aluminum market. However, there are differences in aluminum consumption by end-use category in high (HIC), low (LIC) and middle income countries (MIC). In low- and middle-income countries, aluminum is mainly used for the production of electrical systems and in the construction industry. In high-income countries the main areas of application are products in the transportation sector, including cars, commercial aircraft and railway stock.

It is estimated that the aluminum market will grow in CAGR above 3% in the forecast period until 2025, although earlier data even indicated an increase in aluminum consumption up to 120 Mt. with an average growth rate of about 4.1% per year. The global aluminum market is expected to grow by 6.5% CAGR to reach USD 235.8 billion in 2025. This means that the annual production of bauxite should increase to approx. 570 Mt., and of aluminum oxide to approx. 230 Mt. However, a diversified increase in the use of aluminum is expected in different geographic areas (**Figure 57**). The main driver of the global aluminum market is the growing construction activity in the Asia-Pacific region. In North America, the growing number of construction projects and growing investments in the United States and Canada are driving the market under study. This upward trend is likely to continue, depending on the financing of larger projects. On the other hand, the slowdown in the global automotive industry and the unfavorable conditions resulting from the COVID-19 outbreak are holding back market development, and earlier forecasts are obsolete. Therefore, it is estimated that the construction industry will dominate the global aluminum market in the coming years. The Asia-Pacific region will be the fastest growing in the world in this situation, due to rising consumption in China, India and Japan, with a growing population, rising middle-class income and urbanization. In fact, the Asia-Pacific region will generally dominate the global aluminum market. The electronics manufacturing market in this region will develop rapidly in the coming years due to the numerous Original Equipment Manufacturer OEMs, low cost and availability of raw materials and cheap labor, as well as cooperation with numerous entities in Germany, France and the United States in the field of production services and assembly. China is expected to be the world's largest

Figure 57.
Different scale of growth of aluminum markets in different geographical areas of the world in 2020–2025 due to the diversification of the development of the end-user industry.

market for civil aircraft sales by 2040 among all countries, which will have a significant impact on the demand for aluminum. For example, China is expected to purchase new aircraft from Boeing by 2036 worth USD 1.1 trillion. The growing demand for aluminum is also significantly influenced by the growing demand for cargo transportation, therefore the production of commercial aircraft in Japan will continue to increase, including the production of new generation F-35A fighters and other military aircrafts. Thus, the demand for aluminum in the Asia-Pacific region will increase rapidly in the next two decades due to the rapidly expanding end-user industry.

Aluminum is the only material that more than covers its own collection costs in the consumer disposal stream and is 100% recyclable, retaining its properties for an indefinite period of time. More than 70% of the aluminum produced from the beginning of industrial use of aluminum has been recycled and is still used today. In view of the expected growth of the global aluminum market in 2025 to USD 235.8 billion, and the related expected increase in the production capacity of bauxite mines around the world, one should take into account the probable increase in the share of secondary aluminum from new scrap, proportional to the total consumption. However, the share of aluminum produced from old scrap may decline, as in countries with high economic growth, the share of aluminum used to build new infrastructure with long-term use is significant. It could undoubtedly have a negative impact on greenhouse gas emissions, unless the stricter requirements of the climate policy force an increase in the efficiency of aluminum smelters and the related reduction of energy consumption for aluminum production. Recycling aluminum saves over 90% of energy costs compared to primary production, and thus reduces the use of fossil fuels, including oil, the energy of which would be used to produce fresh aluminum. For the recovery of post-consumer scrap, it is important to diversify the end use of aluminum. For example, statistically, an average of 113,000 aluminum cans are recycled in the world every minute, and their value per year amounts to over USD 800 million. Aluminum used in cars and vehicles can be easily recycled. Many applications in the transport sector, but also in the electronics sector, have a much shorter real life-time and therefore they are more recyclable than electrical systems and construction applications. According to the Aluminum Association, more than half a million tons of aluminum used in cars are recycled annually [419].

The challenges posed by the developing industry in the Industry 4.0 stage and the expectations of the automotive and aviation industries force constant progress in the development of new materials using aluminum. The undoubted advantages of these materials include the density almost three times lower than that of steel, which is the main premise for applications in the area of transport. Newer and newer aluminum alloys with other alloying elements are being developed and implemented. Of course, there are also alloys of other elements in which aluminum is an alloying element. Aluminum matrix composite materials ACMs have a steady share of the systematically growing group of materials using aluminum. This chapter presents a generalization of the results of numerous own studies and provides a detailed overview of the structure and properties and manufacturing technology of several new AMCs selected for presentation due to their advanced manufacturing methods and unexpected properties and the resulting wide application possibilities (**Figure 58**).

Among these new advanced aluminum matrix composites materials, there are basically three groups of such materials [66–80], including:

1. composite materials manufactured by gas-pressure infiltration with liquid aluminum alloys, respectively, eutectic AlSi12 and hypoeutectic AlSi7Mg0.3, constituting the matrix, in which the reinforcement has a skeleton structure,

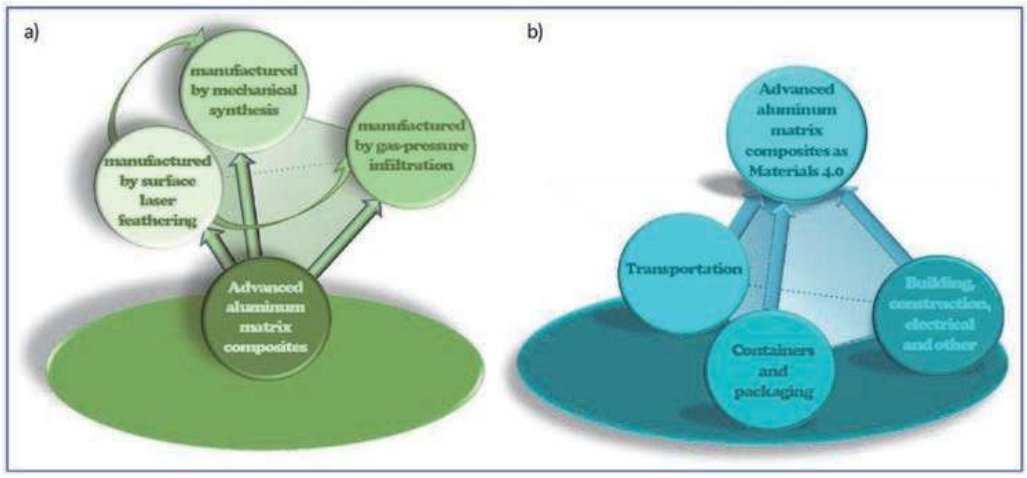

Figure 58.
The scheme (a) of three groups of the new advanced aluminum matrix composites materials presented in the chapter manufactured using advanced technologies of Industry 4.0 stage; (b) the main areas of predicted applications of advanced aluminum matrix composites.

obtained alternatively by sintering Al_2O_3 powder with the participation of carbon fibers enabling, after their removal, obtaining a porous structure, sintering mixtures of HNTs halloysite nanotubes with carbon fibers, after their removal, providing a porous mullite skeleton and selective laser sintering of titanium powder to obtain a skeleton with the porosity of at least 50% with pores with a size of 50–500 μm,

2. nanocomposite materials manufactured by mechanical synthesis using high-energy mechanical milling of a mixture of an aluminum alloy powder for plastic deformation AlMg1SiCu with alternatively halloysite HNTs nanotubes and multi-wall carbon nanotubes MWCNTs and the next two-stage press consolidation and subsequent cold pressing in the first order hot at an elevated temperature in order to produce bars of the assumed diameter,

3. composite surface layers on the substrate of aluminum alloys, alternatively AlMg3, AlMg5, AlMg9, manufactured by surface laser feathering by introducing powder, alternatively tungsten carbide WC/W_2C or silicon carbide SiC with the use of fluxes as agents supporting the operation of the laser beam and facilitating the selective remelting of the aluminum alloys, without the need for additional heat and surface treatment.

The structure, technology, and properties of these materials were presented, as well as the application perspectives, especially in transport and biomedical devices, as well as in connection with the implementation of the Industry 4.0 stage of the Industrial Revolution.

Acknowledgements

The author would like to acknowledge for the cooperation in research realisation his former PhD students Dr Marek Kremzer, Dr Magdalena Kujawa, Dr Anna Achtelik-Franczak, Dr Błażej Tomiczek, Dr Magdalena Macek-Sroka, and Dr Wojciech Pakieła.

Author details

Leszek A. Dobrzański
Medical and Dental Engineering Centre for Research, Design and Production ASKLEPIOS, Gliwice, Poland

*Address all correspondence to: leszek.dobrzanski@centrumasklepios.pl

References

[1] Dobrzański LA. Engineering materials and material design. Fundamentals of materials science and metallurgy. 2nd ed changed and supplemented. Gliwice-Warszawa: WNT;2006. 1596 p. (in Polish)

[2] Mondolfo LF. Aluminum Alloys: Structure and Properties. Changed ed. London: Butterworths/Elsevier;2013. 17 p.

[3] Dobrzański LA. Metals and their alloys. Open Access Library Annal VII, vol. 2. Gliwice: International OCSCO World Press;2017. 982 p. (in Polish)

[4] Totten GE, MacKenzie DS. Handbook of Aluminum: Volume 2: Alloy production and materials manufacturing. New York, NY: Marcel Dekker Inc.;2003.

[5] Buckingham DA, Plunkert PA, Bray EL. Aluminium statistics. U.S. Geological survey [Internet]. Available from: http://minerals.usgs.gov/minerals/pubs/historicalstatistics/ds140-alumi.xlsx [Accessed: 2021-02-10]

[6] Bray EL, Weaver SM. Aluminum in November 2020. U.S. Geological survey [Internet]. Available from: https://prd-wret.s3.us-west-2.amazonaws.com/assets/palladium/production/atoms/files/mis-202011-alumi.pdf [Accessed: 2021-02-10]

[7] Richards JW. Aluminium; its history, occurrence, properties, metallurgy and applications, including its alloys. Philadelphia: H.C. Baird & co.; 1896. 750 p.

[8] Drozdov A. Aluminium: The Thirteenth Element. RUSAL Library; 2007. 240 p.

[9] Clapham JH, Power EE. The Cambridge Economic History of Europe: From the Decline of the Roman Empire. CUP Archive; 1941. 207 p.

[10] Setton KM. The papacy and the Levant: 1204-1571. 1 The thirteenth and fourteenth centuries. American Philosophical Society;1976.

[11] Örsted HC. Overview of the Royal Danish Science Society's Proceedings and the Work of its Members, from 31 May 1824 to 31 May 1825. 15-16 pp. (in Danish)

[12] Royal Danish Academy of Sciences and Letters. The philosophical and historical dissertations of the Royal Danish Science Society. 1827. xxv–xxvi pp. (in Danish)

[13] Wöhler F. Ueber das Aluminium. Annalen der Physik und Chemie. 1827; 87:146-161. DOI:10.1002/andp.18270870912

[14] Venetski S. Silver' from clay. Metallurgist. 1969;13: 451–453. DOI: 10.1007/BF00741130

[15] Evans JW. Metal Production: Electrometallurgy. In: Buschow KHJ, Cahn RW, Flemings MC, Ilschner B, Kramer EJ, Mahajan S, Veyssière P, editors. Encyclopedia of Materials: Science and Technology. 2nd ed. Pergamon; 2003. p. 1-12. DOI: 10.1016/B0-08-043152-6/01888-X

[16] Tabereaux AT, Peterson RD. Chapter 2.5 - Aluminum Production. In: Seetharaman S, editor. Treatise on Process Metallurgy, Vol. 3. Elsevier; 2014. P. 839-917. DOI: 10.1016/B978-0-08-096988-6.00023-7

[17] Panigrahi J, Sharma SC. Chapter 12 - Simulation, Control, and Optimization of Water Systems in Industrial Plants. In: Ranade VV, Bhandari VM, editors. Industrial Wastewater Treatment, Recycling and Reuse. Butterworth-Heinemann; 2014. p. 463-487. DOI: 10.1016/B978-0-08-099968-5.00012-X

[18] Haupin W. Aluminum Production and Refining. In: Buschow KHJ, Cahn RW, Flemings MC, Ilschner B, Kramer EJ, Mahajan S, Veyssière P, editors. Encyclopedia of Materials: Science and Technology. 2nd ed. Pergamon; 2003. p. 132-141. DOI: 10.1016/B0-08-043152-6/00029-2

[19] Bray EL. Aluminum in January 2021. U.S. Geological survey [Internet]. Available from: https://pubs.usgs.gov/periodicals/mcs2021/mcs2021-aluminum.pdf [Accessed: 2021-02-10]

[20] Bray EL. Bauxite and Alumina in January 2018. U.S. Geological survey [Internet]. Available from: https://s3-us-west-2.amazonaws.com/prd-wret/assets/palladium/production/mineral-pubs/bauxite/mcs-2018-bauxi.pdf [Accessed: 2021-02-10]

[21] Bray EL. Bauxite and Alumina in January 2020. U.S. Geological survey [Internet]. Available from: https://pubs.usgs.gov/periodicals/mcs2020/mcs2020-bauxite-alumina.pdf [Accessed: 2021-02-10]

[22] Bray EL. Bauxite and Alumina – 2017 [advance release]. U.S. Geological survey [Internet]. Available from: https://prd-wret.s3.us-west-2.amazonaws.com/assets/palladium/production/atoms/files/myb1-2017-bauxi.pdf [Accessed: 2021-02-10]

[23] Bray EL. Bauxite and Alumina in January 2021. U.S. Geological survey [Internet]. Available from: https://pubs.usgs.gov/periodicals/mcs2021/mcs2021-bauxite-alumina.pdf [Accessed: 2021-02-10]

[24] Types of Aluminum [Internet]. Available from: https://www.thomasnet.com/articles/metals-metal-products/types-of-aluminum/ [Accessed: 2021-02-10]

[25] Hirsch J. 23 - Aluminium sheet fabrication and processing. In: Lumley R, editor. Woodhead Publishing Series in Metals and Surface Engineering, Fundamentals of Aluminium Metallurgy. Woodhead Publishing; 2011. p. 719-746. DOI: 10.1533/9780857090256.3.719

[26] The Aluminum Association. International Alloy Designations and Chemical Composition Limits for Wrought Aluminum and Wrought Aluminum Alloys [Internet]. 2015. Available from: https://www.aluminum.org/sites/default/files/Teal%20Sheets.pdf [Accessed: 2021-02-10]

[27] ASTM B209M – 14. Standard Specification for Aluminum and Aluminum-Alloy Sheet and Plate (Metric). [Internet]. 2014. Available from: https://www.astm.org/Standards/B209M.htm [Accessed: 2021-02-10]

[28] ISO 3522:2007. Aluminium and aluminium alloys - Castings - Chemical composition and mechanical properties [Internet]. 2007. Available from: https://www.iso.org/committee/50152/x/catalogue/ [Accessed: 2021-02-10]

[29] ISO 6361-5:2011. Wrought aluminium and aluminium alloys — Sheets, strips and plates — Part 5: Chemical composition [Internet]. 2015. Available from: https://www.iso.org/obp/ui/#iso:std:iso:6361:-5:ed-1:v1:en [Accessed: 2021-02-10]

[30] Xometry Europe. Aluminium Alloys: Cross-Reference Table of Designation Standards [Internet]. 2019. Available from: https://xometry.de/en/aluminium-alloys-cross-reference-table-of-designation-standards/ [Accessed: 2021-02-10]

[31] Blaz L, Sugamata M, Kaneko J, Sobota J, Wloch G, Bochniak W, Kula A. Structure and properties of 6061+26 mass% Si aluminium alloy produced via coupled rapid solidification and KOBO-extrusion powder. Journal of Materials Processing Technology. 2009;209:

4329-4336. DOI: 10.1016/j.jmatprotec.2008.11.012

[32] Esawi AMK, Borady MAE. Carbon nanotube-reinforced aluminium strips. Composites Science and Technology. 2008;68:486-492. DOI: 10.1016/j.compscitech.2007.06.030

[33] Fogagnolo JB, Ruiz-Navas EM, Robert MH, Torralba JM. The effects of mechanical alloying on the compressibility of aluminium matrix composite powder. Materials Science and Engineering A. 2003;355:50-55. DOI: 10.1016/S0921-5093(03)00057-1

[34] Fogagnolo JB, Velasco F, Robert MH, Torralba JM. Effect of mechanical alloying on the morphology, microstructure and properties of aluminium matrix composite powders. Materials Science and Engineering A 2003;342: 131-143. DOI: 10.1016/S0921-5093(02)00246-0

[35] Gómez de Salazar JM, Barrena MI. The influence of Si and Mg rich phases on the mechanical properties of 6061 Al-matrix composites reinforced with Al_2O_3. Journal of Materials Science. 2002;37:1497-1502. DOI: 10.1023/A:1014967324577

[36] Mao J, Imai T, Dong S, Saito N, Shigematsu I, Kojima S, Ishikawa T. Superplasticity of nitride mullite short fiber-reinforced 6061 aluminium composites. Scripta Materialia. 2003;49:1061-1066. DOI: 10.1016/j.scriptamat.2003.08.017

[37] Ruiz-Navas EM, Fogagnolo JB, Velasco F, Ruiz-Prieto JM, Froyen L. One step production of aluminium matrix composite powders by mechanical alloying. Composites Part A. 2006;37:2114-2120. DOI: 10.1016/j.compositesa.2005.11.016

[38] Sivasankaran S, Sivaprasad K, Narayanasamy R, Iyer VK. Effect of strengthening mechanisms on cold workability and instantaneous strain hardening behavior during grain refinement of AA 6061-10 wt.% TiO_2 composite prepared by mechanical alloying. Journal of Alloys and Compounds. 2010;507:236-244. DOI: 10.1016/j.jallcom.2010.07.168

[39] Sivasankaran S, Sivaprasad K, Narayanasamy R, Iyer VK. Synthesis, structure and sinterability of 6061 AA100−x–x wt.% TiO_2 composites prepared by high-energy ball milling. Journal of Alloys and Compounds. 2010;491:712-721. DOI: 10.1016/j.jallcom.2009.11.051

[40] Son HT, Kim TS, Suryanarayana C, Chun BS. Homogeneous dispersion of graphite in a 6061 aluminum alloy by ball milling. Materials Science and Engineering A. 2003;348:163-169. DOI: 10.1016/S0921-5093(02)00749-9

[41] Wang L, Choi H, Myoung J-M, Lee W. Mechanical alloying of multi-walled carbon nanotubes and aluminium powders for the preparation of carbon/metal composites. Carbon. 2009;47:3427-3433. DOI: 10.1016/j.carbon.2009.08.007

[42] Wang RM, Surappa MK, Tao CH, Li CZ, Yan MG. Microstructure and interface structure studies of SiCp-reinforced Al (6061) metal-matrix composites. Materials Science and Engineering A. 1998;254:219-226. DOI: 10.1016/S0921-5093(98)00686-8

[43] Wu Y, Kim G-Y, Russell AM. Effects of mechanical alloying on an Al6061-CNT composites fabricated by semi-solid powder processing. Materials Science and Engineering A. 2012;538:164-172. DOI: 10.1016/j.msea.2012.01.025

[44] Wu Y, Kim G-Y, Russell AM. Mechanical alloying of carbon nanotube and Al6061 powder for metal matrix composites. Materials Science and

Engineering A. 2012;532:558-566. DOI: 10.1016/j.msea.2011.10.121

[45] Xia X, McQueen HJ. Deformation behaviour and microstructure of a 20% Al_2O_3 reinforced 6061 Al composite. Applied Composite Materials. 1997; 4:333-347. DOI: 10.1023/A: 1008862719958

[46] Adamiak M. The structure and selected properties of the EN AW6061 aluminium alloy base composites reinforced with Ti_3Al intermetallic particles. Composites. 2006;6:70-75. (in Polish)

[47] Adamiak M. Application of mechanical milling to composites materials production. Archives of Foundry. 2006;21:361-367. (in Polish)

[48] Arik H, Ozcatalbas Y, Turker M. Dry sliding wear behavior of in situ Al-Al_4C_3 metal matrix composite produced by mechanical alloying technique. Materials and Design. 2006;27:799-804. DOI: 10.1016/j.matdes.2005.01.024

[49] Bonollo F, Ceschini L, Garagnani GL. Mechanical and impact behaviour of (Al_2O_3)p/2014 and (Al_2O_3)p/6061 Al metal matrix composites in the 25-200°C range. Applied Composite Materials. 1997;4: 173-185. DOI: 10.1007/BF02481779

[50] Cui Y, Geng L, Yao CK. Interfacial bonding mechanisms and mechanical properties of squeeze-cast 6061 Al matrix composite reinforced with self-propagating high-temperature synthesized SiC particulates. Journal of Materials Science Letters. 1997;16: 788-790. DOI: 10.1023/A:1018514021685

[51] Dobrzański LA, Tomiczek B, Adamiak M. Manufacturing of EN AW6061 matrix composites reinforced by halloysite nanotubes. Journal of Achievements in Materials and Manufacturing Engineering. 2011;49: 82-89.

[52] Fogagnolo JB, Pallone EMJA, Martin DR, Kiminami CS, Bolfarini C, Botta WJ. Processing of Al matrix composites reinforced with Al-Ni compounds and Al_2O_3 by reactive milling and reactive sintering. Journal of Alloys and Compounds. 2009;471: 448-452. DOI: 10.1016/j. jallcom.2008.03.125

[53] Fogagnolo JB, Robert MH, Ruiz-Navas EM, Torralba JM. 6061 Al reinforced with zirconium dibromide particles processed by conventional powder metallurgy and mechanical alloying. Journal of Materials Science. 2004;39:127-132. DOI: 10.1023/B: JMSC.0000007736.03608.e5

[54] Fogagnolo JB, Robert MH, Torralba JM. Mechanically alloyed AlN particle- reinforced Al-6061 matrix composites: Powder processing, consolidation and mechanical strength and hardness of the as-extruded materials. Materials Science and Engineering A. 2006; 426:85-94. DOI: 10.1016/j. msea.2006.03.074

[55] Fogagnolo JB, Ruiz-Navas EM, Robert MH, Torralba JM. 6061 Al reinforced with silicon nitride particles processed by mechanical milling. Scripta Materialia. 2002;47: 243-248. DOI: 10.1016/S1359-6462(02) 00133-1

[56] Adamczyk J. Theoretical metallography. Vol. 2: Plastic deformation, strengthening and cracking. Gliwice: Silesian University of Technology Publishing House; 2012. (in Polish)

[57] Lin YC, Li HC, Liou SS, Shie MT. Mechanism of plastic deformation of powder metallurgy metal matrix composites of Cu-Sn/SiC and 6061/SiC under compressive stress. Materials Science and Engineering A. 2004;373: 363-369. DOI: 10.1016/j. msea.2004.02.011

[58] Parvin N, Assadifard R, Safarzadeh P, Sheibani S, Marashi P. Preparation and mechanical properties of SiC-reinforced Al6061 composite by mechanical alloying. Materials Science and Engineering A. 2008;492:134-140. DOI: 10.1016/j.msea.2008.05.004

[59] Qin S, Liu C, Chen J, Zhang G, Wang W. Characterization of thermal residual strain in SiCp/6061 Al composites by ultramicrohardness. Journal of Materials Science Letters. 1999;18:1099-1100. DOI: 10.1023/A:1006616109746

[60] Shakeri HR, Wang Z. Effect of alternative aging process on the fracture and interfacial properties of particulate Al_2O_3-reinforced Al (6061) metal matrix composite. Metallurgical and Materials Transactions A. 2006;33:1699-1713. DOI: 10.1007/s11661-002-0179-1

[61] Tomiczek B, Dobrzański LA. Composite materials with an aluminum alloy matrix EN AW6061 reinforced with nanotubes obtained from halloysite. In: Pacyna J, editor. Works of the XXXIX School of Materials Science and Engineering. Monograph. Kraków– Krynica; 2011. p. 342-346. (in Polish)

[62] Zhao N, Nash P, Yang X. The effect of mechanical alloying on SiC distribution and the properties of 6061 aluminum composite. Journal of Materials Processing Technology. 2005;170:586-592. DOI: 10.1016/j.jmatprotec.2005.06.037

[63] Dobrzański LA, Włodarczyk A, Adamiak M. Structure, properties and corrosion resistance of PM composite materials based on EN AW-2124 aluminum alloy reinforced with the Al_2O_3 ceramic particles. Journal of Materials Processing Technology. 2005;162:27-32. DOI: 10.1016/j.jmatprotec.2005.02.006

[64] Lu L, Lai MO, Ng CW. Enhanced mechanical properties of an Al based metal matrix composite prepared using mechanical alloying. Materials Science and Engineering A. 1998;252:203-211. DOI: 10.1016/S0921-5093(98)00676-5

[65] Włodarczyk-Fligier A, Dobrzański LA, Kremzer M, Adamiak M. Manufacturing of aluminium matrix composite materials reinforced by Al_2O_3 particles. Journal of Achievements in Materials and Manufacturing Engineering. 2008;27:99-102.

[66] Dobrzański LA, project manager. Research Project Report UMO-2013/08/M/ST8/00818. Investigations of structure and properties of newly created porous biomimetic materials fabricated by selective laser sintering, BIOLASIN. Silesian University of Technology; 2013-2016. (in Polish)

[67] Dobrzański LA, project manager. Research Project Report UMO-2012/07/B/ST8/04070. Determining the importance of the effect of the one-dimensional nanostructural materials on the structure and properties of newly developed functional nanocomposite and nanoporous materials, NANOCOPOR. Silesian University of Technology; 2013-2016. (in Polish)

[68] Dobrzański LA, project manager. Research Project Report UMO-2011/03/B/ST08/06076. Synergism of reinforcing with mineral halloysite nanotubes and as a result of the heat treatment of newly developer composite materials with the matrix made of aluminium alloys. Silesian University of Technology; 2012-2015. (in Polish)

[69] Dobrzański LA, contractor. Research Project Report UMO-2011/01/B/ST8/06663. Improving the functional properties of elements of light casting aluminium alloys heat treated by laser remelting and/or alloying the surface with carbides and/or ceramic particles.

Silesian University of Technology; 2011-2014. (in Polish)

[70] Dobrzański LA, project manager. Research Project Report UDA-POKL.04.01.01-00-003/09-00. Opening and development of engineering and PhD studies in the field of nanotechnology and materials science, INFONANO. Silesian University of Technology; 2009-2014. (in Polish)

[71] Dobrzański LA, project manager. Research Project Report UDA-POIG.01.01.01-00.23/08-00. Foresight of surface properties formation leading technologies of engineering materials and biomaterials, FORSURF. Silesian University of Technology; 2009-2012. (in Polish)

[72] Dobrzański LA, project manager. Research Project Report R15 007 02; development project. Improving the functional properties of elements of light casting magnesium and aluminium alloys heat treated by optimizing their chemical composition and by laser remelting and/or alloying the surface with carbides and/or ceramic particles. Silesian University of Technology; 2007-2009. (in Polish)

[73] Dobrzański LA, project manager. Research Project Report KBN Nr 3 T08A 041 30. Shaping the properties of composite Al-Al_2O_3 materials by changing the porosity, wettability and shape of the Al_2O_3 phase and infiltration conditions. Silesian University of Technology; 2006-2007. (in Polish)

[74] Dobrzański LA, project manager. Research Project Report KBN Nr 3 T08A 022 27. Development of a methodology for automated evaluation of the quality and structural defects in Al and Mg alloys with the use of artificial intelligence tools. Silesian University of Technology; 2004-2006. (in Polish)

[75] Kremzer M. Structure and properties of EN AC-AlSi12 matrix composite materials produced by pressure infiltration [PhD thesis]. Dobrzański LA, supervisory guidance. Gliwice: Silesian University of Technology; 2008. (in Polish)

[76] Tomiczek B. Structure and properties of nanostructured composite materials reinforced with halloysite [PhD thesis]. Dobrzański LA, supervisory guidance. Gliwice: Silesian University of Technology; 2013. (in Polish)

[77] Pakieła W. Influence of laser fusion of silicon and tungsten carbides on the structure and properties of the surface layer of Al-Mg alloys [PhD thesis]. Dobrzański LA, supervisory guidance. Gliwice: Silesian University of Technology; 2015. (in Polish)

[78] Kujawa M. AlSi12 infiltrated composite materials reinforced with sintered halloysite nanotubes [PhD thesis]. Dobrzański LA, supervisory guidance. Gliwice: Silesian University of Technology; 2015. (in Polish)

[79] Macek M. Structure and properties of aluminum nanocomposite materials reinforced with carbon nanotubes [PhD thesis]. Dobrzański LA, supervisory guidance. Gliwice: Silesian University of Technology; 2016. (in Polish)

[80] Achtelik-Franczak A. Engineering composite materials with the reinforcement of microporous titanium selectively sintered by laser [PhD thesis]. Dobrzański LA, supervisory guidance. Gliwice: Silesian University of Technology; 2016. (in Polish)

[81] Dobrzański LA, Kremzer M. Manufacture of composite materials by the infiltration of ceramic skeletons sintered with aluminum alloy. In: Proceedings of the IV Polish-Ukrainian Scientific and Technical Conference - Mechanics and Informatics;

Khmelnitskiy, Ukraine, 2006. p. 141-145. (in Polish)

[82] Dobrzański LA, Kremzer M, Nagel A. Application of pressure infiltration to the manufacturing of aluminium matrix composite materials with different reinforcement shape. Journal of Achievements in Materials and Manufacturing Engineering. 2007; 24:183-186.

[83] Dobrzański LA, Kremzer M, Gołombek K, Nagel A. Aluminium matrix composites fabricated by pressure infiltration process. Materials Engineering. 2007;28:520-523.

[84] Dobrzański LA, Kremzer M, Nowak AJ, Nagel A. Composite materials based on porous ceramic preforms infiltrated by aluminium alloy. Journal of Achievements in Materials and Manufacturing Engineering. 2007; 20:95-98.

[85] Dobrzański LA, Kremzer M, Drak M. Modern composite materials manufactured by pressure infiltration method. Journal of Achievements in Materials and Manufacturing Engineering. 2008;30:121-128.

[86] Dobrzański LA, Kremzer M, Gołombek K. Structure and Properties of Aluminum Matrix Composites Reinforced by Al_2O_3 Particles. Materials Science Forum. 2008;591-593:188-192. DOI: 10.4028/www.scientific.net/MSF.591-593.188

[87] Dobrzański LA, Kremzer M, Nowak AJ, Nagel A. Aluminium matrix composites fabricated by infiltration method. Archives of Material Science and Engineering. 2009;36:5-11.

[88] Dobrzański LA, Kremzer M, Nagel A. Structure and properties of ceramic preforms based on Al_2O_3 particles. Journal of Achievements in Materials and Manufacturing Engineering. 2009;35:7-13.

[89] Tomiczek B, Dobrzański LA. Structure and selected properties of composite materials reinforced with halloysite nanotubes. In: Pacyna J, editor. Works of the XL School of Materials Science and Engineering. Monograph. Cracow; 2012. p. 293-298 (in Polish)

[90] Dobrzański LA, Tomiczek B, Adamiak M, Gołombek K. Mechanically milled aluminium matrix composites reinforced with halloysite nanotubes. Journal of Achievements in Materials and Manufacturing Engineering. 2012; 55:654-660.

[91] Labisz K, Tański T, Dobrzański LA, Janicki D, Korcina K. HPDL laser alloying of Al-Si-Cu alloy with Al_2O_3 powder. Archives of Materials Science and Engineering. 2013;63:36-45.

[92] Dobrzański LA, Achtelik-Franczak A, Król M. Computer aided design in Selective Laser Sintering (SLS) – application in medicine. Journal of Achievements in Materials and Manufacturing Engineering 2013;60: 66-75.

[93] Dobrzański LA, Tomiczek B, Pawlyta M. Król M. Aluminium AlMg1SiCu matrix composite materials reinforced with halloysite particles. Archives of Metallurgy and Materials. 2014;59:335-338. DOI: 10.2478/amm-2014-0055

[94] Dobrzański LA, Tomiczek B, Matula G, Gołombek K. Role of halloysite nanoparticles and milling time on the synthesis of AA 6061 aluminium matrix composites. Advanced Materials Research. 2014;939:84-89. DOI: 10.4028/www.scientific.net/AMR.939.84

[95] Dobrzański LA, Macek M, Tomiczek B. Effect of carbon nanotubes content on morphology and properties of AlMg1SiCu matrix composite

powders. Archives of Materials Science and Engineering. 2014;69:12-18.

[96] Tomiczek B, Pawlyta M, Adamiak M, Dobrzański LA. Effect of milling time on microstructure of AA6061 composites fabricated via mechanical alloying. Archives of Metallurgy and Materials 2015; 60:789-793. DOI: 10.1515/amm-2015-0208

[97] Tomiczek B, Kujawa M, Matula G, Kremzer M, Tański T, Dobrzański LA. Aluminium AlSi12 alloy matrix composites reinforced by mullite porous preforms. Materialwissenschaft und Werkstofftechnik. 2015;46:368-376. DOI: 10.1002/mawe.201500411

[98] Dobrzański LA, Reimann Ł, Kujawa M, Tomiczek B. Corrosion behaviour of aluminium matrix composites reinforced with sintered halloysite nanotubes. Journal of Achievements in Materials and Manufacturing Engineering. 2015;73: 92-99.

[99] Tomiczek AE, Dobrzański LA, Macek M. Effect of milling time on microstructure and properties of AA6061/MWCNTS composite powders. Archives of Metallurgy and Materials. 2015;60:3029-3034. DOI: 10.1515/amm-2015-0484

[100] Dobrzański LA, Macek M, Tomiczek B, Pakieła W, Kremzer M. Influence of the milling time and MWCNT content on the wear properties of the AlMg1SiCu/MWCNT nanocomposites. Archives of Materials Science and Engineering. 2015;74:77-84.

[101] Dobrzański LA, Macek M, Tomiczek B, Nuckowski PM, Nowak AJ. The influence of the dispersion method on the microstructure and properties of MWCNTs/AA6061 composites. Archives of Metallurgy and Materials. 2016;61:1229-1234. DOI: 10.1515/amm-2016-0203

[102] Kujawa M, Dobrzański LA, Matula G, Kremzer M, Tomiczek B. Manufacturing of porous ceramic preforms based on halloysite nanotubes (HNTS). Archives of Metallurgy and Materials. 2016;61:917-922. DOI: 10.1515/amm-2016-0155

[103] Pawlyta M, Tomiczek B, Dobrzański LA, Kujawa M, Bierska-Piech B. Transmission electron microscopy observations on phase transformations during aluminium/mullite composites formation by gas pressure infiltration. Materials Characterization. 2016;114:9-17. DOI: 10.1016/j.matchar.2016.02.003

[104] Labisz K, Tański T, Janicki D, Borek W, Lukaszkowicz K, Dobrzański L.A. Effect of laser feeding on heat treated aluminium alloy surface properties. Archives of Metallurgy and Materials. 2016;61:741-746. DOI: 10.1515/amm-2016-0126

[105] Kujawa M, Suwak R, Dobrzański LA, Gerle A, Tomiczek B. Thermal characterization of halloysite materials for porous ceramic preforms. Archives of Materials Science and Engineering. 2021.

[106] Dobrzański LA, Kremzer M, Dziekońska M. Al_2O_3 preforms infiltrated by liquid aluminium alloy by deposition Ni-P coating. Archives of Materials Science and Engineering. 2012;55:14-21.

[107] Kujawa M, Kremzer M, Dobrzański LA. Manufacturing of aluminium matrix composite with gas pressure infiltration method. Proceedings of the 19th International Seminar of Ph.D. Students SEMDOK. 29-31.01.2014; Terchova, Slovakia; 2014. p. 38-41.

[108] Kujawa M, Dobrzański LA, Kremzer M. Production of porous ceramic skeletons based on mineral nanotubes obtained from halloysite.

Proceedings of the XLI School of Materials Science and Engineering. 24-27.09.2013; Cracow-Krynica; 2013. p. 319-325. (in Polish)

[109] Dobrzański LA, Tomiczek B, Pawlyta M, Nuckowski P. TEM and XRD study of nanostructured composite materials reinforced with the halloysite particles. Materials Science Forum. 2014;783-786:1591-1596. DOI: 10.4028/www.scientific.net/MSF.783-786.1591

[110] Dobrzański LA, Tomiczek B, Pawlyta M, Gołombek K. EN AW-AlMg1SiCu alloy matrix composite materials reinforced with halloysite particles manufactured by mechanical milling. Materials Engineering. 2014; 198:102-105.

[111] Tomiczek B, Dobrzański LA. Composite materials based on EN AW-AlMg1SiCu aluminium alloy reinforced with halloysite particles. Journal of Achievements in Materials and Manufacturing Engineering. 2013;61: 39-46.

[112] Dobrzański LA, Kremzer M, Adamiak M. The influence of reinforcement shape on wear behaviour of aluminium matrix composite materials. Journal of Achievements in Materials and Manufacturing Engineering. 2010;42:26-32.

[113] Bolewski A. Detailed mineralogy. Warsaw: Geological Publishing House; 1975. (in Polish)

[114] Stoch L. Clay minerals. Warsaw: Geological Publishing House; 1974. (in Polish)

[115] Szymański A. Technical Mineralogy. Warsaw: PWN; 1997. (in Polish)

[116] Das S, Kordijazi A, Akbarzadeh O, Rohatgi PK. An innovative process for dispersion of graphene nanoparticles and nickel spheres in A356 alloy using pressure infiltration technique. Engineering Reports. 2020;2:e12110. DOI: 10.1002/eng2.12110

[117] Shao P, Chen G, Ju B, Yang W, Zhang Q, Wang Z, Tan X, Pei Y, Zhong S, Hussain M, Wu G. Effect of hot extrusion temperature on graphene nanoplatelets reinforced Al6061 composite fabricated by pressure infiltration method. Carbon. 2020;162: 455-464. DOI: 10.1016/j.carbon.2020.02.080

[118] Zhang Q, Dong S, Ma S, Hou X, Yang W, Zhang Y, Wu G. Microstructure and compressive behavior of lamellar Al_2O_3p/Al composite prepared by freeze-drying and mechanical-pressure infiltration method. Science and Engineering of Composite Materials. 2020;27:1-9. DOI: 10.1515/secm-2020-0001

[119] Garcia-Cordovilla C, Louis E, Narciso J. Pressure infiltration of packed ceramic particulates by liquid metals. Acta Materialia 1999;47:4461-4479. DOI: 10.1016/S1359-6454(99)00318-3

[120] Daoud A. Microstructure and tensile properties of 2014 Al alloy reinforced with continuous carbon fibers manufactured by gas pressure infiltration. Materials Science and Engineering A. 2005;391:114-120. DOI: 10.1016/j.msea.2004.08.075

[121] Cook AJ, Werner PS. Pressure infiltration casting of metal matrix composites. Materials Science and Engineering A. 1991;144:189-206. DOI: 10.1016/0921-5093(91)90225-C

[122] Albiter A, Contreras A, Salazar M, Gonzalez-Rodriguez JG. Corrosion behaviour of aluminium metal matrix composites reinforced with TiC processed by pressureless infiltration. Journal of Applied Electrochemistry. 2006;36:303-308. DOI: 10.1007/s10800-005-9073-z

[123] Alonso A, Pamies A, Narciso J, Garcia-Cordovilla C, Louis E. Evaluation of the wettability of liquid aluminum with ceramic particulates (SiC, TiC, Al_2O_3) by means pressure infiltration. Metallurgical Transactions A. 1993;24:1423-1432. DOI: 10.1007/BF02668210

[124] Altinkok N, Demir A, Ozsert I, Processing of Al_2O_3/SiC ceramic cake preforms and their liquid metal infiltration. Composites A. 2003;34: 577-582. DOI: 10.1016/S1359-835X(03) 00125-8

[125] Canadan E, Ahlatci H, Cimenoglu H. Abrasive wear behaviour of Al-SiC composites produced by pressure infiltration technique. Wear. 2001;247:133-138. DOI: 10.1016/ S0043-1648(00)00499-3

[126] Cardinal S, R'Mili M, Merle P. Improvement of high pressure infiltration behavior of alumina platelet preforms: manufacture and characterization of hybrid performs. Composites A. 1998;29:1433-1441. DOI: 10.1016/S1359-835X(98)00026-8

[127] Carreno-Morelli E, Cutart T, Schaller R, Bonjour C. Processing and characterization of aluminium-based MMCs produced by gas pressure infiltration. Materials Science and Engineering A. 1998;251:48-57. DOI: 10.1016/S0921-5093(98)00649-2

[128] Chung WS, Lin SJ. Ni-Coated SiC_p reinforced aluminum composites processed by vacuum infiltration. Materials Research Bulletin. 1996;31: 1437-1447. DOI: 10.1016/S0025-5408 (96)00150-X

[129] Cornie JA. Advanced pressure infiltration casting technology produces near-absolute net-shape metal matrix composite components cost competitively. Materials Technology. 1995;10:43-48. DOI: 10.1080/ 10667857.1995.11752588

[130] Eardley ES, Flower HM. Infiltration and solidification of commercial purity aluminium matrix composites. Materials Science and Engineering A. 2003;359:303-312. DOI: 10.1016/S0921-5093(03)00357-5

[131] Assar A-EM. Fabrication of metal matrix composite by infiltration process – part 2: experimental study. Journal of Materials Processing Technology. 1999;86:152-158. DOI: 10.1016/S0924-0136(98)00304-5

[132] Garbellini O, Morando C, Biloni H, Papacio H. Infiltration of Saffil alumina fiber with AlCu and AlSi alloys. Scripta Materialia. 1999;41:187-193. DOI: 10.1016/S1359-6462(99)00141-4

[133] Luo ZP, Song YG, Zhang SQ. A TEM study of the microstructure of SiCp/Al composite prepared by pressureless infiltration method. Scripta Materialia. 2001;45:1183-1189. DOI: 10.1016/S1359-6462(01)01148-4

[134] McCullough C, Deve HE, Chanel TE. Mechanical response of continuous fiber-reinforced Al_2O_3-Al composites produced by pressure infiltration casting. Materials Science and Engineering A. 1994;189:147-154. DOI: 10.1016/0921-5093(94)90410-3

[135] Molina JM, Saravanan RA, Apron R, Garcia-Cordovilla C, Louis E, Narciso J. Pressure infiltration of liquid aluminium into packed SiC particulate with a bimodal size distribution. Acta Materialia. 2002;50:247-257. DOI: 10.1016/S1359-6454(01)00348-2

[136] Peng LM, Cao JW, Noda K, Han KS. Mechanical properties of ceramic-metal composites by pressure infiltration of metal into porous ceramics. Materials Science and Engineering A. 2004;374:1-9. DOI: 10.1016/j.msea.2003.12.027

[137] Srinivasa Rao B, Jayram V. Pressureless infiltration of Al-Mg based

alloys into Al_2O_3 preforms: mechanism and phenomenology. Acta Materialia. 2001;49:2373-2385. DOI: 10.1016/S1359-6454(01)00158-6

[138] Wannasin J, Flemings MC. Fabrication of metal matrix composites by high-pressure centrifugal infiltration process. Journal of Materials Processing Technology. 2005;169:143-149. DOI: 10.1016/j.jmatprotec.2005.03.004

[139] Zitnansky M, Martinovic M. Infiltration of the metal through a bundle of continual fibres. Journal of Materials Processing Technology. 2000; 106:163-166. DOI: 10.1016/S0924-0136(00)00609-9

[140] Maj J, Basista M, Węglewski W, Bochenek K, Strojny-Nędza A, Naplocha K, Panzner T, Tatarková M, Fiori F. Effect of microstructure on mechanical properties and residual stresses in interpenetrating aluminum-alumina composites fabricated by squeeze casting. Materials Science and Engineering A. 2018;715:154-162. DOI: 10.1016/j.msea.2017.12.091

[141] Dobrzański LA, Kremzer M, Nagel A, Huchler B. Fabrication of ceramic preforms based on Al_2O_3 CL 2500 powder. Journal of Achievements in Materials and Manufacturing Engineering. 2006;18:71-74.

[142] Dobrzański LA, Kremzer M, Nagel A, Huchler B. Structure and properties of porous preforms manufactured on the base of Al_2O_3 powder. Archives of Foundry. 2006;21: 149-154. (in Polish)

[143] Kremzer M, Dobrzański LA. Manufacture of porous ceramic frames based on Al_2O_3 powder. Works of the XXXIV School of Materials Science and Engineering. Kraków-Krynica;2006. p. 241-244. (in Polish)

[144] Mattern A, Huchler B, Stadenecker D, Oberacker R, Nagel A, Hoffmann MJ. Preparation of interpenetrating ceramic-metal composites. Journal of European Ceramic Society. 2004;24:3399-3408. DOI: 10.1016/j.jeurceramsoc.2003.10.030

[145] Naplocha K, Janus A, Kaczmar JW, Samsonowicz Z. Technology and mechanical properties of ceramic preforms for composite materials. Journal of Materials Processing Technology. 2000;106:119-122. DOI: 10.1016/S0924-0136(00)00601-4

[146] Dobrzański LA, Kremzer M, Adamiak M. Structure and tribological properties of aluminium matrix composites fabricated by pressure infiltration method. In: Proceedings of the 16th International Federation for Heat Treatment and Surface Engineering Congress; 2007.

[147] Dobrzański LA, Kremzer M, Gołombek K. Structure and properties of aluminum matrix composites reinforced by Al_2O_3 particles. In: Proceedings of the 6th International Latin American Conference on Powder Technology; 2007.

[148] Dobrzański LA, Kremzer M, Nagel A. Aluminium EN AC – AlSi12 alloy matrix composite materials reinforced by Al_2O_3 porous performs. Archives of Material Science and Engineering. 2007;28:593-596.

[149] Dobrzański LA, Kremzer M, Nagel A, Huchler B. Composite materials based on the porous Al_2O_3 ceramics infiltrated with the EN AC – AlSi12 alloy. In: Proceedings of the 3rd Scientific Conference MMME; Gliwice-Wisła; 2005. (CD-ROM).

[150] Dobrzański LA, Kremzer M, Nagel A, Huchler B. Composite materials based on Al_2O_3 porous ceramics infiltrated with EN AC-AlSi12 alloy, Composites. 2005;5:35-41.

[151] Dobrzański LA, Kremzer M, Nagel A. Influence of reinforcements shape on the structure and properties of Al-Al_2O_3 composite materials. In: Proceedings of the 11th International Research/Expert Conference Trends in the Development of Machinery and Associated Technology; 2007. p. 1479-1482.

[152] Dobrzański LA, Kremzer M. Structure and properties of EN AC-AlSi12 alloy reinforced by ceramic fibres and particles. In: Proceedings of PM 2006 World Congress and Exhibition; Busan, Korea; 2006. (CD-ROM)

[153] Dobrzański LA, Kremzer M. Manufacture of composite materials by the infiltration of ceramic skeletons sintered with aluminum alloy. Trailer of the Khmelnytsky National University. 2006;2:141-144. (in Polish)

[154] Dobrzański LA, Krupiński M, Konieczny J. The structure and properties of composite materials with an aluminum alloy matrix reinforced with SiC particles. In: Proceedings of the 12th International Scientific Conference AMME; Gliwice-Zakopane; 2003. p. 229-232. (in Polish)

[155] Morgiel J, Naplocha K, Pomorska M, Kaczmar J. Microstructure and tensile properties of composites with high strength aluminium alloys matrix reinforced with Saffil™ fibers. Composites. 2011;11:136-141.

[156] Zhang H, Maljkovic N, Mitchell BS. Structure and interfacial properties of nanocrystalline aluminum/mulite composites. Materials Science and Engineering A. 2002;326: 317-323. DOI: 10.1016/S0921-5093(01) 01500-3

[157] Zhiping L, Yinggang S, Shaoqing Z, Miller DJ. Interfacial microstructure in a B_4C/Al composite fabricated by pressureless infiltration. Metallurgical and Materials Transactions A. 2012;43: 281-293. DOI: 10.1007/s11661-011-0817-6

[158] Shang-Nan C, Jow-Lay H, Ding-Fwu L, Horng-Hwa L. The mechanical properties and microstructure of Al_2O_3/aluminum alloy composites fabricated by squeeze casting. Journal of Alloys and Compounds. 2007;436:124-130. DOI: 10.1016/j.jallcom.2006.07.062

[159] Loehman RE, Ewsuk KG, Fahrenholtz WG, Lakshman BB. Ceramic-metal composite formation by reactive metal penetration. Key Engineering Materials. 1996;127-131: 431-438. DOI: 10.4028/www.scientific.net/KEM.127-131.431

[160] Loehman RE, Ewsuk KG, Tomsia AP. Synthesis of Al_2O_3-Al composites by reactive metal penetration. Journal of American Society. 1996;79:27-32. DOI: 10.1111/j.1151-2916.1996.tb07876.x

[161] Naga SM, El-Maghraby A, El-Rafei AM. Properties of Ceramic - Metal Composites Formed by Reactive Metal Penetration. American Ceramic Society Bulletin. 2007;86:9301-9306.

[162] Sobczak J, Sobczak N. Squeeze Cast Aluminum and Magnesium Matrix Composites Reinforced with Short Alumina Fibers - Structure and Chemistry Characterization. Composites 2001;1:2155-159.

[163] Potoczek M, Śliwa RE. Microstructure and physical properties of AlMg/Al_2O_3 interpenetrating composites fabricated by metal infiltration into ceramic foams. Archives of Metallurgy and Materials. 2011;56: 1265-1269.

[164] Valdez S, Campillo B, Pérez R, Martínez L, García H A. Synthesis and microstructural characterization of Al-Mg alloy - SiC particle composite. Materials Letters. 2008;62:2623-2625. DOI: 10.1016/j.matlet.2008.01.002

[165] Freitas M, Pianaro SA, Nadal FN, Tebcherani SM, Berg EAT. Preparation and characterization of SiC/kaolin/Al composite materials by squeeze-casting. Cerâmica. 2009;55:271-280. DOI: 10.1590/S0366-69132009000300006

[166] Breslin MC, Ringnalda J, Xu L, Fuller M, Seeger J, Daehn GS, Otani T, Fraser HL. Processing, microstructure, and properties of co-continuous alumina-aluminum composites. Materials Science and Engineering A. 1995;195:113-119. DOI: 10.1016/0921-5093(94)06510-1

[167] Li W, Long JP, Jing S, Shen BL, Gao SJ, Tu MJ. Aging characteristics of short mulite fiber reinforced Al-4.0Cu-1.85Mg metal matrix composite. Journal of Materials Engineering and Performance. 2003;12:19-22. DOI: 10.1361/105994903770343420

[168] Dobrzański LA, Dobrzański LB, Dobrzańska-Danikiewicz AD. Overview of conventional technologies using the powders of metals, their alloys and ceramics in Industry 4.0 stage. Journal of Achievements in Materials and Manufacturing Engineering. 2020;98:56-85. DOI: 10.5604/01.3001.0014.1481

[169] Kim BM, Cho YK, Yoon SY, Stevens R, Park HC. Mullite whiskers derived from kaolin. Ceramics International. 2009;35:579-583. DOI: 10.1016/j.ceramint.2008.01.017

[170] Aksay IA, Dabbs DM, Sarikaya M. Mullite for structural, electronic, and optical applications. Journal of American Ceramic Society. 1991;74:2343-2358. DOI: 10.1111/j.1151-2916.1991.tb06768.x

[171] Kong LB, Zhang TS, Chen YZ, Ma J, Boey F, Huang H. Microstructural composite mullite derived from oxides via a high-energy ball milling process. Ceramics International. 2004;30:1313-1317. DOI: 10.1016/j.ceramint.2003.12.022

[172] Puff Z, Sałaciński R. Possibilities of obtaining mullite material with the participation of Al_2O_3 nanopowder. Glass and Ceramics. 2008;59:12-14. (in Polish)

[173] Anggono J. Mullite ceramics: its properties, structure, and synthesis. Jurnal Teknik Mesin Universitas Kristen Petra. 2005;7:1-10. DOI: 10.9744/jtm.7.1.pp. 1-10.

[174] Esharghawi A, Penot C, Nardou F. Contribution to porous mullite synthesis from clays by adding Al and Mg powders. Journal of the European Ceramic Society. 2009;29:31-38. DOI: 10.1016/j.jeurceramsoc.2008.05.036

[175] Cao GH, Shen GJ, Liu ZG, Wu SQ. Interface study of mullite short fibers reinforced Al-12Si alloy composites. Journal of Materials Science Letters. 2001;20:501-503. DOI: 10.1023/A:1010959912780

[176] Zawrah MF, Aly MH. In situ formation of Al_2O_3-SiC-mulite from Al-matrix composites. Ceramics International. 2006;32:21-28. DOI: 10.1016/j.ceramint.2004.12.005

[177] She JH, Mechnich P, Schneider H, Kanka B, Schmücker M. Infiltration behaviors of porous mullite/mullite preforms in aluminum-chloride solutions. Journal of Materials Science Letters. 2000;19:1887-1891. DOI: 10.1023/A:1006726425129

[178] Naplocha K, Granat K. The structure and properties of hybrid preforms for composite. Journal of Achievements in Materials and Manufacturing Engineering. 2007;22:35-38.

[179] Kaczmar JW, Kurzawa A. Structure and properties of porous ceramic preforms made of α-alumina particles. Archives of Foundry Engineering. 2010;10:157-162.

[180] Yamanaka T, Choi YB, Matsugi K, Yanagisawa O, Sasaki G. Influence of preform preparation condition on infiltration of molten aluminum. Journal of Materials Processing Technology. 2007;187-188:530-532. DOI: 10.1016/j.jmatprotec.2006.11.217

[181] Navacerrada MA, Fernández P, Díaz C, Pedrero A. Thermal and acoustic properties of aluminium foams manufactured by the infiltration process. Applied Acoustics. 2013;74: 496-501. DOI: 10.1016/j.apacoust.2012.10.006

[182] Zhao YY, Tao XF. Behaviour of metal matrix syntactic foams in compression. Proceedings of the Materials Science and Technology Conference; 2009. p. 1785-1794.

[183] Potoczek M, Śliwa RE, Myalski J, Śleziona J. Metal-ceramic interpenetrating composites produced by pressure infiltration of metal into ceramic foams. Ores and Non-ferrous Metals. 2009;54:688-692.

[184] Sobczak N, Jaworska L, Podsiadło M, Smuk B, Nowak R, Kurtyka P, Twardowska A. Nitride and carbide preforms for infiltration process. Archives of Materials Science and Engineering. 2007;28:653-656.

[185] Luyten J, Mullens S, Cooymans J, De Wilde AM, Thijs I, Kemps R. Different methods to synthesize ceramic foams. Journal of the European Ceramic Society. 2009;29: 829-832. DOI: 10.1016/j.jeurceramsoc.2008.07.039

[186] Hufenbach W, Gude M, Czulak A, Śleziona J, Dolata-Grosz A, Dyzia M. Development of textile-reinforced carbon fibre aluminium composites manufactured with gas pressure infiltration methods. Journal of Achievements in Materials and manufacturing Engineering. 2009;35: 177-183.

[187] Jiang J, Wang Y. Microstructure and mechanical properties of the rheoformed cylindrical part of 7075 aluminum matrix composite reinforced with nano-sized SiC particles. Materials and Design. 2015;79: 32-41. DOI: 10.1016/j.matdes.2015.04.040

[188] Liu Q, Ke L, Liu F, Huang C, Xing L. Microstructure and mechanical property of multi-walled carbon nanotubes reinforced aluminum matrix composites fabricated by friction stir processing. Materials and Design. 2013; 45:343-348. DOI: 10.1016/j.matdes.2012.08.036

[189] Su H, Gao W, Feng Z, Lu Z. Processing, microstructure and tensile properties of nano-sized Al_2O_3 particle reinforced aluminum matrix composites. Materials and Design. 2012; 36:590-596. DOI: 10.1016/j.matdes.2011.11.064

[190] Bandyopadhyay A, Espana F, Balla VK, Bose S, Ohgami Y, Davies NM. Influence of porosity on mechanical properties and in vivo response of Ti6Al4 implants. Acta Biomaterialia. 2010;6:1640-1648. DOI: 10.1016/j.actbio.2009.11.011

[191] Bibb R, Thompson D, Winder J. Computed tomography characterisation of additive manufacturing materials. Medical Engineering & Physics. 2011;33: 590-596. DOI: 10.1016/j.medengphy.2010.12.015

[192] Cader M, Trojnacki M. Analysis of the applicability of additive technology to fabrication of mobile robots construction. Measurements. Automation. Robotics. 2013;2:200-207. (in Polish)

[193] Contreras A, Lopez VH, Bedolla E. Mg/TiC composites manufactured by pressureless melt infiltration. Scripta Materialia. 2004;51:249-253. DOI: 10.1016/j.scriptamat.2004.04.007

[194] Dimitrov D, Schreve K, Beer N. Advances in three dimensional printing - state of the art and future perspectives. Rapid Prototyping Journal. 2006;12: 136-147. DOI: 10.1108/ 13552540610670717

[195] Dobrzański LA, Dobrzańska-Danikiewicz AD, Malara P, Gaweł TG, Dobrzański LB, Achtelik-Franczak A. Fabrication of scaffolds from Ti6Al4V powders using the computer aided laser method. Archives of Metallurgy and Materials. 2015;60:1065-1070. DOI: 10.1515/amm-2015-0260

[196] Dobrzański LA. Overview and general ideas of the development of constructions, materials, technologies and clinical applications of scaffolds engineering for regenerative medicine. Archives of Materials Science and Engineering. 2014;69:53-80.

[197] Esen Z, Bor S. Processing of titanium foams using magnesium spacer particles. Scripta Materialia. 2007;56: 341-344. DOI: 10.1016/j. scriptamat.2006.11.010

[198] Eshraghi S, Das S. Mechanical and microstructural properties of polycaprolactone scaffolds with one-dimensional, two-dimensional, and three-dimensional orthogonally oriented porous architectures produced by selective laser sintering, Acta Biomaterialia. 2010;6:2467-2476. DOI: 10.1016/j.actbio.2010.02.002

[199] Fukuda A, Takemoto M, Saito T, Fujibayashi S, Neo M, Pattanayak DK, Matsushita T, Sasaki K, Nishida N, Kokubo T, Nakamura T. Osteoinduction of porous Ti implants with a channel structure fabricated by selective laser melting. Acta Biomaterialia. 2011;7: 2327-2336. DOI: 10.1016/j. actbio.2011.01.037

[200] Gasser A, Backes G, Kelbassa I, Weisheit A, Wissenbach K. Laser additive manufacturing: laser metal deposition (LMD) and selective laser melting (SLM) in turbo-engine applications. Laser Material Processing. 2010;2:58-63. DOI: 10.1002/ latj.201090029

[201] Karageorgiou V, Kaplan D. Porosity of 3D biomaterial scaffolds. Biomaterials. 2005;26:5474-5491. DOI: 10.1016/j.biomaterials.2005.02.002

[202] Klimek M. The use of SLS technology in making permanent dental restorations. Prosthetics. 2012;12:47-55. (in Polish)

[203] Furumoto T, Koizumi A, Alkahari MR, Anayama R, Hosokawa A, Tanaka R, Ueda T. Permeability and strength of a porous metal structure fabricated by additive manufacturing. Journal of Materials Processing Technology. 2015;219:10-16. DOI: 10.1016/j.jmatprotec.2014.11.043

[204] Kolan KC, Doiphode ND, Leu MC. Selective laser sintering and freeze extrusion fabrication of scaffolds for bone repair using 13-93 bioactive glass: a comparison. In: Proceedings of the Solid Freeform Fabrication Symposium; Austin, Texas; 2010.

[205] Li JP, Habibovic P, van den Doel M, Wilson CE, de Wijn JR, van Blitterswijk CA, de Groot K. Bone ingrowth in porous titanium implants produced by 3D fiber deposition. Biomaterials. 2007;28: 2810-2820. DOI: 10.1016/j. biomaterials.2007.02.020

[206] Mazzoli A. Selective laser sintering in biomedical engineering. Medical and Biological Engineering and Computing. 2013;51:245-256. DOI: 10.1007/ s11517-012-1001-x

[207] Melchels FPW, Domingos MAN, Klein TJ, Malda J, Bartolo PJ, Hutmacher DW. Additive manufacturing of tissues and organs. Progress in Polymer Science. 2012;37:

1079-1104. DOI: 10.1016/j.progpolymsci.2011.11.007

[208] Nouri A, Hodgson PD, Wen C. Biomimetic Porous Titanium Scaffolds for Orthopedic and Dental Applications. In: Mukherjee A, editor. Biomimetics. Learning from Nature. IntechOpen; 2010. p. 415-450. DOI: 10.5772/8787

[209] Sachlos E, Czernuszka JT. Making tissue engineering scaffolds work. Review: the application of solid freeform fabrication technology to the production of tissue engineering scaffolds. European Cells & Materials. 2003;5:29-39. DOI: 10.22203/eCM.v005a03

[210] Salmoria GV, Fancello EA, Roesler CRM, Dabbas F. Functional graded scaffold of HDPE/HA prepared by selective laser sintering: microstructure and mechanical properties. International Journal of Advanced Manufacturing Technology. 2013;65:1529-1534. DOI: 10.1007/s00170-012-4277-y

[211] Simancik F. Metallic foams - ultra light materials for structural applications. Materials Engineering. 2001;5:823-828.

[212] Song Y, Yan Y, Zhang R, Xu D, Wang F. Manufacturing of the die of an automobile deck part based on rapid prototyping and rapid tooling technology. Journal of Materials Processing Technology. 2002;120:237-242. DOI: 10.1016/S0924-0136(01)01165-7

[213] Thomas CL, Gaffney TM, Kaza S, Lee CH. Rapid prototyping of large scale aerospace structures. In: Proceedings of Aerospace Applications Conference IEEE. 1996;4:219-230.

[214] Veiseh M, Edmondson D. Bone as an Open Cell Porous Material. ME 599K: Special Topics in Cellular Solids; 2003.

[215] Weisensel L, Travitzky N, Sieber H, Greil P. Laminated object manufacturing (LOM) of SiSiC composites. Advanced Engineering Materials. 2004;6:899-903. DOI: 10.1002/adem.200400112

[216] Xie F, He X, Cao S, Qu X. Structural and mechanical characteristics of porous 316L stainless steel fabricated by indirect selective laser sintering. Journal of Materials Processing Technology. 2013;213:838-843. DOI: 10.1016/j.jmatprotec.2012.12.014

[217] Meenashisundaram GK, Wang N, Maskomani S, Lu S, Anantharajan SK, Dheen ST, Nai SML, Fuh JYH, Wei J. Fabrication of Ti + Mg composites by three-dimensional printing of porous Ti and subsequent pressureless infiltration of biodegradable Mg. Materials Science and Engineering C. 2020;108:110478. DOI: 10.1016/j.msec.2019.110478

[218] Dobrzański LA, Dobrzańska-Danikiewicz AD, Czuba ZP, Dobrzański LB, AchtelikFranczak A, Malara P, Szindler M, Kroll L. Metallic skeletons as reinforcement of new composite materials applied in orthopaedics and dentistry. Archives of Materials Science and Engineering. 2018;92:53-85.DOI: 10.5604/01.3001.0012.6585

[219] Jurczyk M. Mechanical synthesis. Poznan: Poznan University of Technology Publishing House; 1998. (in Polish)

[220] Ozdemir I, Ahrens S, Mücklich S, Wielage B. Nanocrystalline Al-Al_2O_{3p} and SiC_p composites produced by high-energy ball milling. Journal of Materials Processing Technology. 2008;205:111-118. DOI: 10.1016/j.jmatprotec.2007.11.085

[221] Suryanarayana C. Mechanical alloying and milling. Progress in

Materials Science. 2001;46:1-184. DOI: 10.1016/S0079-6425(99)00010-9

[222] Kadi S, Lellou S, Marouf-Khelifa K, Schott J, Gener-Batonneau I, Khelifa A. Preparation, characterisation and application of thermally treated Algerian halloysite. Microporous and Mesoporous Materials. 2012;158:47-54. DOI: 10.1016/j.micromeso.2012.03.014

[223] MacKenzie KJD, Meinhold RH, Brown IWM, White GV. The formation of mullite from kaolinite under various reaction atmospheres. Journal of European Ceramic Society. 1996;16: 115-119. DOI: 10.1016/0955-2219(95) 00143-3

[224] Perera DS, Allott G. Mullite morphology in fired kaolinite/halloysite clays. Journal of Materials Science Letters. 1985;4:1270-1272. DOI: 10.1007/ BF00723478

[225] Tezuka N, Low I-M, Davies IJ, Prior M, Studer A. In situ neutron diffraction investigation on the phase transformation sequence of kaolinite and halloysite to mullite. Physica B. 2006;385-386:555-557. DOI: 10.1016/j. physb.2006.05.357

[226] Goda ES, Yoon KR, El-sayed SH, Hong SE. Halloysite nanotubes as smart flame retardant and economic reinforcing materials: A review. Thermochimica Acta. 2018;669:173-184. DOI: 10.1016/j.tca.2018.09.017

[227] Miyazaki M, Kamitani M, Takashi N, Kano J, Saito F. Amorphization of kaolinite and media motion in grinding by a double rotating cylinders mill – a comparison with a tumbling ball mill. Advanced Powder Technology. 2000;11:235-244. DOI: 10.1163/156855200750172349

[228] Schmücker M, Schneider H, MacKenzie KJD. Mechanical amorphization of mullite and thermal recrystallization. Journal of Non-Crystalline Solids. 1998;226: 99-104. DOI: 10.1016/S0022-3093(98) 00366-4

[229] Valášková M, Barabaszová K, Hundáková M, Ritz M, Plevová E. Effects of brief milling and acid treatment on two ordered and disordered kaolinite structures. Applied Clay Science. 2011;54:70-76. DOI: 10.1016/j.clay.2011.07.014

[230] Vizcayno C, de Gutiérrez RM, Castello R, Rodriguez E, Guerrero CE: Pozzolan obtained by mechanochemical and thermal treatments of kaolin. Applied Clay Science. 2010;49:405-413. DOI: 10.1016/j.clay.2009.09.008

[231] Arakawa S, Hatayama T, Matsugi K, Yanagisawa O. Effect of heterogeneous precipitation on age-hardening of Al_2O_3 particle dispersion Al-4mass%Cu composite produced by mechanical alloying. Scripta Materialia. 2000;42:755-760. DOI: 10.1016/ S1359-6462(99)00426-1

[232] Couper MJ, Parson NC. Precipitation Strengthening and Alloy Design for 6061 Al-Mg-Si Alloys In: Starke, Jr. EA, Sanders, Jr. TH, Cassada WA. Aluminium Alloys – Their Physical and Mechanical Properties 1. Wiley-VCH GmbH & Co. KGaA; 2008. p. 98-104.

[233] Maisonnette D, Suery M, Nelias D, Chaudet P, Epicier T. Effects of heat treatments on the microstructure and mechanical properties of a 6061 aluminium alloy. Materials Science and Engineering A. 2011;528:2718-2724. DOI: 10.1016/j.msea.2010.12.011

[234] Hirsch J, Skrotzki B, Gottstein G, editors. Aluminium Alloys. Their Physical and Mechanical Properties. Weinheim: Wiley-VCH Verlag GmbH & Co. KGaA; 2008.

[235] Jia DC, Li XL, Zhou Y, Han HQ. Effect of SiC particulate sizes on the

mechanical properties of Al-6Ti-6Nb matrix composites prepared by a mechanical alloying technique. Journal of Materials Science Letters. 1999;18: 2029-2032. DOI: 10.1023/A: 1006706505141

[236] Stobrawa J, Rdzawski Z, Głuchowski W, Malec W. Microstructure and properties of CuNi2Si1 alloy processed by continuous RCS method. Journal of Achievements in Materials and Manufacturing Engineering. 2009;37:466-479.

[237] NaturalNano [Internet]. 2015. Available from: www.naturalnano.com [Accessed: 2021-02-10]

[238] Wang L, Hu J, Li ZJ, Fei WD. Fracture behavior of aluminium borate whisker- reinforced aluminium alloy 6061 composite. Materials Science and Engineering A. 2008;497:358-362. DOI: 10.1016/j.msea.2008.07.018

[239] Kurzydłowski K, Lewandowska M, editors. Engineering, structural and functional nanomaterials. Warsaw: PWN; 2010. (in Polish)

[240] Hebda M, Wachal A. Tribology. Warsaw: WNT; 1980. (in Polish)

[241] Naplocha K, Kaczmar JW. Wear mechanisms of fiber reinforced composite materials based on 2024 and 7075 aluminum alloys. Journal of Achievements in Materials and Manufacturing Engineering. 2011;49: 180-187.

[242] Esawi AMK, Morsi K, Sayed A, Abdel Gawad A, Borah P. Fabrication and properties of dispersed carbon nanotube–aluminum composites. Materials Science and Engineering A. 2009;508:167-173. DOI: 10.1016/j.msea.2009.01.002

[243] Liu ZY, Xiao BL, Wang WG, Ma ZY. Tensile Strength and Electrical Conductivity of Carbon Nanotube Reinforced Aluminum Matrix Composites Fabricated by Powder Metallurgy Combined with Friction Stir Processing. Journal of Materials Science & Technology. 2014;30:649-655. DOI: 10.1016/j.jmst.2014.04.016

[244] Morsi K, Esawi A. Effect of mechanical alloying time and carbon nanotube (CNT) content on the evolution of aluminum (Al)–CNT composite powders. Journal of Materials Science. 2007;42:4954-4959. DOI: 10.1007/s10853-006-0699-y

[245] Nouri N, Ziaei-Rad S, Adibi S, Karimzadeh F. Fabrication and mechanical property prediction of carbon nanotube reinforced Aluminum nanocomposites. Materials and Design. 2012;34:1-14. DOI: 10.1016/j.matdes.2011.07.047

[246] Peng T, Chang I. Mechanical alloying of multi-walled carbon nanotubes reinforced aluminum composite powder. Powder Technology. 2014;266:7-15. DOI: 10.1016/j.powtec.2014.05.068

[247] Chen B, Li Z, Shen J, Li S, Jia L, Umeda J, Kondoh K, Li J.S. Mechanical properties and strain hardening behavior of aluminum matrix composites reinforced with few-walled carbon nanotubes. Journal of Alloys and Compounds. 2020;826: 154075. DOI: 10.1016/j.jallcom.2020.154075

[248] Guo B, Du Y, Yan N, Song M. Mechanical properties and microstructures of Al-10Mg-4.5Si matrix composites reinforced by carbon nanotubes. Journal of Alloys and Compounds. 2019;792:860-868. DOI: 10.1016/j.jallcom.2019.04.101

[249] Turan ME. Investigation of mechanical properties of carbonaceous (MWCNT, GNPs and C60) reinforced hot-extruded aluminum matrix composites. Journal of Alloys and

Compounds. 2019;788:352-360. DOI: 10.1016/j.jallcom.2019.02.25

[250] Mokdad F, Chen DL, Liu ZY, Xiao BL, Ni DR, Ma ZY. Deformation and strengthening mechanisms of a carbon nanotube reinforced aluminum composite. Carbon. 2016;104:64-77. DOI: 10.1016/j.carbon.2016.03.038

[251] Bradbury CR, Gomon J-K, Kollo L, Kwon H, Leparoux M. Hardness of Multi Wall Carbon Nanotubes reinforced aluminium matrix composites. Journal of Alloys and Compounds. 2014;585:362-367. DOI: 10.1016/j.jallcom.2013.09.142

[252] Li H, Kang J, He C, Zhao N, Liang C, li B. Mechanical properties and interfacial analysis of aluminum matrix composites reinforced by carbon nanotubes with diverse structures. Materials Science and Engineering A. 2013;577:120-124. DOI: 10.1016/j.msea.2013.04.035

[253] Pérez-Bustamante R, Pérez-Bustamante F, Estrada-Guel I, Santillán-Rodríguez CR, Matutes-Aquino JA, Herrera-Ramírez JM, Miki-Yoshida M, Martínez-Sánchez R. Characterization of Al2024-CNTs composites produced by mechanical alloying. Powder Technology. 2011;212:390-396. DOI: 10.1016/j.powtec.2011.06.007

[254] Pérez-Bustamante R, Pérez-Bustamante F, Estrada-Guel I, Licea-Jiménez L, Miki-Yoshida M, Martínez-Sánchez R. Effect of milling time and CNT concentration on hardness of CNT/Al2024 composites produced by mechanical alloying. Materials Characterization. 2013;75:13-19. DOI: 10.1016/j.matchar.2012.09.005

[255] Simões S, Viana F, Reis MAL, Vieira MF. Improved dispersion of carbon nanotubes in aluminum nanocomposites. Composite Structures. 2014;108:992-1000. DOI: 10.1016/j.compstruct.2013.10.043

[256] Esawi AMK, Morsi K, Sayed A, Taher M, Lanka S. Effect of carbon nanotube (CNT) content on the mechanical properties of CNT-reinforced aluminium composites. Composites Science and Technology. 2010;70:2237-2241. DOI: 10.1016/j.compscitech.2010.05.004

[257] Esawi AMK, Morsi K, Sayed A, Taher M, Lanka S. The influence of carbon nanotube (CNT) morphology and diameter on the processing and properties of CNT-reinforced aluminium composites. Composites Part A. 2011;42:234-243. DOI: 10.1016/j.compositesa.2010.11.008

[258] Javadi AH, Mirdamadi Sh, Faghihisani MA, Shakhesi S, Soltani R. Fabrication of well-dispersed, multiwalled carbon nanotubes-reinforced aluminum matrix composites. New Carbon Materials. 2012;27:161-165. DOI: 10.1016/S1872-5805(12)60010-9

[259] Kwon H, Park DH, Silvain JF, Kawasaki A. Investigation of carbon nanotube reinforced aluminum matrix composite materials. Composites Science and Technology. 2010;70:546-550. DOI: 10.1016/j.compscitech.2009.11.025

[260] Morsi K, Esawi AMK, Lanka S, Sayed A, Taher M. Spark plasma extrusion (SPE) of ball-milled aluminum and carbon nanotube reinforced aluminum composite powders. Composites Part A. 2010;41:322-326. DOI: 10.1016/j.compositesa.2009.09.028

[261] Poirier D, Gauvin R, Drew RAL. Structural characterization of a mechanically milled carbon nanotube/aluminum mixture. Composites Part A. 2009;40:1482-1489. DOI: 10.1016/j.compositesa.2009.05.025

[262] Ram HRA, Koppad PG, Kashyap KT. Nanoindentation studies

on MWCNT/aluminum alloy 6061 nanocomposites. Materials Science and Engineering A. 2013;559:920-923. DOI: 10.1016/j.msea.2012.08.143.

[263] Wu Y, Kim G-Y. Carbon nanotube reinforced aluminum composite fabricated by semi-solid powder processing. Journal of Materials Processing Technology. 2011;211: 1341-1347. DOI: 10.1016/j.jmatprotec.2011.03.007

[264] Housaer F, Beclin F, Touzin M, Tingaud D, Legris A, Addad A. Interfacial characterization in carbon nanotube reinforced aluminum matrix composites. Materials Characterization. 2015;110:94-101. DOI: 10.1016/j.matchar.2015.10.014

[265] Ci L, Ryu Z, Jin-Phillipp NY, Rühle M. Investigation of the interfacial reaction between multi-walled carbon nanotubes and aluminium. Acta Materialia. 2006;54:5367-5375. DOI: 10.1016/j.actamat.2006.06.031

[266] Laha T, Kuchibhatla S, Seal S, Li W, Agarwal A. Interfacial phenomena in thermally sprayed multiwalled carbon nanotube reinforced aluminum nanocomposite. Acta Materialia. 2007; 55:1059-1066. DOI: 10.1016/j.actamat.2006.09.025

[267] Zhou W, Sasaki S, Kawasaki A. Effective control of nanodefects in multiwalled carbon nanotubes by acid treatment. Carbon. 2014;78:121-129. DOI: 10.1016/j.carbon.2014.06.055

[268] Liu ZY, Xiao BL, Wang WG, Ma ZY. Modelling of carbon nanotube dispersion and strengthening mechanisms in Al matrix composites prepared by high energy ball milling-powder metallurgy method. Composites Part A. 2017;94:189-198. DOI: 10.1016/j.compositesa.2016.11.029

[269] Wang W, Li Q, Ma R, Cui Y, Cao X, Wang X. Effects of the Si contents of an infiltrating aluminium alloy on the microstructure and strength of SiC matrix composites. Ceramics International. 2017;43:12526-12533.DOI: 10.1016/j.ceramint.2017.06.125

[270] Kwon H, Estili M, Takagi K, Miyazaki T, Kawasaki A. Combination of hot extrusion and spark plasma sintering for producing carbon nanotube reinforced aluminum matrix composites. Carbon. 2009;47:570-577. DOI: 10.1016/j.carbon.2008.10.041

[271] Yan H, Qiu H. Fabrication of carbon nanotube reinforced A356 nanocomposites. Journal of Materials Research. 2016;31:2277-2283. DOI: 10.1557/jmr.2016.258

[272] Zhou W, Yamamoto G, Fan Y, Kwon H, Hashida T, Kawasaki A. In-situ characterization of interfacial shear strength in multi-walled carbon nanotube reinforced aluminum matrix composites. Carbon. 2016;106: 37-47. DOI: 10.1016/j.carbon.2016.05.015

[273] Zhou W, Yamaguchi T, Kikuchi K, Nomura N, Kawasaki A. Effectively enhanced load transfer by interfacial reactions in multi-walled carbon nanotube reinforced Al matrix composites. Acta Materialia. 2017;125: 369-376. DOI: 10.1016/j.actamat.2016.12.022

[274] Liu X, Liu E, Li J, He C, Zhao N. Investigation of the evolution and strengthening effect of aluminum carbide for in-situ preparation of carbon nanosheets/aluminum composites. Materials Science and Engineering A. 2019;764:138139. DOI: 10.1016/j.msea.2019.138139

[275] Raviathul Basariya M, Srivastava VC, Mukhopadhyay NK. Microstructural characteristics and mechanical properties of carbon nanotube reinforced aluminum alloy composites produced by ball milling.

Materials and Design. 2014;64:542-549. DOI: 10.1016/j.matdes.2014.08.019

[276] Choi HJ, Lee SM, Bae DH. Wear characteristic of aluminum-based composites containing multi-walled carbon nanotubes. 2010;270:12-18. DOI: 10.1016/j.wear.2010.08.024

[277] Afzal N, Rafique M, Javaid W, Ahmad R, Farooq A, Saleem M, Khaliq Z. Influence of carbon ion implantation energy on aluminum carbide precipitation and electrochemical corrosion resistance of aluminum. Nuclear Instruments and Methods in Physics Research Section B: Beam Interactions with Materials and Atoms. 2018;436:84-91. DOI: 10.1016/j.nimb.2018.09.008

[278] Yolshina LA, Muradymov RV, Korsun IV, Yakovlev GA, Smirnov S.V. Novel aluminum-graphene and aluminum-graphite metallic composite materials: Synthesis and properties. Journal of Alloys and Compounds. 2016; 663:449-459. DOI: 10.1016/j.jallcom.2015.12.084

[279] Chen B, Shen J, Ye X, Imai H, Umeda J, Takahashi M, Kondoh K. Solid-state interfacial reaction and load transfer efficiency in carbon nanotubes (CNTs)-reinforced aluminum matrix composites. Carbon. 2017;114:198-208. DOI: 10.1016/j.carbon.2016.12.013

[280] Dobrzański LA, Dobrzańska-Danikiewicz AD. Surface treatment of engineering materials. Open Access Library, vol. 5. Gliwice: International OCSCO World Press; 2011. 480 p. (in Polish)

[281] Feng W, Patel SH, Young M-Y, Zunino III JL, Xanthos M. Smart polymeric coatings—recent advances. Advances in Polymer Technology. 2007; 26:1-13. DOI: 10.1002/adv.20083

[282] Firouzi A, Del Gaudio C, lamastra FR, Montesperelli G, Bianco A. Electrospun polymeric coatings on aluminum alloy as a straightforward approach for corrosion protection. Journal of Applied Polymer Science. 2015;132:41250. DOI: 10.1002/app.41250

[283] Wankhede RG, Morey S, Khanna AS, Birbilis N. Development of water-repellent organic–inorganic hybrid sol–gel coatings on aluminum using short chain perfluoro polymer emulsion. Applied Surface Science. 2013;283:1051-1059. DOI: 10.1016/j.apsusc.2013.07.066

[284] Galvão TLP, Bouali AC, Serdechnova M, Yasakau KA, Zheludkevich ML, Tedim J. Chapter 16 - Anticorrosion thin film smart coatings for aluminum alloys. In: Makhlouf ASH, Abu-Thabit NY, editors. Advances in Smart Coatings and Thin Films for Future Industrial and Biomedical Engineering Applications. Elsevier; 2020. p. 429-454. DOI: 10.1016/B978-0-12-849870-5.00007-0

[285] Xiong G, Elam JW, Feng H, Han CY, Wang H-H, Iton LE, Curtiss LA, Pellin MJ, Kung M, Kung H, Stair PC. Effect of Atomic Layer Deposition Coatings on the Surface Structure of Anodic Aluminum Oxide Membranes. The Journal of Physical Chemistry B. 2005;109:14059-14063. DOI: 10.1021/jp0503415

[286] Sharma K. Spatial atomic layer deposition on flexible porous substrates: ZnO on anodic aluminum oxide films and Al_2O_3 on Li ion battery electrodes. Journal of Vacuum Science & Technology A. 2016;34:01A146. DOI: 10.1116/1.4937728

[287] Hennessy JJ, Balasubramanian K, Moore CS, Jewell AD, Nikzad S, France KC, Quijada MA. Performance and prospects of far ultraviolet aluminum mirrors protected by atomic layer deposition. Journal of

Astronomical Telescopes, Instruments, and Systems. 2016;2:041206. DOI: 10.1117/1.JATIS.2.4.041206

[288] Elam JW, Xiong G, Han CY, Wang H-H, Birrell JP, Welp U, Hryn JN, Pellin MJ, Baumann TF, Poco JF, Satcher Jr. JH. Atomic Layer Deposition for the Conformal Coating of Nanoporous Materials. Journal of Nanomaterials. 2006;2006:64501. DOI: 10.1155/JNM/2006/64501

[289] Kennedy E, Byrne G, Collins DN. A review of the use of high power diode lasers in surface hardening. Journal of Materials Processing Technology. 2004; 155-156:1855-1860. DOI: 10.1016/j.jmatprotec.2004.04.276

[290] Dobrzański LA, Bonek M, Hajduczek E, Klimpel A, Lisiecki A. Application of high power diode laser (HPDL) for alloying of X40CrMoV5-1 steel surface layer by tungsten carbides. Journal of Materials Processing Technology. 2004;155-156:1956-1963. DOI: 10.1016/j.jmatprotec.2004.04.058

[291] Dobrzański LA, Bonek M, Piec M, Jonda E. Diode laser modification of surface gradient layer properties of a hot-work tool steel. Materials Science Forum. 2006;532-533:657-660. DOI: 10.4028/www.scientific.net/MSF.532-533.657

[292] Chi Y, Gu G, Yu H, Chen C. Laser surface alloying on aluminum and its alloys: A review. Optics and Lasers in Engineering. 2018;100:23-37. DOI: 10.1016/j.optlaseng.2017.07.006

[293] Dobrzański LA, Dobrzańska-Danikiewicz AD. Applications of Laser Processing of Materials in Surface Engineering in the Industry 4.0 Stage of the Industrial Revolution. Materials Performance and Characterization. 2019;8:1091-1129. DOI: 10.1520/MPC20190203

[294] Dobrzański LA, Dobrzański LB, Dobrzańska-Danikiewicz AD, Kraszewska M. Manufacturing powders of metals, their alloys and ceramics and the importance of conventional and additive technologies for products manufacturing in Industry 4.0 stage. Archives of Materials Science and Engineering. 2020;102:13-41. DOI: 10.5604/01.3001.0014.1452

[295] Dobrzański LA, Dobrzański LB, Dobrzańska-Danikiewicz AD. Manufacturing technologies thick-layer coatings on various substrates and manufacturing gradient materials using powders of metals, their alloys and ceramics. Journal of Achievements in Materials and Manufacturing Engineering. 2020;99:14-41. DOI: 10.5604/01.3001.0014.1598

[296] Yue TM, Yan LJ, Chan CP, Dong CF, Man HC, Pang GKH. Excimer laser surface treatment of aluminum alloy AA7075 to improve corrosion resistance. Surface and Coatings Technology. 2004;179:158-164. DOI: 10.1016/S0257-8972(03)00850-8

[297] Zhang QY, Li XQ, Wang DY, Tian YS, Aleem BJA. Laser surface treatment of Aluminum alloys. Mater Heat Treatment. 2010;39:120-125.

[298] Ji H, Xu Y, Lu ZS, Zhou DR. Progress in strengthening of aluminium alloy surface by laser. Material Science and Technology. 2003;11:220-224.

[299] Gordani GR, ShojaRazavi R, Hashemi SH, Isfahani ARN. Laser surface alloying of an electroless Ni–P coating with Al-356 substrate. Optics and Lasers in Engineering. 2008;46: 550-557. DOI: 10.1016/j.optlaseng.2008.02.002

[300] Staia MH, Cruz M, Dahotre NB. Microstructural and tribological characterization of an A-356 aluminum alloy superficially modified by laser alloying. Thin Solid Films. 2000; 377-378:665-674. DOI: 10.1016/S0040-6090(00)01448-6

[301] Chuang YC, Le SC, Lin HC. Effect of temperature on the sliding wear behavior of laser surface alloyed Ni-base on Al–Mg–Si alloy. Applied Surface Science. 2006;253:1404-1410. DOI: 10.1016/j.apsusc.2006.02.014

[302] Vaziri SA, Shahverdi HR, Torkamany MJ, Shabestari SG. Effect of laser parameters on properties of surface-alloyed Al substrate with Ni. Optics and Lasers in Engineering. 2009; 47:971-975. DOI: 10.1016/j.optlaseng.2009.04.007

[303] Liu W, Li X, Yu XT, Mo YM. Laser surface alloyed technology on Al alloys. Science and Technology of Overseas Building Materials. 2006;4:56-58.

[304] Kadolkar P, Dahotre NB. Effect of processing parameters on the cohesive strength of laser surface engineered ceramic coatings on aluminum alloys. Materials Science and Engineering A. 2003;342:183-191. DOI: 10.1016/S0921-5093(02)00286-1

[305] Nath S, Pityana S, Majumdar JD. Laser surface alloying of aluminium with WC+Co+NiCr for improved wear resistance. Surface and Coatings Technology. 2012;206:3333-3341. DOI: 10.1016/j.surfcoat.2012.01.038

[306] Geng H, Niu Y, Tian X, Chen C, Hou X. Laser surface strengthening process of Al-Si base alloy. Journal of Materials Science and Technology. 2001;17:115-118.

[307] Chong PH, Man HC, Yue TM. Microstructure and wear properties of laser surface-cladded Mo·WC MMC on AA6061 aluminum alloy. Surface and Coatings Technology. 2001;145: 51-59. DOI: 10.1016/S0257-8972(01)01286-5

[308] Almeida A, Petrov P, Nogueira I, Vilar R. Structure and properties of Al—Nb alloys produced by laser surface alloying. Materials Science and Engineering A. 2001;303:273-280. DOI: 10.1016/S0921-5093(00)01838-4

[309] Rajamure RS, Vora HD, Srinivasan SG, Dahotre NB. Laser alloyed Al—W coatings on aluminum for enhanced corrosion resistance. Applied Surface Science. 2015;328:205-214. DOI: 10.1016/j.apsusc.2014.12.037

[310] Watkins KG, McMahon MA, Steen WM. Microstructure and corrosion properties of laser surface processed aluminium alloys: a review. Materials Science and Engineering A. 1997;231:55-61. DOI: 10.1016/S0921-5093(97)00034-8

[311] Yilbas BS, Karatas C, Karakoc H, Aleem BJA, Khan S, Al-Aqeeli N. Laser surface treatment of aluminum based composite mixed with B_4C particles. Optics and Laser Technology. 2015;66: 129-137. DOI: 10.1016/j.optlastec.2014.08.014

[312] Staia MH, Cruz M, Dahotre NB. Wear resistance of a laser alloyed A-356 aluminum/WC composite. Wear. 2001; 251:1459-1468. DOI: 10.1016/S0043-1648(01)00789-X

[313] Man HC, Kwok CT, Yue TM. Cavitation erosion and corrosion behaviour of laser surface alloyed MMC of SiC and SiN on Al alloy AA6061. Surface and Coating Technology. 2000; 132:11-20. DOI: 10.1016/S0257-8972(00)00729-5

[314] Vreeling JA, k VO, Hamstra GA, Pei YT, De Hosson JTM. In-situ microscopy investigation of failure mechanisms in Al/SiC_p metal matrix composite produced by laser embedding. Scripta Materialia. 2000;42: 589-595. DOI: 10.1016/S1359-6462(99)00404-2

[315] Man HC, Zhang S, Cheng FT, Yue TM. In situ synthesis of TiC reinforced surface MMC on Al6061 by laser surface alloying. Scripta Materialia.

2002;46:229-234. DOI: 10.1016/S1359-6462(01)01230-1

[316] Tomida S, Nakata K, Saji S, Kubo T. Formation of metal matrix composite layer on aluminum alloy with TiC-Cu powder by laser surface alloying process. Surface and Coating Technology. 2001;142:585-589. DOI: 10.1016/S0257-8972(01)01172-0

[317] Dubourg L, Ursescu D, Hlawka F, Cornet A. Laser cladding of MMC coatings on aluminium substrate: influence of composition and microstructure on mechanical properties. Wear. 2005;258:1745-1754. DOI: 10.1016/j.wear.2004.12.010

[318] Dobrzański LA. Significance of materials science for the future development of societies. Journal of Materials Processing Technology. 2006; 175:133-148. DOI: 10.1016/j.jmatprotec.2005.04.003

[319] Dobrzański LA, Dobrzański LB. Approach to the design and manufacturing of prosthetic dental restorations according to the rules of the Industry 4.0. Materials Performance and Characterization. 2020;9:394-476. DOI: 10.1520/MPC20200020

[320] Dobrzański LA, Dobrzański LB. Dentistry 4.0 Concept in the Design and Manufacturing of Prosthetic Dental Restorations. Processes. 2020;8:525. DOI: 10.3390/pr8050525

[321] Dobrzański LA. Role of materials design in maintenance engineering in the context of industry 4.0 idea. Journal of Achievements in Materials and Manufacturing Engineering. 2019;96: 12-49. DOI: 10.5604/01.3001.0013.7932

[322] Dobrzański LA, Dobrzańska-Danikiewicz AD. Why are Carbon-Based Materials Important in Civilization Progress and Especially in the Industry 4.0 Stage of the Industrial Revolution?. Materials Performance and Characterization. 2019;8:337-370. DOI: 910.1520/MPC20190145

[323] Dobrzański LA. Chapter 5 - Effect of heat and surface treatment on the structure and properties of the Mg-Al-Zn-Mn casting alloys. In: Dobrzański LA, Totten GE, Bamberger M, editors. Magnesium and Its Alloys. Boca Raton, FL: CRC Press; 2019. p. 91-202.

[324] Dobrzański LA. Fundamentals of material design methodology. Gliwice: Silesian University of Technology Publishing House; 2009. (in Polish)

[325] Dobrzańska-Danikiewicz AD. The State of the Art Analysis and Methodological Assumptions of Evaluation and Development Prediction for Materials Surface Technologies. Journal of Achievements in Materials and Manufacturing Engineering. 2011; 49:121-141.

[326] Materials Selection in Mechanical Design. Oxford, UK: Pergamon Press; 1992.

[327] Waterman NA, Ashby MF, editors. The Materials Selector. 3 vols. London: Chapman & Hall; 1997.

[328] Ashby MF. Materials Selection in Mechanical Design. 4th ed. Burlington, MA: Butterworth-Heinemann; 2011.

[329] Ashby MF, Jones DRH. Engineering Materials 1: An Introduction to Properties, Applications and Design. Waltham, MA: Butterworth-Heinemann; 2012.

[330] Ashby MF, Jones DRH. Engineering Materials 2: An Introduction to Microstructures and Processing. Waltham, MA: Butterworth-Heinemann; 2013.

[331] Oztemel E, Gursev S. Literature Review of Industry 4.0 and Related Technologies. Journal of Intelligent

Manufacturing. 2020;31: 127-182. DOI: 10.1007/s10845-018-1433-8

[332] Dobrzański LA. Structural Phenomena Accompanying the Production of Composite and Nanocomposite Materials Using Selected Technologies. Invited lecture at the 22nd Physical Metallurgy and Materials Science Conference: Advanced Materials and Technologies; 9-12 June 2019; Bukowina Tatrzańska, Poland.

[333] Dobrzański LA. Role of Materials Design in Maintenance Engineering in the Context of Industry 4.0 Idea. Invited lecture at the International Maintenance Technologies Congress and Exhibition; 26-28 September 2019; Denizli, Turkey.

[334] Dobrzański LA. The role of materials engineering in stage 4.0 of the technological revolution. Invited lecture at the 24th Seminar of the Polish Society of Materials Science; 12-15 May 2019; Jachranka, Poland. (in Polish)

[335] Dobrzański LA. The importance of materials engineering in stage 4.0 of the technological revolution. Invited lecture in the Institute of Fundamental Technological Research, Polish Academy of Sciences; 27 May 2019; Warsaw, Poland. (in Polish)

[336] Dobrzański LA. Stage 4.0 of the Technological Revolution in the Context of the Development of Engineering & Dental Materials. Invited lecture in the Lviv Polytechnic National University; 3 June 2019; Lviv, Ukraine.

[337] Jose R, Ramakrishna S. Materials 4.0: Materials Big Data Enabled Materials Discovery. Applied Materials Today. 2018;10: 127-132. DOI: 10.1016/j.apmt.2017.12.015

[338] United Nations General Assembly. Transforming Our World: The 2030 Agenda for Sustainable Development: A/RES/70/1. New York: United Nations; 2015.

[339] Dobrzański LA. Fundamentals of materials science and metallurgy. Engineering materials with the basics of material design. Warsaw, Poland: WNT; 2002. (in Polish)

[340] Dobrzański LA. Metallic engineering materials. Warsaw, Poland: WNT; 2004. (in Polish)

[341] Dobrzański LA. Fundamentals of materials science. Gliwice, Poland: Silesian University of Technology Publishing House; 2012. (in Polish)

[342] Dobrzański LA, Dobrzańska-Danikiewicz AD. Surface engineering of materials: a compendium of knowledge and an academic textbook. Gliwice: International OCSCO World Press; 2018. 1138 p. (in Polish)

[343] Dobrzański LA. Materials Design as an Important Element of Advanced Products' Engineering Design and Manufacturing. In: 17th International Congress of Mechanical Engineering. São Paulo, Brazil: Associação Brasileira de Ciências Mecânicas; 2003. (CD-ROM)

[344] Dobrzański LA. Contemporary development trends in materials science and material engineering. Materials Engineering. 2003;24:271-278. (in Polish)

[345] Dobrzański LA. Significance of Materials Science and Engineering for Advances in Design and Manufacturing Processes, Computer Integrated Manufacturing. In: Skołud B, Krenczyk D, editors. Advanced Design and Management. Warsaw, Poland: WNT; 2003. p. 128-140.

[346] Dobrzański LA. The importance of the development of materials science and materials engineering to improve

the quality of life of modern societies. Wisnyk Technologiczno University of Podilla, Khmelnytsky, Ukraine. 2003;I: 34-47. (in Polish)

[347] Dobrzański LA. Heat Treatment as Fundamental Technological Process of Formation of Structure and Properties of Metals. In: 8th Seminar of the International Federation for Heat Treatment and Surface Engineering. Winterthur, Switzerland: International Federation for Heat Treatment and Surface Engineering, 2001. p. 1-12.

[348] Dobrzański LA. Significance of Materials Science for Advances in Products Design and Manufacturing. Invited lecture at the General Assembly of the International Academy for Production Engineering; 22-28 August 2004; Cracow, Poland.

[349] Dobrzański LA. Computational Materials Science as a Method of Design of Contemporary Engineering Materials and Products. In: 10th Seminary of Research and Education Programmes in Materials Engineering. Myczkowce, Poland: Polish Society of Materials Science, 2004. p. 55-88. (in Polish)

[350] Ruehle M, Dosch H, Mittemeijer E, van de Voorde MH, editors. European White Book on Fundamental Research in Materials Science. Stuttgart, Germany: Max-Planck-Institute für Metallforschung; 2001.

[351] Dieter GE, editor. ASM Handbook Volume 20: Materials Selection and Design. Materials Park, OH: ASM International; 1997.

[352] Japan Business Federation. Society 5.0: Co-Creating the Future (Excerpt). Tokyo: Keidanren; 2018.

[353] Japan Business Federation. Toward Realization of the New Economy and Society (Outline). Tokyo: Keidanren; 2016.

[354] Japan Business Federation. Japan's Initiatives–Society 5.0. Tokyo: Keidanren; 2016.

[355] Harayama Y. Society 5.0: Aiming for a New Human-Centered Society. Hitachi Review. 2017;66:8-13.

[356] Government of Japan Cabinet Office. Society 5.0 [Internet]. 2019. Available from: http://web.archive.org/web/20190710182953/https://www8.cao.go.jp/cstp/society5_0/index.html [Accessed: 2021-02-10]

[357] Fukuyama M. Society 5.0: Aiming for a New Human-Centered Society. Japan SPOTLIGHT. 2018;July/August: 47-50.

[358] Kagermann H, Wahlster W, Helbig J. Recommendations for Implementing the Strategic Initiative INDUSTRIE 4.0: Final Report of the Industrie 4.0 Working Group. Bonn, Germany: Federal Ministry of Education and Research; 2013.

[359] Kagermann H. Chancen von Industrie 4.0 Nutzen. In: Industrie 4.0 in Produktion, Automatisierung und Logistik. Wiesbaden, Germany: Springer Fachmedien Wiesbaden; 2014. p. 603-614.

[360] Hermann M, Pentek T, Otto B. Design Principles for Industrie 4.0 Scenarios: A Literature Review. Dortmund, Germany: Technische Universität Dortmund; 2015.

[361] Rüßmann M, Lorenz M, Gerbert P, Waldner M, Justus J, Engel P, Harnisch M. Industry 4.0: The Future of Productivity and Growth in Manufacturing Industries. Boston, MA: Boston Consulting Group; 2015.

[362] European Commission. Commission Sets Out Path to Digitise European Industry. IP/16/1407 [Internet]. 2016. Available from: http://web.archive.org/web/

20200403145542/https://ec.europa.eu/commission/presscorner/detail/en/IP_16_1407 [Accessed: 2021-02-10]

[363] Danieluk K. Digital Innovation Hubs on Smart Factories in New EU Member States [Internet]. 2017. Available from: https://ec.europa.eu/futurium/en/implementing-digitising-european-industry-actions/digital-innovation-hubs-smart-factories-new-eu [Accessed: 2021-02-10]

[364] Lu BH, Bateman RJ, Cheng K. RFID Enabled Manufacturing: Fundamentals, Methodology and Applications. International Journal of Agile Systems and Management. 2006;1:73-92. DOI: 10.1504/IJASM. 2006.008860

[365] Giusto D, Iera A, Morabito G, Atzori L, editors. The Internet of Things. New York: Springer; 2010.

[366] Zhu Q, Wang R, Chen Q, Liu Y, Qin W. IOT Gateway: Bridging Wireless Sensor Networks into Internet of Things. In: 2010 IEEE/IFIP International Conference on Embedded and Ubiquitous Computing. Piscataway, NJ: The Institute of Electrical and Electronics Engineers; 2010. p. 347-352.

[367] Wan J, Yan H, Liu Q, Zhou K, Lu R, Li D. Enabling Cyber-Physical Systems with Machine-to-Machine Technologies. International Journal of Ad Hoc and Ubiquitous Computing. 2013;13:187-196. DOI: 10.1504/IJAHUC.2013.055454

[368] Gubbi J, Buyya R, Marusic S, Palaniswami M. Internet of Things (IoT): A Vision, Architectural Elements, and Future Directions. Future Generation Computer Systems. 2013;29: 1645-1660. DOI: 10.1016/ j. future.2013.01.010

[369] Zhong RY, Li Z, Pang LY, Pan Y, Qu T, Huang GQ. RFID-Enabled Real-Time Advanced Planning and Scheduling Shell for Production Decision Making. International Journal of Computer Integrated Manufacturing. 2013;26:649-662. DOI: 10.1080/0951192X.2012.749532

[370] Wu D-Z, Greer MJ, Rosen DW, Schaefer D. Cloud Manufacturing: Strategic Vision and State-of-the-Art. Journal of Manufacturing Systems. 2013;32:564-579. DOI: 10.1016/j. jmsy.2013.04.008

[371] Moreno-Vozmediano R, Montero RS, Llorente IM. Key Challenges in Cloud Computing: Enabling the Future Internet of Services. IEEE Internet Computing. 2013;17: 18-25. DOI: 10.1109/MIC.2012.69

[372] Lee J, Kao H-A, Yang S. Service Innovation and Smart Analytics for Industry 4.0 and Big Data Environment. Procedia CIRP. 2014; 16:3-8. DOI: 10.1016/j.procir. 2014.02.001

[373] Bi Z, Xu LD, Wang C. Internet of Things for Enterprise Systems of Modern Manufacturing. IEEE Transactions on Industrial Informatics. 2014;10:1537-1546. DOI: 10.1109/TII.2014.2300338

[374] Brettel M, Friederichsen N, Keller M, Rosenberg M. How Virtualization, Decentralization, and Network-Building Change the Manufacturing Landscape: An Industry 4.0 Perspective. International Journal of Mechanical, Aerospace, Industrial, Mechatronic, and Manufacturing Engineering. 2014;8: 37-44.

[375] Buer S-V, Strandhagen JO, Chan FTS. The Link between Industry 4.0 and Lean Manufacturing: Mapping Current Research and Establishing a Research Agenda. International Journal of Production Research. 2018;56:2924-2940. DOI: 10.1080/00207543.2018.1442945

[376] Patel P, Cassou D. Enabling High-Level Application Development for the Internet of Things. Journal of Systems and Software. 2015;103:62-84. DOI: 10.1016/j.jss.2015.01.027

[377] Zhang Y, Zhang G, Wang J, Sun S, Si S, Yang T. Real-Time Information Capturing and Integration Framework of the Internet of Manufacturing Things. International Journal of Computer Integrated Manufacturing. 2015;28:811-822. DOI: 10.1080/0951192X.2014.900874

[378] Qiu X, Luo H, Xu G, Zhong R-Y, Huang GQ. Physical Assets and Service Sharing for IoT-Enabled Supply Hub in Industrial Park (SHIP). International Journal of Production Economics. 2015; 159:4-15. DOI: 10. 1016/j.ijpe.2014.09.001

[379] Posada J, Toro C, Barandiaran I, Oyarzun D, Stricker D, de Amicis R, Pinto EB, Eisert P, Döllner J, Vallarino I. Visual Computing as a Key Enabling Technology for Industrie 4.0 and Industrial Internet. IEEE Computer Graphics and Applications. 2015;35: 26-40. DOI: 10.1109/MCG.2015.45

[380] Farooq MU, Waseem M, Mazhar S, Khairi A, Kamal T. A Review on Internet of Things (IoT). International Journal of Computer Applications. 2015;113:1-7. DOI: 10.5120/19787-1571

[381] Lee J, Bagheri B, Kao H-A. A Cyber-Physical Systems Architecture for Industry 4.0-Based Manufacturing Systems. Manufacturing Letters. 2015;3: 18-23. DOI: 10.1016/j.mfglet.2014.12.001

[382] Almada-Lobo F. The Industry 4.0 Revolution and the Future of Manufacturing Execution Systems (MES). Journal of Innovation Management. 2015;3:16-21. DOI: 10.24840/2183-0606_003.004_0003

[383] Wamba SF, Akter S, Edwards A, Chopin G, Gnanzou D. How 'Big Data' Can Make Big Impact: Findings from a Systematic Review and a Longitudinal Case Study. International Journal of Production Economics. 2015;165: 234-246. DOI: 10.1016/j.ijpe.2014.12.031

[384] Yin YH, Nee AYC, Ong SK, Zhu JY, Gu PH, Chen LJ. Automating Design with Intelligent Human-Machine Integration. CIRP Annals. 2015;64: 655-677. DOI: 10.1016/j.cirp.2015.05.008

[385] Colin M, Galindo R, Hernández O. Information and Communication Technology as a Key Strategy for Efficient Supply Chain Management in Manufacturing SMEs. Procedia Computer Science. 2015;55:833-842. DOI: 10.1016/j.procs.2015.07.152

[386] Hozdic E. Smart Factory for Industry 4.0: A Review. International Journal of Modern Manufacturing Technologies. 2015;7:28-35.

[387] Zhong RY, Huang GQ, Lan S, Dai QY, Zhang T, Xu C. A Two-Level Advanced Production Planning and Scheduling Model for RFID-Enabled Ubiquitous Manufacturing. Advanced Engineering Informatics. 2015;29: 799-812. DOI: 10.1016/j.aei.2015.01.002

[388] Wang S, Wan J, Zhang D, Li D, Zhang C. Towards Smart Factory for Industry 4.0: A Self-Organized Multi-Agent System with Big Data Based Feedback and Coordination. Computer Networks. 2016;101:158-168. DOI: 10.1016/j.comnet.2015.12.017

[389] Monostori L, Kádár B, Bauernhansl T, Kondoh S, Kumara S, Reinhart G, Sauer O, Schuh G, Sihn W, Ueda K. Cyber-Physical Systems in Manufacturing. CIRP Annals. 2016;65: 621-641. DOI: 10.1016/j.cirp.2016.06.005

[390] Zhong RY, Lan S, Xu C, Dai Q, Huang GQ. Visualization of RFID-Enabled Shopfloor Logistics Big Data in Cloud Manufacturing. International

Journal of Advanced Manufacturing Technology. 2016;84:5-16. DOI: 10.1007/s00170-015-7702-1

[391] Georgakopoulos D, Jayaraman PP, Fazia M, Villari M, Ranjan R. Internet of Things and Edge Cloud Computing Roadmap for Manufacturing. IEEE Cloud Computing. 2016;3:66-73. DOI: 10.1109/MCC. 2016.91

[392] Zhong RY, Newman ST, Huang GQ, Lan S. Big Data for Supply Chain Management in the Service and Manufacturing Sectors: Challenges, Opportunities, and Future Perspectives. Computers & Industrial Engineering. 2016;101:572-591. DOI: 10.1016/j.cie.2016.07.013

[393] Misra G, Kumar V, Agarwal A, Agarwal K. Internet of Things (IoT) – A Technological Analysis and Survey on Vision, Concepts, Challenges, Innovation Directions, Technologies, and Applications (An Upcoming or Future Generation Computer Communication System Technology). American Journal of Electrical and Electronic Engineering. 2016;4:23-32. DOI: 10.12691/ajeee-4-1-4

[394] Schumacher A, Erol S, Sihn W. A Maturity Model for Assessing Industry 4.0 Readiness and Maturity of Manufacturing Enterprises. Procedia CIRP. 2016;52:161-166. DOI: 10.1016/j.procir.2016.07.040

[395] Sipsas K, Alexopoulos K, Xanthakis V, Chryssolouris G. Collaborative Maintenance in Flow-Line Manufacturing Environments: An Industry 4.0 Approach. Procedia CIRP. 2016;55:236-241. DOI: 10.1016/j.procir.2016.09. 013

[396] Qin J, Liu Y, Grosvenor R. A Categorical Framework of Manufacturing for Industry 4.0 and Beyond. Procedia CIRP. 2016;52:173-178. DOI: 10.1016/j.procir.2016.08.005

[397] DIN SPEC 91345:2016-04. Referenzarchitekturmodell Industrie 4.0 (RAMI4.0). Berlin: Beuth Verlag; 2016.

[398] Dobrzański LA. Comparative Analysis of Mechanical Properties of Scaffolds Sintered from Ti and Ti6Al4V Powders. Lecture at the22nd Winter International Scientific Conference on Achievements in Mechanical and Materials Engineering; 6-9 December 2015; Zakopane, Poland.

[399] Adolphs P, Auer S, Bedenbender H, Billmann M, Hankel M, Heidel R, Hoffmeister M, Huhle H, Jochem M, Kiele-Dunsche M, Koschnick G, Koziolek H, Linke L, Pichler R, Schewe F, Schneider K, Waser B. Structure of the Administration Shell: Continuation of the Development of the Reference Model for the Industrie 4.0 Component. Berlin: Federal Ministry for Economic Affairs and Energy; 2016.

[400] Bahrin MAK, Othman MF, Azli NHN, Talib MF. Industry 4.0: A Review on Industrial Automation and Robotic. Jurnal Teknologi. 2016;78:137-143. DOI: 10.11113/jt.v78.9285

[401] Mosterman PJ, Zander J. Industry 4.0 as a Cyber-Physical System Study. Software & Systems Modeling. 2016;15:17-29. DOI: 10.1007/s10270-015-0493-x

[402] Harrison R, Vera D, Ahmad B. Engineering Methods and Tools for Cyber-Physical Automation Systems. Proceedings of the IEEE. 2016;104:973-985. DOI: 10.1109/JPROC.2015.2510665

[403] Stock T, Seliger G. Opportunities of Sustainable Manufacturing in Industry 4.0. Procedia CIRP. 2016;40:536-541. DOI: 10.1016/j.procir.2016.01.129

[404] Pfeiffer S. Robots, Industry 4.0 and Humans, or Why Assembly Work Is More than Routine Work. Societies. 2016;6:16. DOI: 10.3390/soc6020016

[405] Gorkhali A, Xu LD. Enterprise Application Integration in Industrial Integration: A Literature Review. Journal of Industrial Integration and Management. 2016;1:1650014. DOI: 10.1142/S2424862216500147

[406] Zhong RY, Xu X, Klotz E, Newman ST. Intelligent Manufacturing in the Context of Industry 4.0: A Review. Engineering. 2017;3:616-630. DOI: 10.1016/J.ENG.2017.05.015

[407] Thoben K-D, Wiesner S, Wuest T. 'Industrie 4.0' and Smart Manufacturing – A Review of Research Issues and Application Examples. International Journal of Automation Technology. 2017;11: 4-16. DOI: 10.20965/ijat.2017.p0004

[408] Xu X. Machine Tool 4.0 for the New Era of Manufacturing. International Journal of Advanced Manufacturing Technology. 2017;92: 1893-1900. DOI: 10.1007/s00170-017-0300-7

[409] Li B-H, Hou B-C, Yu W-T, Lu X-B, Yang C-W. Applications of Artificial Intelligence in Intelligent Manufacturing: A Review. Frontiers of Information Technology & Electronic Engineering. 2017;18:86-96. DOI: 10.1631/FITEE.1601885

[410] Lu Y. Industry 4.0: A Survey on Technologies, Applications and Open Research Issues. Journal of Industrial Information Integration. 2017;6:1-10. DOI: 10.1016/j.jii.2017.04.005

[411] Vaidya S, Ambad P, Bhosle S. Industry 4.0 – A Glimpse. Procedia Manufacturing. 2018;20:233-238. DOI: 10.1016/j.promfg.2018.02.034

[412] Kumar K, Zindani D, Davim JP. Industry 4.0: Developments towards the Fourth Industrial Revolution. Singapore: Springer Nature Singapore Pte Ltd.; 2019.

[413] Łobaziewicz M. Zarządzanie inteligentnym przedsiębiorstwem w dobie przemysłu 4.0. Toruń, Poland: Towarzystwo Naukowe Organizacji i Kierownictwa; 2019.

[414] Ardito L, Petruzzelli AM, Panniello U, Garavelli AC. Towards Industry 4.0: Mapping Digital Technologies for Supply Chain Management-Marketing Integration. Business Process Management Journal. 2019;25:323-346. DOI: 10.1108/BPMJ-04-2017-0088

[415] Boston Consulting Group. Embracing Industry 4.0 and Rediscovering Growth [Internet]. 2019. Available from: https://www.bcg.com/pl-pl/capabilities/operations/embracing-industry-4.0-rediscovering- growth.aspx [Accessed: 2021-02-10]

[416] Tietenberg T, Lewis L, Environmental and Natural Resource Economics. London: Pearson Education; 2003.

[417] Tay SI, Lee TC, Hamid NAA, Ahmad ANA. An Overview of Industry 4.0: Definition, Components, and Government Initiatives. Journal of Advanced Research in Dynamical and Control Systems. 2018;10:1379-1387.

[418] Dobrzański LA, Dobrzański LB, Dobrzańska-Danikiewicz AD, Dobrzańska J. The Concept of Sustainable Development of Modern Dentistry. Processes. 2020;8:1605. DOI: 10.3390/pr8121605

[419] Aluminum Market - Industry Analysis, Market Size, Share, Trends, Application Analysis, Growth And Forecast 2019-2025 [Internet]. Available

from: https://www.industryarc.com/Research/Aluminium-Market-Research-503190 [Accessed: 2021-02-10]

[420] Aluminum Market - Growth, Trends, and Forecast (2020-2025) [Internet]. 2020. Available from: https://www.researchandmarkets.com/reports/5025633/aluminum-market-growth-trends-and-forecast [Accessed: 2021-02-10]

[421] The Aluminum Association. The Economic Impact of Aluminum. Aluminum Drives Modern Manufacturing [Internet]. Available from: https://www.aluminum.org/aluminum-advantage/economic-impact-aluminum [Accessed: 2021-02-10]